research report

Design of Cold-Formed Steel Plain Channels

RESEARCH REPORT RP01-2

FEBRUARY 2001
REVISION 2006

Committee on Specifications
for the Design of Cold-Formed
Steel Structural Members

American Iron and Steel Institute

The material contained herein has been developed by researchers based on their research findings. The material has also been reviewed by the American Iron and Steel Institute Committee on Specifications for the Design of Cold-Formed Steel Structural Members. The Committee acknowledges and is grateful for the contributions of such researchers.

The material herein is for general information only. The information in it should not be used without first securing competent advice with respect to its suitability for any given application. The publication of the information is not intended as a representation or warranty on the part of the American Iron and Steel Institute, or of any other person named herein, that the information is suitable for any general or particular use or of freedom from infringement of any patent or patents. Anyone making use of the information assumes all liability arising from such use.

DESIGN OF COLD-FORMED STEEL PLAIN CHANNELS

FINAL REPORT

By

FANG YIU
PROFESSOR TEOMAN PEKÖZ, PROJECT DIRECTOR

A PROJECT SPONSORED BY
THE AMERICAN IRON AND STEEL INSTITUTE

Date Submitted 14 February 2001

SCHOOL OF CIVIL AND ENVIRONMENTAL
ENGINEERING
CORNELL UNIVERSITY
HOLLISTER HALL, ITHACA NY 14853-3501

ABSTRACT

Though channels are seemingly simple members, their accurate design presents special challenges. The topics under study include the behavior of channels in compression, bending about both principal axes and under the action of axial load and biaxial bending. The post local-buckling behavior of thin-walled channels and the inelastic reserve load carrying capacity of thick-walled channels are considered in the proposed design procedures.

The scope of the research includes plate elements subjected to various types of stress gradients. Physical test results coupled with extensive finite element studies are used to formulate design procedures.

TABLE OF CONTENTS

1. INTRODUCTION

Cold-formed steel plain channels shown in Figure1.1 are used in several applications such as bracing members in racks and tracks in steel framed housing. This report gives an overview of the design procedures developed for laterally braced beams, columns and beam-columns of plain channels. These formulations are based on experimental and finite element studies. Current design procedures were found to be inaccurate. For example, the minor axis bending capacity of plain channels is conservatively predicted by the AISI Specification, particularly when k=0.43 is assumed for flanges.

The design procedures developed are applicable to cross-sections in the range of practical sections used in the industry, namely $b_2 / b_1 \leq 1$. The recommendations treat members that are made up of elements that may be in the post-buckling or post yielding range. The design procedures developed are consistent with AISI Specification for calculating the overall capacity of plain channels.

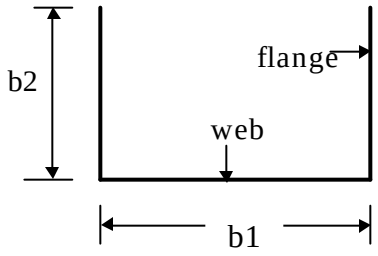

Figure 1.1 Plain Channel

2. REVIEW OF PREVIOUS RESEARCH -- EXPERIMENTAL AND ANALYTICAL WORK

Available experimental and analytical work on beams, columns and beam-columns of plain channels are reviewed.

2.1 Beams

2.1.1 Minor Axis Bending

- El Mahi and Rhodes' Experiments from UK [1985]-- Minor Axis Bending with Stiffened Element in Tension

84 tests were performed on plain channel specimens and 17 tee specimens at University of Strathclyde for the Cold Rolled Sections Association, and subsequently as part of ECSC research project no. 7210/SA/608. Of these 17 channels and 7 tee tests were undertaken for exploration purposes. Therefore the results for 67 channels and 10 tees were reported. The channels were tested as beams under pure moment loading with the unstiffened elements having their free edges in compression. Table 2.1 shows the basic cross-sectional dimensions. The typical cross section is presented in Figure 2.1.

An effective width approach was proposed in the post buckling range along with the use of post yield capacity for thicker elements to determine failure moment. The proposed effective width equation had a slight conservatism to take account of imperfections. In addition, Dr. Rhodes pointed out the slight anomaly in this proposed method.

Table 2.1 El Mahi & Rhodes' Cross Section Information

	t(mm)	b_1(mm)	b_2(mm)	q	span(mm)	$F_y(N/mm^2)$
1	1.55	49.17	12.38	0	500	270
2	1.56	49.97	25.89	0	500	270
3	1.58	49.65	36.8	0	500	270
4	1.56	52.25	51.56	0	500	270
5	1.18	51.03	13.18	0	500	270
6	1.17	50.8	25.03	0	500	270
7	1.17	51.2	38.59	0	500	270
8	1.18	50.73	51.68	0	500	270
9	1.18	51.44	23.86	13.5	500	270
10	1.18	52.07	23.54	29	500	270
11	1.18	51.44	23.86	46	500	270
12	1.18	52.12	49.53	15.5	500	270
13	1.18	52.38	49.5	29	500	270
14	1.18	52.39	49.58	47.5	500	270
15	1.17	51.15	13.9	0	700	270
16	1.15	52.19	25.59	0	700	270
17	1.17	49.63	40.1	0	700	270
18	1.17	50.39	52.13	0	700	270
19	1.52	51.19	13.21	0	700	270
20	1.57	53.68	25.26	0	700	270
21	1.57	52.41	38.59	0	700	270
22	1.57	51.14	51.29	0	700	270
23	1.59	50	25.4	16	700	270
24	1.62	52.07	24.13	28	700	270
25	1.57	52.07	24.13	46	700	270
26	1.63	51.44	49.53	15	700	270
27	1.62	53.34	48.26	29	700	270
28	1.63	53.34	49.34	45	700	270
29	0.55	51.8	12.5	0	700	270
30	0.55	51.5	25.8	0	700	270
31	0.56	51.5	38.5	0	700	270
32	0.54	52	51	0	700	270
33	0.55	52	23	15	700	270
34	0.56	49.5	23.5	29	700	270
35	0.55	50	23.5	45	700	270
36	0.54	49	40	16	700	270
37	0.55	49.5	49	30	700	270
38	0.55	50	49	44	700	270
39	0.703	50.5	51	0	305	279

40	0.71	50.5	38.4	0	305	279

(Continued Table 2.1)

41	0.708	50.8	25.5	0	305	279
42	0.71	50.8	51.5	0	305	279
43	0.71	50.3	50.3	0	305	279
44	0.7	51	25.6	0	305	279
45	0.81	52	26	0	700	184
46	0.81	52.5	33.2	0	700	184
47	0.81	54	41	0	700	184
48	0.815	53.5	45.5	0	700	184
49	0.8	53	51	0	700	184
481	0.815	53.5	45.5	0	700	184
491	0.8	53	51	0	700	184
50	1.2	54.5	26	0	700	262
51	1.2	53	33.5	0	700	262
52	1.205	53.5	46	0	700	262
53	1.21	53.5	41	0	700	262
54	1.2	54	51	0	700	262
55	1.21	54	51	0	700	262
56	0.81	51	40	25	700	184
57	0.805	51	40	35	700	184
58	0.81	50.5	40.5	40	700	184
59	0.8	51	40	46	700	184
60	0.815	51	40	49	700	184
61	0.8	50.5	40	55	700	184
62	0.81	51	40	60	700	184
63	1.2	51	40	35	700	262
64	1.21	50	40.5	40	700	262
65	1.205	5.1	40	46	700	262
66	1.2	5.1	40	53	700	262
67	1.21	50.5	40.5	60	700	262

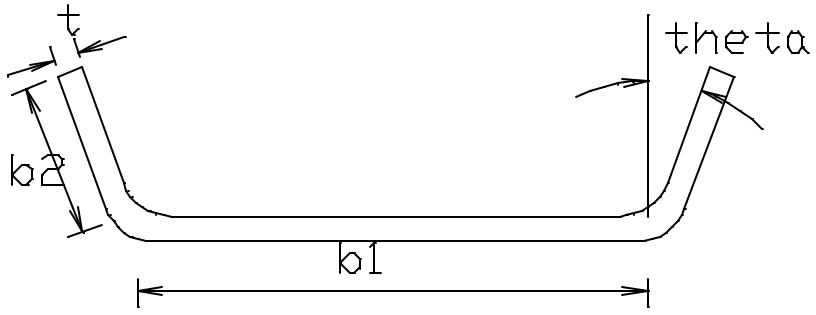

Figure 2.1 El Mahi & Rhodes's Cross Section

- Enjiky's Experiments from United Kingdom[1985]-- Minor Axis Bending with Stiffened Element in Tension, Minor Axis Bending with Stiffened Element in Compression

Plain channel sections in bending (using 0.5m and 1m spans) with their unstiffened and stiffened components in compression were tested at Oxford Polytechnic. These channel sections had a range of width to thickness ratios for compression components 3-92 for unstiffened and 14-184 for stiffened components. Tables 2.2.1 and 2.2.2 show the basic cross-sectional dimensions for stiffened element in tension and in compression, respectively. The typical cross section is presented in Figure 2.2.

Inelastic post-buckling analysis of plain channel sections was carried out by yield line theory. Recommendations on safety factors, experimental techniques, and some other issues to UK Specification Design were suggested.

Table 2.2.1 Enjiky's Cross Section Information
with Minor Axis Bending with Stiffened Element in Tension

Specimen	Section Size	Yield Stress	span	
Experiment Reference	(DxBxt) mm	N/mm^2	L mm	Q mm
M9	30x8x1.6	232.5	1000	300
M10	45x16x1.6	232.5	1000	300
M11	60x24x1.6	232.5	1000	300
M12	75x32x1.6	232.5	1000	300
M13	90x40x1.6	232.5	1000	300
M14	105x48x1.6	232.5	1000	300
M15	120x56x1.6	232.5	1000	300
M16	135x64x1.6	232.5	1000	300
Q1	160x80x1.6	183	1000	300

Q2	210x105x1.6	183	1000	300
Q3	240x120x1.6	183	1000	300
Q4	270x135x1.6	183	1000	300
Q5	300x150x1.6	183	1000	300

(Continued Table 2.2.1)

A1	100x50x1.6	230.6	500	200
A2	100x50x1.6	230.6	500	200
A3	100x50x1.6	230.6	500	200
A4	100x50x1.6	230.6	500	200
C1	100x50x1.6	230.6	500	200
C2	100x50x1.6	230.6	500	200
9	30x8x1.6	232.5	500	200
10	45x16x1.6	232.5	500	200
11	60x24x1.6	232.5	500	200
12	75x32x1.6	232.5	500	200
13	90x40x1.6	232.5	500	200
14	105x48x1.6	232.5	500	200
15	120x56x1.6	232.5	500	200
16	135x64x1.6	232.5	500	200
Q6	160x80x1.6	183	500	200
Q7	210x105x1.6	183	500	200
Q8	240x120x1.6	183	500	200
Q9	270x135x1.6	183	500	200
Q10	300x150x1.6	183	500	200

Table 2.2.2 Enjiky's Cross Section Information

with Minor Axis Bending with Stiffened Element in Compression

Specimen	Section Size	Yield Stress	span	
Experiment Reference	(DxBxt) mm	N/mm2	L mm	Q mm
M1	30x8x1.6	232.5	1000	300
M2	45x16x1.6	232.5	1000	300
M3	60x24x1.6	232.5	1000	300
M4	75x32x1.6	232.5	1000	300
M5	90x40x1.6	232.5	1000	300
M6	105x48x1.6	232.5	1000	300
M7	120x56x1.6	232.5	1000	300
M8	135x64x1.6	232.5	1000	300
P1	160x80x1.6	183	1000	300
P2	210x105x1.6	183	1000	300

P3	240x120x1.6	183	1000	300
P4	270x135x1.6	183	1000	300
P5	300x150x1.6	183	1000	300
1	30x8x1.6	232.5	500	200
2	45x16x1.6	232.5	500	200

(Continued Table 2.2.2)

3	60x24x1.6	232.5	500	200
4	75x32x1.6	232.5	500	200
5	90x40x1.6	232.5	500	200
6	105x48x1.6	232.5	500	200
7	120x56x1.6	232.5	500	200
8	135x64x1.6	232.5	500	200
P6	160x80x1.6	183	500	200
P7	210x105x1.6	183	500	200
P8	240x120x1.6	183	500	200
P9	270x135x1.6	183	500	200
P10	300x150x1.6	183	500	200
Y1	60x24x1.6	210	1000	300
Y2	75x32x1.6	210	1000	300
Y3	90x40x1.6	210	1000	300
Y4	105x48x1.6	210	1000	300
Y5	120x56x1.6	210	1000	300
Y6	135x64x1.6	210	1000	300
Y7	160x80x1.6	210	1000	300
Y8	210x105x1.6	210	1000	300
Y9	240x120x1.6	210	1000	300
Y10	270x135x1.6	210	1000	300
Y11	300x150x1.6	210	1000	300

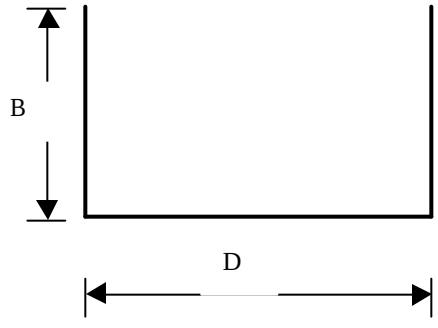

Figure 2.2 Enjiky's Cross Section

- P. Jayabalan's Experiments from India[1989]-- Minor Axis Bending with Stiffened Element in Tension, Minor Axis Bending with Stiffened Element in Compression

Nine beam tests (using 2m span) were carried out on plain channel sections at India Institute of Technology Madras with 6 specimens having unstiffened components in compression and 3 specimens having stiffened components in compression. Table 2.3 shows the basic cross-sectional dimensions. The typical cross section is presented in Figure 2.3.

Effective width equation for unstiffened elements in post local buckling range, considering the effect of imperfection, was suggested. However, those specimens that did not experience local buckling were ignored by this work. Moreover, most of the dimensions of specimen cross sections were not commonly used in industry.

Table 2.3 Jayabalan's Cross Section Information

Specimen	Type	D(mm)	W(mm)	T(mm)	R(mm)
B1	F	96.3	51.1	1.97	6.5
B2	S	97.4	50.3	1.96	6
B3	F	126.1	52.8	1.98	6.5
B4	S	181.1	53.8	2.01	7
B5	F	184.1	50.2	2.03	7
B6	S	126.5	50.3	2.03	6.5
B7	F	99.9	51.5	5.94	6.5
B8	F	131.1	52.7	5.94	7
B9	F	19	50.7	5.97	7

F stands for the case of maximum compression at free edge and

S stands for the case of maximum compression at supported edge

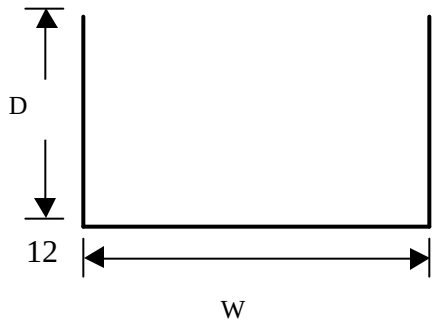

Figure 2.3 Jayabalan's Cross Section

- Julie Cohen's Work from US [1987]-- Minor Axis Bending with Stiffened Element in Tension

An iterative effective width approach was suggested and post-yield strain reserve capacity was utilized for cross sections of not slender flanges. But, there were some geometry restrictions for the proposed effective width equation such as, $H/t \le 50$; $q \le 45^o$; and $H/W1 \le 1$(H is flange width; W1 is web width; t is thickness; q is the angle between flange and the line perpendicular to web). Thus, not all experimental data can be evaluated by this approach.

2.1.2 Major Axis Bending

- Reck's Experiments from Cornell University

Four specimens were tested by Reck at Cornell University and reported by Venkatakrishnan Kalyanaraman in 1976, while only three of them are available for evaluation. Table 2.4 shows the basic cross-sectional dimensions. The typical cross-section is shown in Figure 2.4.

Table 2.4 Reck's Cross Section

	Reck's Specimen					
	Bc (in.)	Bt (in.)	D (in.)	t (in.)	L (in.)	Fy kips
UP-9	1.68	1.671	3.978	0.06	60	42
UP-10	1.22	1.241	4.013	0.035	60	36
UP-11	1.417	1.446	4.005	0.0347	60	36
UP-12	1.616	1.648	4.001	0.0355	60	N/A

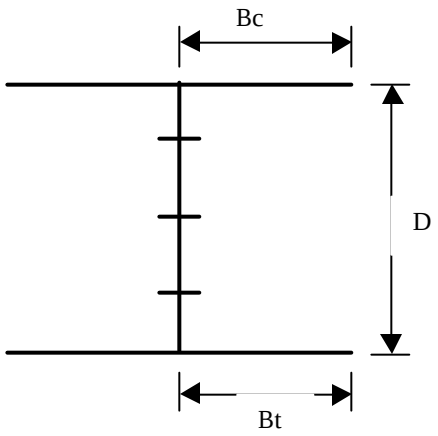

Figure 2.4 Reck's Cross Section

- Asko Talja's Experiments from Finland [1990]

Two specimens were bent about the axis of symmetry of the profile. Plain channels were side by side and the webs were connected together with a plate. Table 2.5 shows the basic cross-sectional dimensions. The typical cross-section is shown in Figure 2.5.

Table 2.5 Asko's Cross Section

Name	fy	t (mm)	r (mm)	a (mm)	b (mm)	l_1 (mm)	l_2 (mm)	l_3 (mm)
UU1 / MR1	620	6.05	8	121	37	250	750	1250
UU1 / MR2	620	6.05	8	121	37	1250	1750	2150

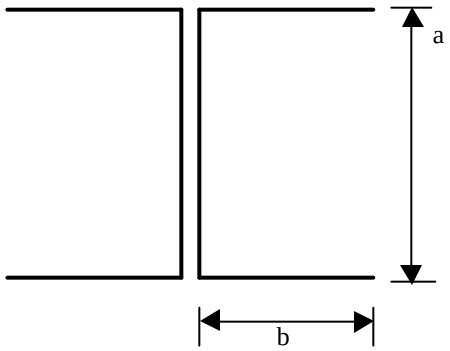

Figure 2.5 Asko's Cross Section

2.2 Columns

- Mulligan & Pekoz's Experiments from USA[1983]--Flat-ended Stub Column with Uniform Compression

Eleven press-braked stub column tests were carried out on plain channel sections at Cornell University to study the interaction of local buckling between plate elements. The column length was determined to be short enough to preclude the overall buckling modes, but be long enough so as not to restrict the local buckling behavior. Initial imperfections were measured. The basic cross-sectional dimensions are presented in Table 2.6. The typical cross-section is shown in Figure 2.6.

Table 2.6 Mulligan & Pekoz's Cross Section Information

Specimen		W1(in.)	w2(in.)	t(in.)	OR(in.)	L(in.)	Fy(ksi)
SC/1	60x30	3.230	1.609	0.0484	0.168	9.976	32.79
SC/1	90x30	4.609	1.612	0.0478	0.164	10.94	32.79
SC/1	120x30	6.102	1.612	0.0472	0.172	8.961	32.79
SC/2	120x30	6.117	1.605	0.0482	0.168	16.85	32.79
SC/1	40x60	2.051	3.095	0.0480	0.152	15.14	51.62
SC/2	40x60	2.095	3.093	0.0481	0.152	15.14	51.62

(Continued Table 2.6)

SC / 1	60x60	3.058	3.080	0.0479	0.125	9.141	51.62
SC / 1	100x60	5.070	3.077	0.0481	0.125	15.14	51.62
SC / 1	120x60	6.125	2.973	0.0474	0.156	18.98	32.79
SC / 1	180x60	8.844	2.984	0.0476	0.164	17.98	32.79
SC / 2	180x60	8.852	2.980	0.0476	0.164	24.98	32.79

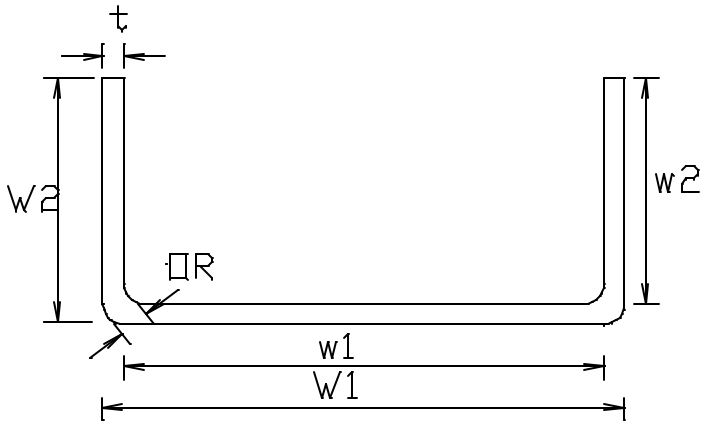

Figure 2.6 Mulligan & Pekoz's Cross Section

- Asko Talja's Experiments from Finland[1990]--Flat-ended Column with Uniform Compression

Twelve roll-formed high-strength steels (HSS) column tests were carried out on plain channel sections at Technical Research Center of Finland. Channel columns were tested under uniform compression in a fixed end condition. The basic cross-sectional dimensions are presented in Table 2.7. The typical cross-section is shown in Figure 2.7.

Table 2.7 Asko Talja's Cross Section

		Asko Talja's Cross Section				
Specimen	bw (mm)	bf (mm)	t (mm)	R (mm)	L (mm)	Fy (N/mm^2)
U127x40x6 a)	127.0	40.6	5.98	7.5	240	609
b)	127.0	40.6	5.98	7.5	650	609
c)	127.0	40.6	5.98	7.5	1000	609
d)	127.0	40.6	5.98	7.5	1400	609
U186x80x6 a)	186.4	79.8	5.96	7.5	490	570
b)	186.4	79.8	5.96	7.5	1200	570
c)	186.4	79.8	5.96	7.5	2100	570
d)	186.4	79.8	5.96	7.5	3100	570
U286x80x6 a)	287.0	78.9	5.94	7.25	560	576
b)	287.0	78.9	5.94	7.25	1400	576
c)	287.0	78.9	5.94	7.25	2200	576
d)	287.0	78.9	5.94	7.25	3100	576

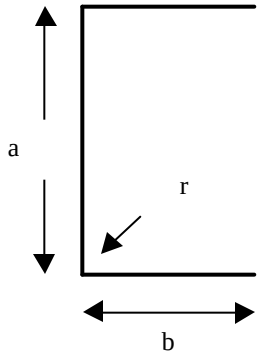

Figure 2.7 Asko Talja's Cross Section

- Ben Young's Experiments from Australia[1997]--Flat-ended and Pin-ended Columns with Uniform Compression

A series of tests was performed on plain channels press-braked from high strength structural steel sheets at University of Sydney to study the effect of support conditions (fixed-ended, pin-ended) on singly symmetric columns. Geometric imperfections, material properties and residual stresses were

measured on nearly all test specimens before testing. Four different cross section geometries were tested over a range of lengths which involved pure local buckling, distortional buckling as well as overall flexural buckling and flexural-torsional buckling. The shift of the effective centroid was measured experimentally. Tables 2.8.1 and 2.8.2 show the basic cross-sectional dimensions. The data in shaded cells correspond to pin-ended columns; while the other data correspond to fix-ended columns. The cross sectional dimension is presented in Figure 2.8.

Table 2.8.1 Ben Young's Cross Section Information on Series P36

Specimen	Bf (mm)	Bw (mm)	t	t (base metal)	Radius	L (mm)	A (mm^2)	Fy (Mpa)
P36F0280	36.8	96.8	1.51	1.47	0.85	279.9	246	550
P36F1000	36.7	96.6	1.52	1.48	0.85	1000.2	248	550
P36F1500	36.8	97.4	1.5	1.46	0.85	1500.9	245	550
P36F2000	36.8	96.6	1.51	1.48	0.85	2000.6	247	550
P36F2500	36.8	97	1.51	1.48	0.85	2499.4	248	550
P36F3000	36.8	96.9	1.51	1.47	0.85	3000.5	246	550
P36P0280-	36.9	96.6	1.51	1.48	0.85	280	247	550
P36P0315-	37	96.8	1.5	1.46	0.85	314.5	245	550
P36P0815-	36.8	97.5	1.51	1.48	0.85	814.9	249	550
P36P1315-	37	96.6	1.5	1.46	0.85	1315.1	245	550

Table 2.8.2 Ben Young's Cross Section Information on Series P48

Specimen	Bf (mm)	Bw (mm)	t	t (base metal)	Radius	L (mm)	A (mm^2)	Fy (Mpa)
P48F0300	49.6	94.6	1.51	1.47	0.85	*300	280	510
P48F1000	49.7	94.7	1.51	1.47	0.85	999.7	281	510
P48F1500	49.6	95.5	1.51	1.46	0.85	1500.9	280	510
P48F1850	49.6	95.1	1.54	1.49	0.85	1850	284	510
P48F2150	49.5	95.9	1.52	1.47	0.85	2148.9	282	510
P48F2500	49.7	95.4	1.52	1.47	0.85	2499.8	282	510
P48F3000	49.5	96	1.53	1.47	0.85	3001.3	283	510
P48F3500	49.5	95.8	1.52	1.47	0.85	3501.2	282	510

(Continued Table 2.8.2)

P48P0300 +	49.6	94.8	1.51	1.46	0.85	*300	279	510
P48P0565-	49.8	94.5	1.53	1.48	0.85	564.9	283	510
P48P1065	50	94.2	1.52	1.48	0.85	1064.7	282	510
P48P1565-	49.4	95.1	1.52	1.47	0.85	1565	281	510

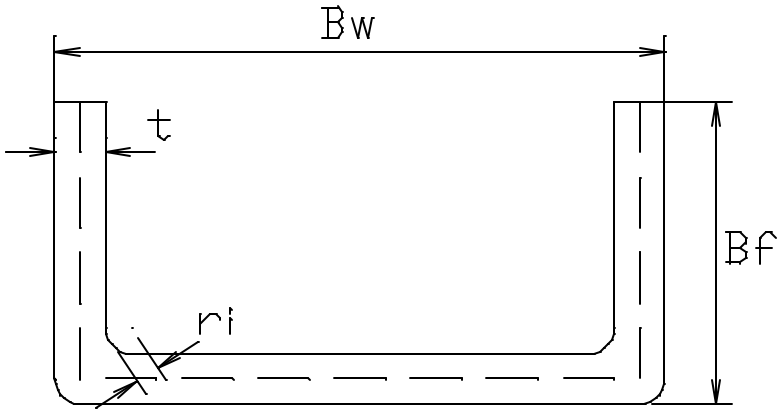

Figure 2.8 Ben Young's Cross Section

- Pekoz's Experiments from USA [1998] -- Flat-ended Column with Uniform Compression

Seven plain channels under uniform compression were tested at Cornell University. The channels were loaded flat-ended between bearing plates. The failure modes were also reported. Imperfections were not measured. Table 2.9 shows the basic cross-sectional dimensions. The typical cross-section is shown in Figure 2.9.

Table 2.9 Pekoz's Cross Section

No.	L(in)	t(in)	a(in)	b(in)	Pult (kips)	Fy (ksi)	failure mode
1	114.85	0.064	3.28	1.52	4.70	51.2	FB
2	114.80	0.060	2.26	1.54	4.00	53.6	FB
3	72.02	0.063	3.25	1.03	4.10	54.5	FB,CFM
4	72.00	0.062	2.30	1.04	4.00	57.8	FB,CFM
5	58.25	0.061	2.25	1.58	6.90	52.5	FTB
6	58.15	0.081	3.23	1.56	14.60	58.4	FB,CFE
7	65.62	0.062	3.26	1.04	5.20	55.1	FB,CFE

FB: flexural buckling
TFB: torsional flexural buckling
CFE: local buckling near the ends due to crippling of flanges
CFM: local buckling at the middle due to crippling of flange

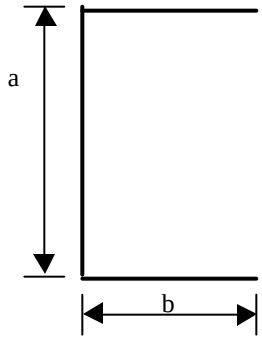

Fig.2.9 Pekoz's Cross Section

2.3 Beam-Columns

2.3.1 Eccentricity of the Load in the Plane of Symmetry

- P. Jayabalan's Experiments from India[1989]-- Flat-ended Column with Eccentric Compression

Twenty columns with non-uniform compression were tested at India Institute of Technology Madras, ten of which were corresponding to the case of maximum compression at the free edge and the remaining were corresponding to the case of maximum compression at the supported edge:

Kex=0.5; Key=0.5; Ket=0.5. Table 2.10 shows the basic cross-sectional dimensions. The typical cross-section is shown in Figure 2.10.

Table 2.10 Jayabalan's Cross sectional Dimensions

NO	Type	D(mm)	W(mm)	t(mm)	R(mm)
C1	F	89.4	59.1	1.8	6
C2	S	96.8	50	1.94	6
C3	F	89.3	59.3	1.78	6
C4	S	89.8	59	1.75	5.5
C5	F	89.7	57.7	1.78	5.5
C6	S	97.4	50.7	1.96	6
C7	F	120.3	56.8	1.73	6
C8	S	120.2	57.7	1.81	6
C9	F	120.3	58.9	1.85	6
C10	S	119.4	56.8	1.74	6
C11	F	120	57.4	1.81	5.5
C12	S	119.7	59.4	1.71	5.5
C13	F	61.5	58	1.77	6
C14	S	59.4	61	1.73	5.5
C15	F	62	59.8	1.81	6
C16	S	61.1	56.9	1.79	5.5
C17	F	184.4	53.1	2.09	6.5
C18	S	184.7	53.1	2.12	7
C19	F	184.7	50.7	2.11	7
C20	S	184.2	49.1	2.15	6.5

F stands for the case of maximum compression at free edge and

S stands for the case of maximum compression at supported edge

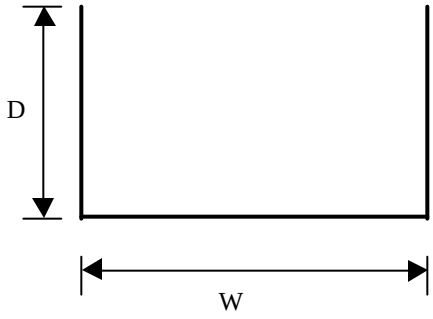

Fig 2.10 Jayabalan's Cross Section

- K. Srinivasa Rao's Experiments from India[1998]--Pin-ended Column with Eccentric Compression

Thirteen plain channels under non-uniform compression were tested at India Institute of Technology Madras to study the torsional-flexural buckling of locally buckled long members with singly symmetric open sections. Table 2.11 shows the basic cross-sectional dimensions. The typical cross-section is shown in Figure 2.11.

Tables 2.11 Srinivasa's Cross Sections

Specimen	Bf(mm)	Bw(mm)	t(mm)	Ri(mm)	L(mm)	ex(mm)
LPCI-11	50.2	42.91	1.48	5.02	598	-1.61
LPCI-12	50.58	41.53	1.49	4.76	902	-2.17
LPCI-21	49.57	43.72	1.48	4.52	1503	10.5
LPCI-31	49.61	43.98	1.48	4.65	1193	-11.8
LPCII-11	90.76	38.12	1.49	2.77	797	1.3
LPCII-12	90.65	38.89	1.48	2.75	1503	3.78
LPCII-21	91.34	37.15	1.49	2.89	1099	9.97
LPCII-22	89.36	42.02	1.49	4.02	1499	28.88
LPCII-23	88.86	42.62	1.47	4.04	2200	43.68
LPCII-31	90.83	38.43	1.48	2.9	1100	-8.26

LPCII-32	89.37	42.05	1.49	3.77	1498	-19.34
LPCIII-33	89.93	42.92	1.49	3.76	2205	-45.32
LPCIII-11	155.5	48.85	1.48	3.77	1097	1.92

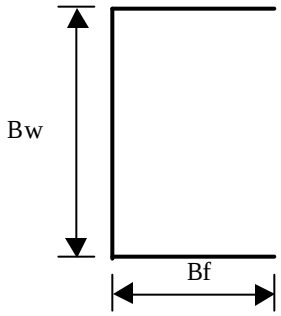

Fig.2.11 Srinivasa's Cross Sections

2.4 Others

Several other researchers have also studied plain channel cross sections, while their experimental results are not available.

Chilver [1953]: Twelve stub columns were tested, while no information was given about geometric imperfections and the lengths of the specimens.

Pekoz [1977]: Twelve stub columns were tested, while no information was given on the lengths of the columns.

Batista et al.[1987]: A series of tests on plain channel columns fabricated by brake-pressing form 1.5, 2.0 and 4.0mm steel sheets was made. Columns were tested between pinned ends under concentric loading or as stub columns. The overall geometric imperfections and residual stresses were measured in some specimens. The long columns mainly failed in flexural or flexural-torsional buckling without local buckling, and some columns failed interactively in local and overall modes.

As none of the existing analytical models are satisfactory for the available experimental data, there is a definite need for the specification to provide some guidance in the design of plain channels.

3. ELASTIC BUCKLING

The determination of the ultimate strength when the plate elements are in the post buckling range is based on the effective width procedure. The effective width procedure necessitates the use of the plate buckling stress or the plate buckling coefficient k.

In AISI Specification, plate buckling coefficients are limited to isolated plates. However, cold-formed sections are composed of interconnected plates. In addition, the buckling of one plate affects the buckling and post-buckling of the remaining plates that comprise the section.

Simple equations for plate buckling coefficient k considering the interaction between plate elements were developed for minor and major axis bending as well as for columns. These equations were obtained by using a computer program CUFSM developed by Schafer (1997) at Cornell University. The dimensions of plain channels are in the ranges of practical applications by the industry.

3.1 Beams

3.1.1 Minor Axis Bending with Stiffened Element in Tension

A parameter study has been carried out for plain channels having minor axis bending with stiffened element in tension. The ratio of flange width b_2 over web width b_1 varies from 0.1 to 1. The cross section is

illustrated in Figure 3.1. The results are shown in Figure 3.2. The stress gradient is displayed in Figure 3.3.

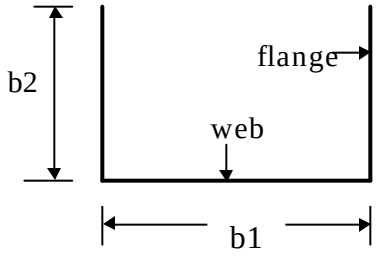

Figure 3.1 Cross Section for Parameter Study

bending about the weak axis

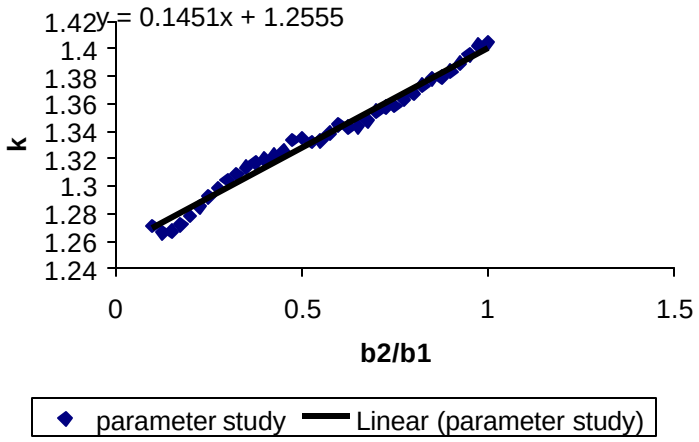

Figure 3.2 k versus b_2/b_1 for Minor Axis Bending with Stiffened Element in Tension

It is found that k is independent of the channel thickness and is an approximate linear function of b_2/b_1. Channels with flanges not at right

angles to the web (hereinafter angled channels) and ordinary plain channels of the same dimensions have almost the same magnitude of k value.

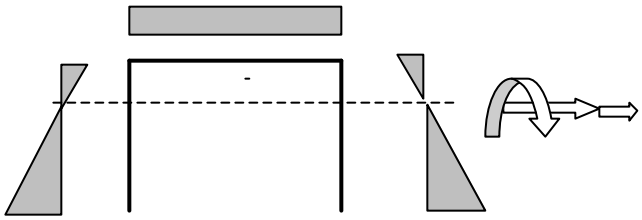

Figure 3.3 Stress Gradient for Minor Axis Bending with Stiffened Element in Tension

$$k_f = 0.1451(\frac{b_2}{b_1}) + 1.2555$$

3.1.2 Minor Axis Bending with Stiffened Element in Compression

A similar parameter study has been carried out for plain channels having minor axis bending with stiffened element in compression. The cross section is illustrated in Figure 3.1. The results are shown in Figure 3.4. The stress gradient is displayed in Figure 3.5.

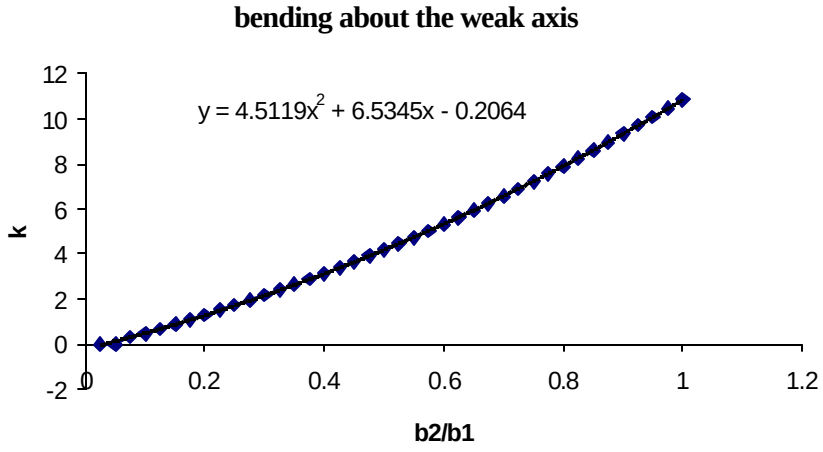

Figure 3.4 k versus b_2 / b_1 for Minor Axis Bending with Stiffened Element in Compression

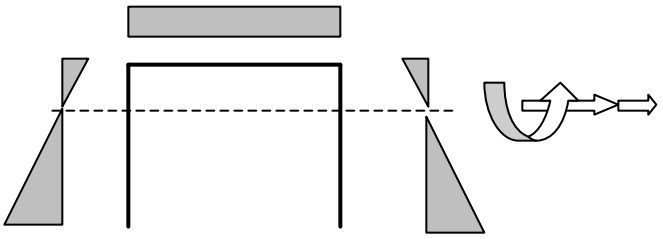

Figure 3.5 Stress Gradient for Minor Axis Bending with Stiffened Element in Compression

$$k_f = 4.5119(\frac{b_2}{b_1})^2 + 6.5345(\frac{b_2}{b_1}) - 0.2064$$

$$k_w = (b_1 / b_2)^2 k_f$$

3.1.3 Major Axis Bending

There are two types of section profiles being tested in this category:

1) Asko type : two plain channel sections have some distance in between, which is shown in Figure 3.6.
2) Reck type: two plain channel sections are closly connected; this type is more like a W cross section with web thickness 2t shown in Figure 3.7.

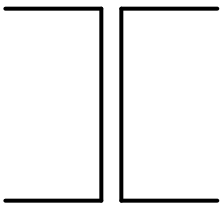

Figure 3.6 Major Axis Bending--Asko Type

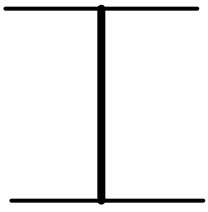

Figure 3.7 Major Axis Bending--Reck Type

3.1.3.1 Plate buckling coefficients obtained from CUFSM for Asko Type

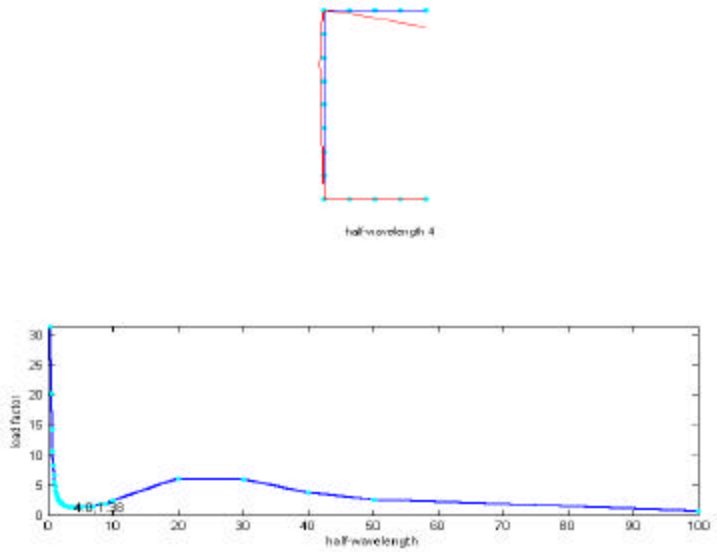

Figure 3.8 results from CUFSM for Asko type channels

Figure 3.8 shows the buckling shape of the plain channel and its corresponding half-wavelength and load factor. A parameter study has also been carried out and the results are shown in Figure 3.9. The stress gradient is displayed in Figure 3.10.

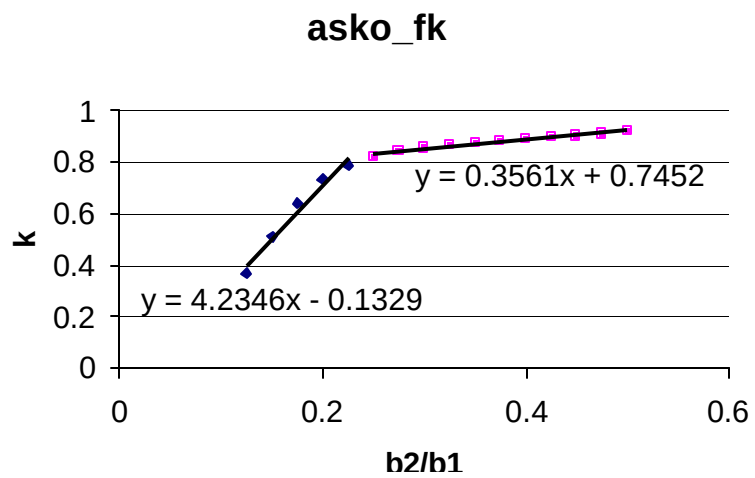

Figure 3.9 k versus b_2/b_1 for Asko type channels

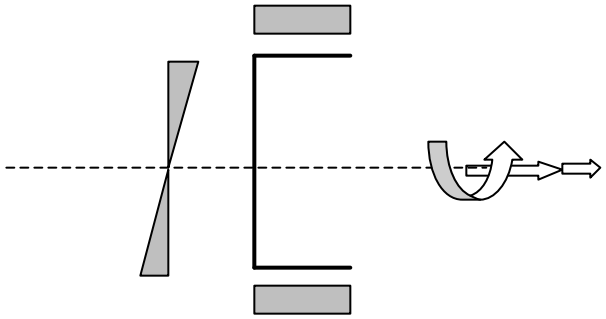

Figure 3.10
Stress Gradient for Major Axis Bending--Asko Type

$$k_f = 0.3561(\frac{b_2}{b_1}) + 0.7452 \text{, when } \frac{b_2}{b_1} > 0.2264$$

$$k_f = 4.2346(\frac{b_2}{b_1}) - 0.1329 \text{, when } \frac{b_2}{b_1} \le 0.2264$$

$$k_w = (b_1 / b_2)^2 k_f$$

3.1.3.2 Plate buckling coefficients obtained from CUFSM for Reck Type

Figure 3.11 shows the buckling shape of the plain channel and its corresponding half-wavelength and load factor. A parameter study also has been carried out and the results are shown in Fig. 3.12. The stress gradient is displayed in Figure 3.13.

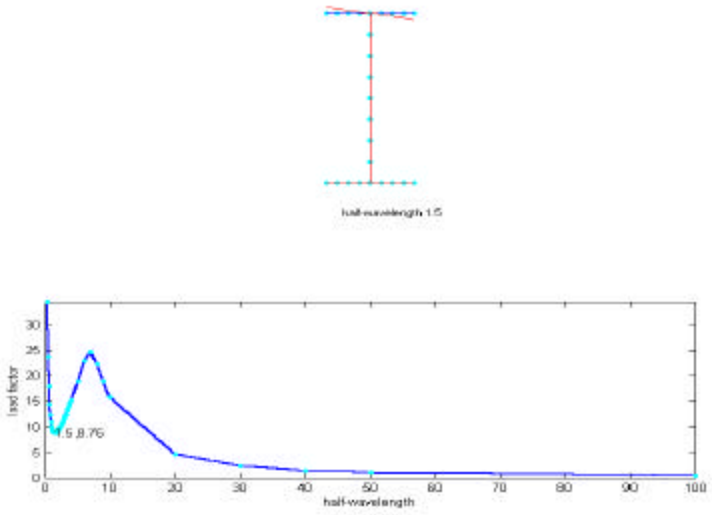

Figure 3.11 Results from CUFSM for Reck Type Channels

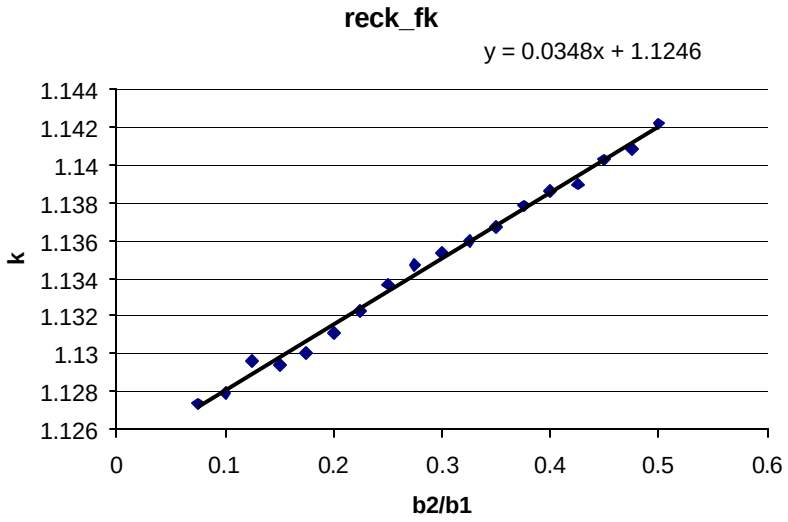

Figure 3.12 k versus b_2 / b_1 for Reck Type Channels

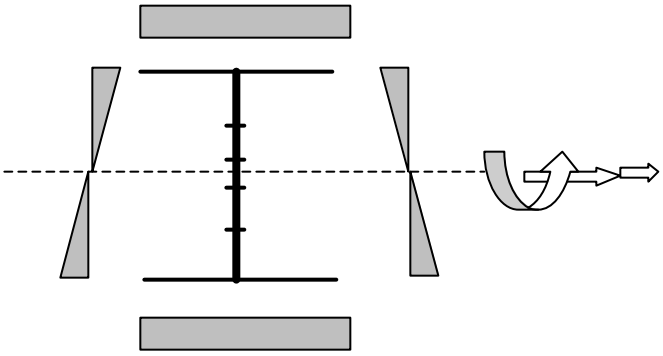

Figure 3.13 Stress Gradient for Major Axis Bending--Reck Type

$$k_f = 0.0348(\frac{b_2}{b_1}) + 1.1246$$

$$k_w = (b_1 / b_2)^2 k_f$$

3.2 Columns

A parameter study has been carried out on plain channel sections of pure compression with b_2 / b_1 changing from 0 to 5. The cross section is

illustrated in Figure 3.1. The results are shown in Figure 3.14. The stress gradient is displayed in Figure 3.17.

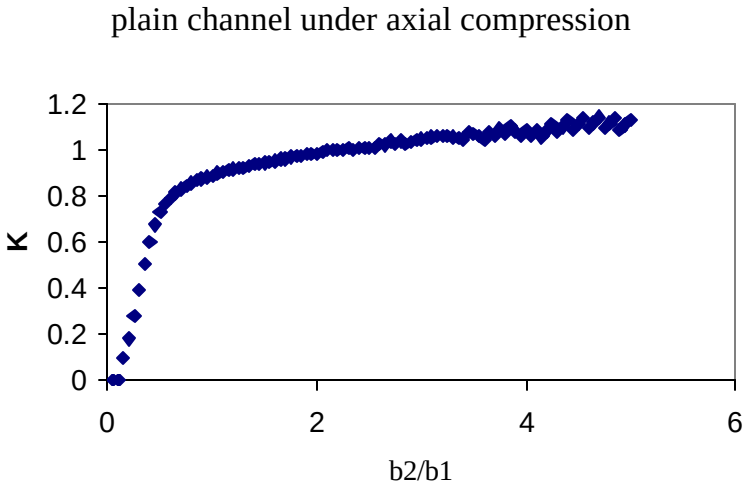

Figure 3.14 k versus b_2 / b_1 for Columns

The web as shown in Fig. 3.15a dominates local buckling of a plain channel with narrow flanges. As the flange width increases, flanges may determine local buckling, as would be the case for the channel shown in Fig. 3.15b. Two-line approximation can be formulated to determine k in Figure 3.16.

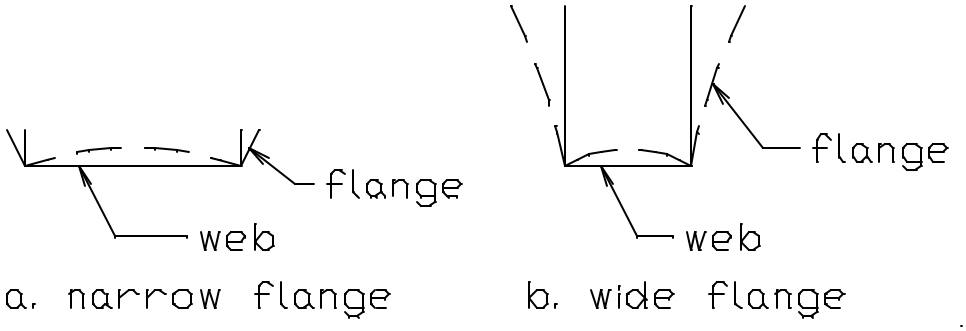

Fig. 3.15 Concentrically loaded channels

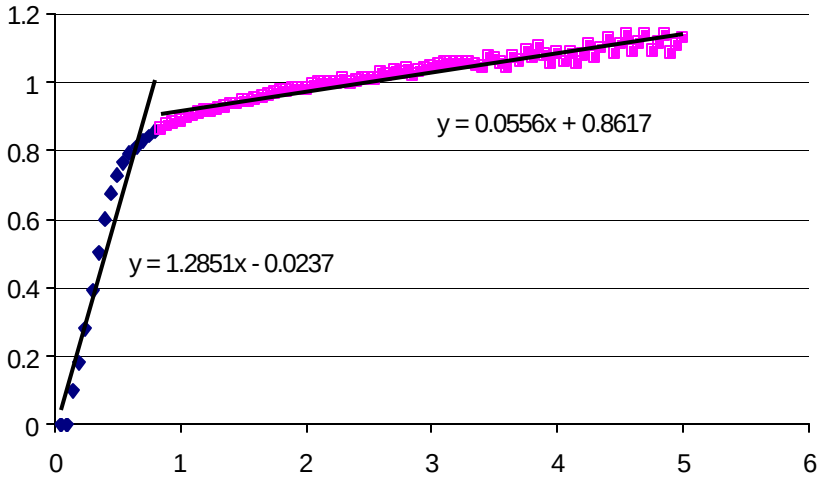

Figure 3.16 formula of k versus b_2 / b_1 for Columns

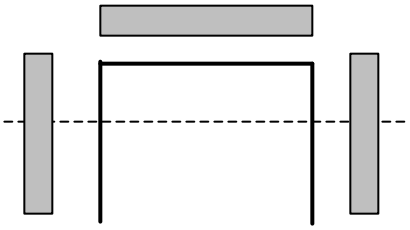

Figure 3.17 Stress Gradient for Columns

$$k_f = 1.2851(\frac{b_2}{b_1}) - 0.0237 \text{, when } \frac{b_2}{b_1} \le 0.7201$$

$$k_f = 0.0556(\frac{b_2}{b_1}) + 0.8617 \text{, when } \frac{b_2}{b_1} > 0.7201$$

4. ULTIMATE STRENGTH: FINITE ELEMENT STUDIES

4.1 Minor Axis Beam Bending with Stiffened Element in Tension

El Mahi and Rhodes' experimental work at University of Strathclyde is studied in 4.1.1 and evaluated by Finite Element Program ABAQUS in Part 4.1.2. Based on the studies in 4.1.1 and 4.1.2, design formulations are proposed in Part 5.1.1. Further parameter studies using abaqus are carried out in 4.1.3.

4.1.1 Studies on Failure Behavior of Laterally Braced Beam

The results from El Mahi and Rhodes' experimental investigation are studied. It is found that different controlling parameters such as flange over web ratio b_2/b_1, flange slenderness b_2/t, beam span L, and inclined angle affect failure loads.

1) Flange Width to Web Depth Ratio b_2/b_1

Test results are grouped by thickness in Figure 4.1.1 for different flange width to web depth ratios. It is clear that the failure load is affected by the ratio b_2/b_1. Higher flange over web ratio results in higher values of failure moment.

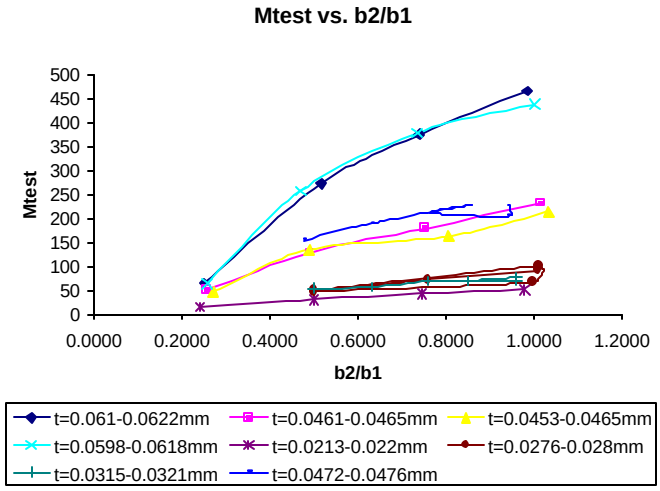

Figure 4.1.1 Effect of Flange over Web Ratio b_2/b_1

2) Flange Slenderness b_2/t

Test results are organized by thickness in Figure 4.1.2 for different flange slenderness. Specimens having lower values of b_2/t ratio fail by yielding instead of buckling elastically. It is also found out that thicker specimens sustain higher loads before failure.

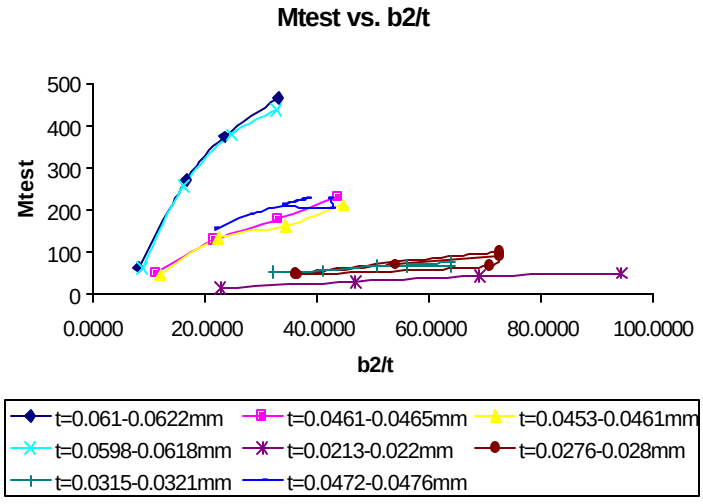

Figure 4.1.2 Effect of Flange Slenderness b_2 / t

3) Beam span L

The failure moment of longer beams is slightly lower than that of shorter beams.

4) Inclined angle

For angled-plain channel specimens, the experimental results showed that the failure moment decreases as theta (shown in Figure 4.1.3) increases. When theta is between 0 and 45 degree, there is slight reduction in the bending moment, whereas when theta is greater than 45, there is notable reduction in the bending moment, as shown in Figure 4.1.4.

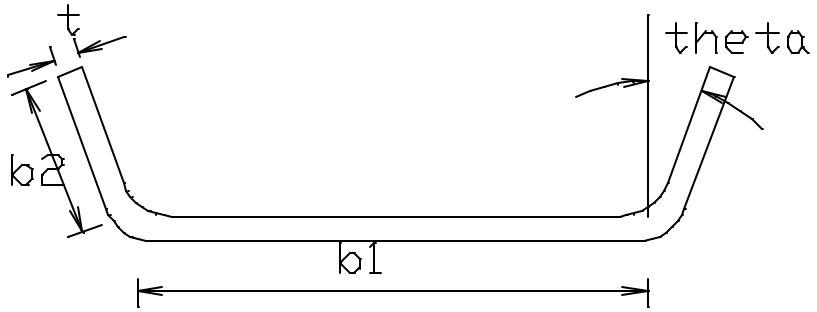

Figure 4.1.3 El Mahi and Rhode's Cross Section

Based on the above study, the strength reduction factor R_f is suggested as follows.

When theta is between 0 and 30 degree, R_f=1.1

When theta is between 30 and 45 degree, $R_F = 1.1 + \frac{1.8 - 1.1}{15}(q - 30)$

When theta is greater than 45 degree, R_f=1.8

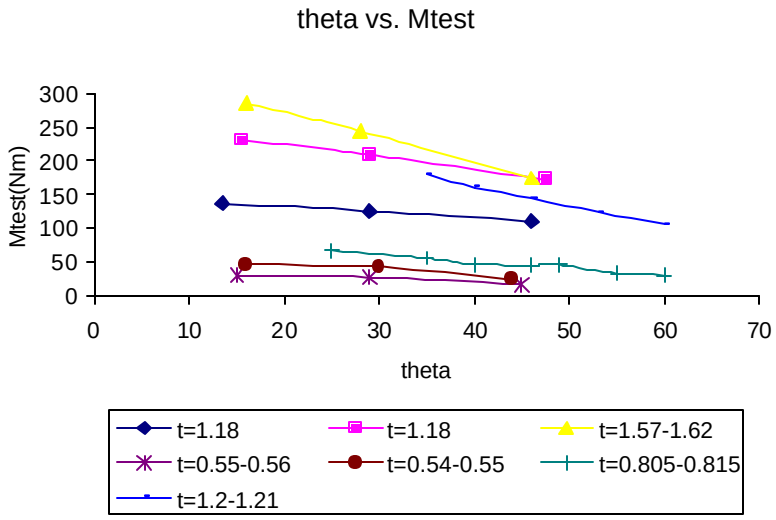

Figure 4.1.4 Effect of Inclined Angle

4.1.2 Verification Studies Using Abaqus

El Mahi and Rhodes' experimental results were used to verify the finite element results.

4.1.2.1 Finite Element Model

--Simply supported beams with cantilevered ends shown in Figure 4.1.5 was modeled

--Element Type: shell element S9R5

--Aspect ratio: 1.02~1.21

--Symmetry was used; half of the beam was modeled

--Imperfection magnitude was 0.1t (t is the plate thickness).

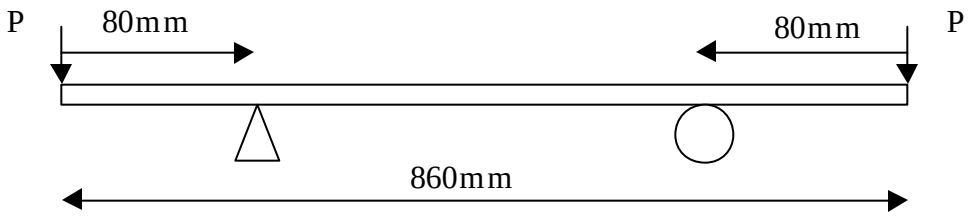

Figure 4.1.5 El Mahi and Rhodes' Experimental Setup

4.1.2.2 Abaqus Results

Midspan Moment -Displacement Diagrams of all specimens of El Mahi and Rhodes experiments were studied and only Spec16, Spec18, Spec22 and Spec32 were presented in Figures 4.1.6, 4.1.7, 4.1.8, and 4.1.9, respectively.

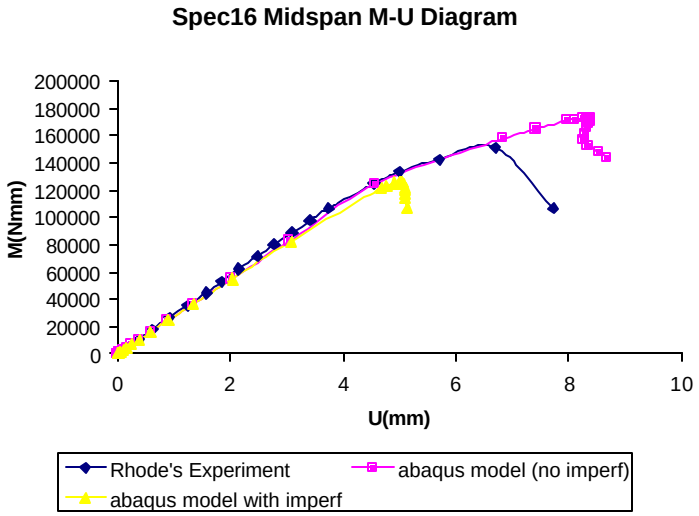

Figure 4.1.6 Midspan Moment -Displacement Diagram of Spec16

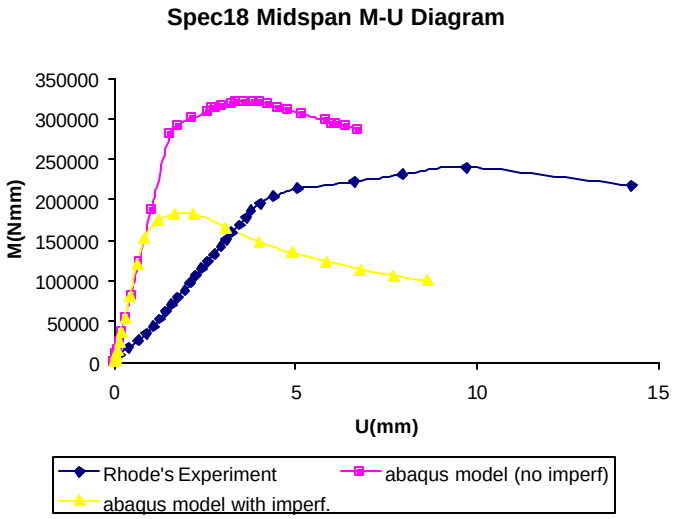

Figure 4.1.7 Midspan Moment -Displacement Diagram of Spec18

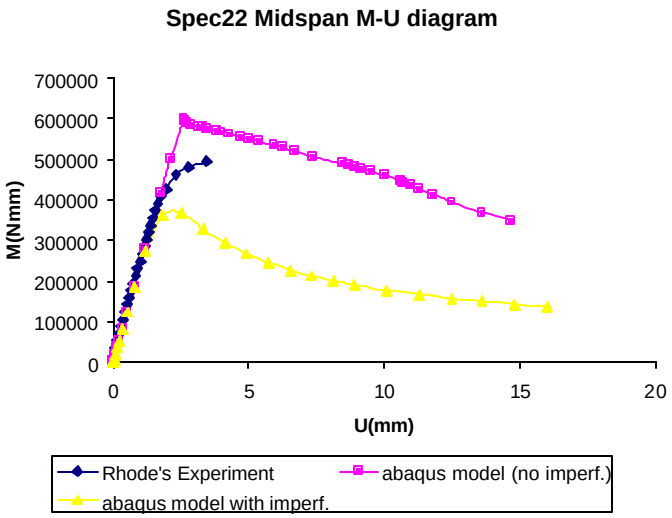

Figure 4.1.8 Midspan Moment -Displacement Diagram of Spec22

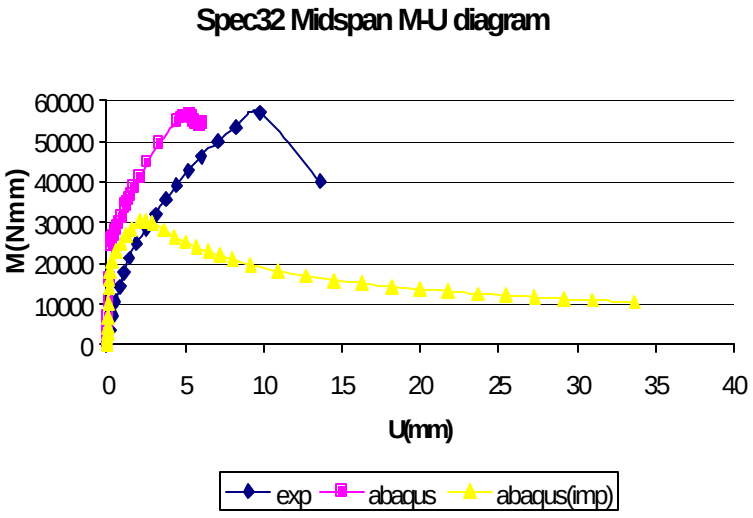

Figure 4.1.9 Midspan Moment -Displacement Diagram of Spec32

4.1.2.3 Observations and Conclusions

1) Generally speaking, most of El Mahi and Rhodes' experimental data are reliable. Within the elastic range, the Abaqus midspan moment-displacement

diagram (hereinafter called M-U diagram) has a good agreement with the experimental data.

2) Abaqus results with and without imperfections are also presented in M-U diagrams. It is important to note that with the introduction of imperfection, the ultimate load is reduced significantly. Imperfection sensitivity is studied in Appendix B.

3) Residual stresses are not included in Abaqus models of 4.1.2 and will be investigated in 4.1.3.

4) In Spec18 and Spec32, tensile strain is observed in Abaqus at free edges before the ultimate load is reached, which is in agreement with El Mahi's experimental finding. However, the deflections in M-U diagram obtained from Abaqus results are found twice difference from experimental results within the elastic range. After communicating with Dr. Rhodes and investigating his test readings, it is found that experimental recording of deflection might not be correct. The ultimate load in experiments falls between Abaqus results with and without considering imperfection.

Based on the above study, an effective width approach in the post buckling range and the use of post yield strain reserve capacity expressed in terms of a ratio, C_y, the post-yield to yield strains, are proposed in Part 5.1.1.

4.1.3 Parameter Studies

As the proposed design formulations were based on only one set of experimental data from one research institute that was available when the research was undertaking. Parameter studies using Abaqus are carried out. Geometric imperfections and residual stresses are two of parameters for finite element studies. Geometric imperfection studies are shown in Appendix B.

4.1.3.1 Residual Stress

Residual stresses may develop during the manufacturing process as a result of non-uniform plastic deformations. They vary an enormous amount for all sections. Ben Schafer (1997) investigated in depth the magnitude and distribution of residual stress in cold-formed steel sections. Based on this work, a longitudinal through thickness flexural residual stress for plain channel roll-formed sections shown in Figure 4.1.10 is introduced in parameter studies. Flexural residual stresses are in tension outside and equal but in compression inside in Figure 4.1.10.

Flexural residual stresses are self-equilibrating through the thickness and thus have a small net effect. However, the early yielding on the face of the plates due to the residual stresses may have influence on the stress distribution and the way the load is carried in the plate.

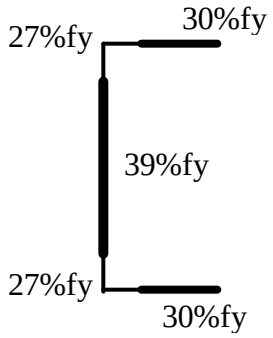

Figure 4.1.10 Distribution and Magnitude of Flexural Residual Stresses

Abaqus results with and without considering residual stresses are shown in Figure 4.1.11. The results indicate that residual stresses' influence on the ultimate load is small.

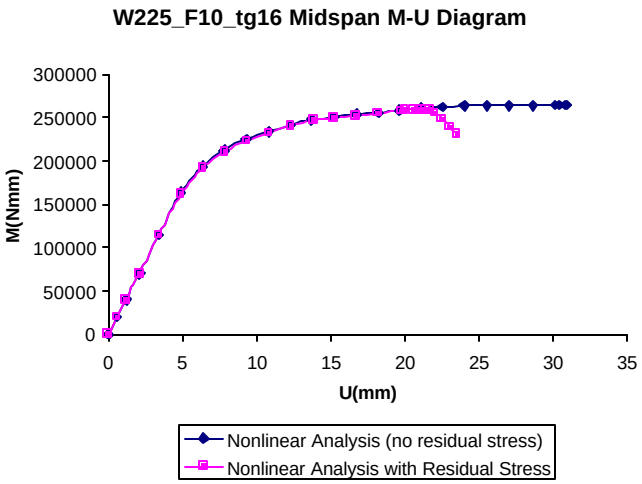

Figure 4.1.11 Effect of Residual Stress on Ultimate Load

4.1.3.2 Models for Parameter Studies

Two models are developed and compared with the experimental data. One is a simply supported beam with end plates shown in Figure 4.1.12. The other is a simply supported beam with beam elements at two ends shown in Figure 4.1.13. Spec21 in El Mahi and Rhodes' test is shown for comparison study. The results of these two models along with the experimental data and the results from the model in Verification Study are presented in Figure 4.1.14.

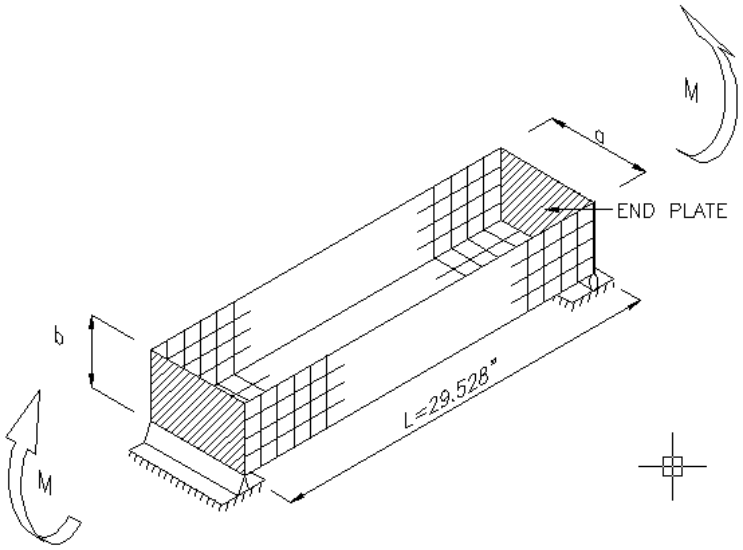

Figure 4.1.12 A Simply Supported Beam with End Plates

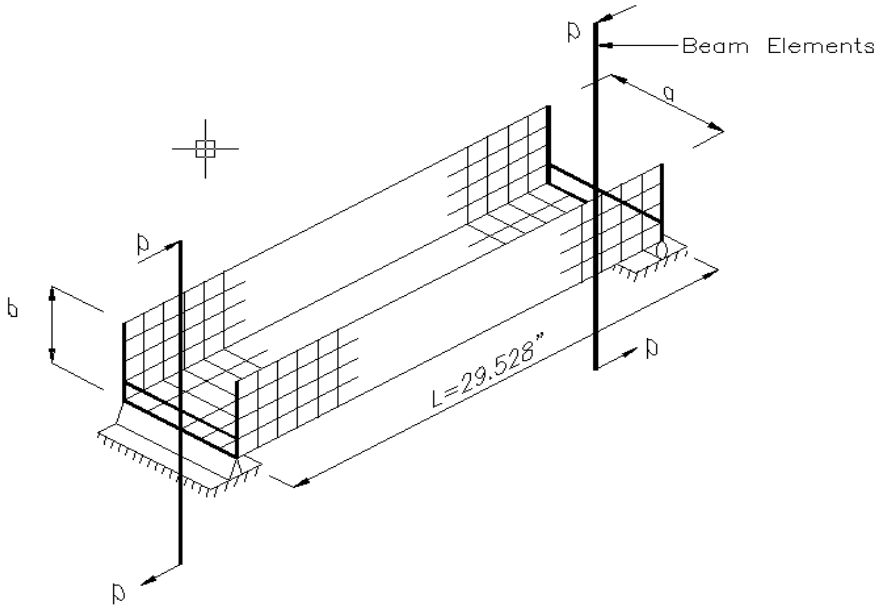

Figure 4.1.13 A Simply Supported Beam

with Beam Elements at Two Ends

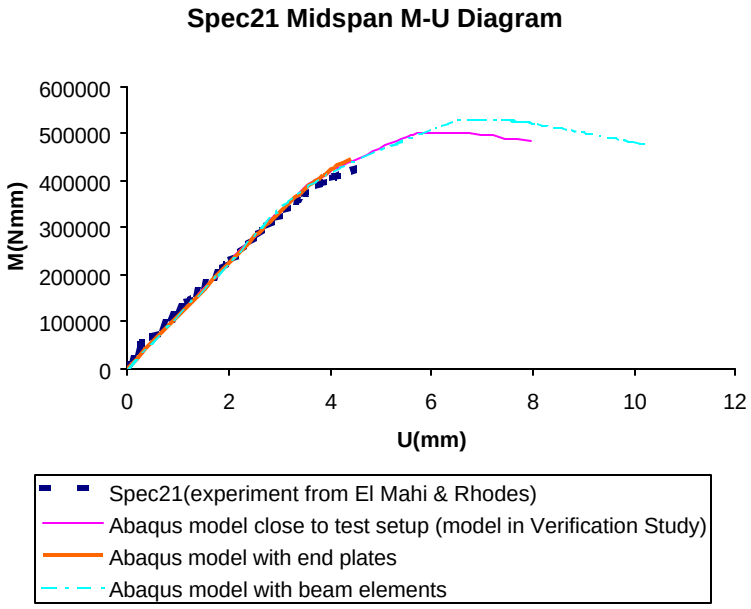

Figure 4.1.14 Comparison of Results from Different Abaqus Model s

Observations and Conclusions:

1) The results from three Abaqus models are compared with the experimental data. Within elastic range, all of these three models have good agreement with experimental data. Abaqus model with end plates can not trace the dropping portion of M-U diagram, while the other two Abaqus models can follow the inelastic range very well.

2) Results from the model with beam elements at two ends matched well with experimental data in elastic range and can follow the descending branch. Hence it is selected for parametric study.

3) Imperfection is not included in Figure 4.1.14 comparison study.

4.1.3.3 Parameter Studies

The objective of this parameter study is three folded:

1) quantify the effects of imperfection and residual stress on the ultimate load of plain channel sections;
2) validate the proposed empirical design formulations in Part 5.1.1;
3) study laterally braced beams of varied flange slendernesses and different dimensions that industries have interest in.

Therefore, the members for parameter studies are selected to be typical sections of industrial practical applications.

4.1.3.3.1 Model Parameters

Model parameters include flange slenderness b_2/t, flange over web ratio b_2/b_1, plate thickness t, imperfections, and residual stresses.

4.1.3.3.2 Model Beam Length

Since the ultimate load of plain channels is influenced by the length of the section, a study on the beam length is conducted.

The geometry of the cross section is taken the same as that of Spec21. in El Mahi and Rhodes' experiment. Only beam length varies from 300mm, 500mm, 700mm to 1000mm. The beam length effects are obvious from Figure 4.1.15. The longer the beam length, the lower the ultimate strength is. A beam length of 750mm is selected in my parameter study. The length is chosen to ensure that the beam would not be subject to lateral buckling.

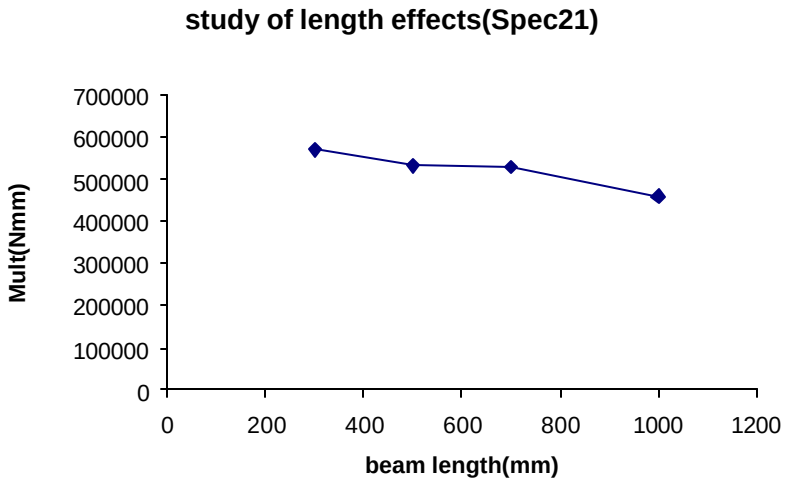

Figure 4.1.15 Study of Beam Length Effect

4.1.3.3.3 Mesh Discretization

A complete study of mesh discretization is computational expensive. A nonlinear analysis is conducted and the result is compared with the experimental data. It is assumed that good agreement with experimental data implies an adequate mesh for nonlinear analysis. The result is presented in Figure 4.1.16.

4.1.3.3.4 Residual Stress

Residual stresses are included in parameter study. The residual stress distribution and magnitude is shown in Figure 4.1.10.

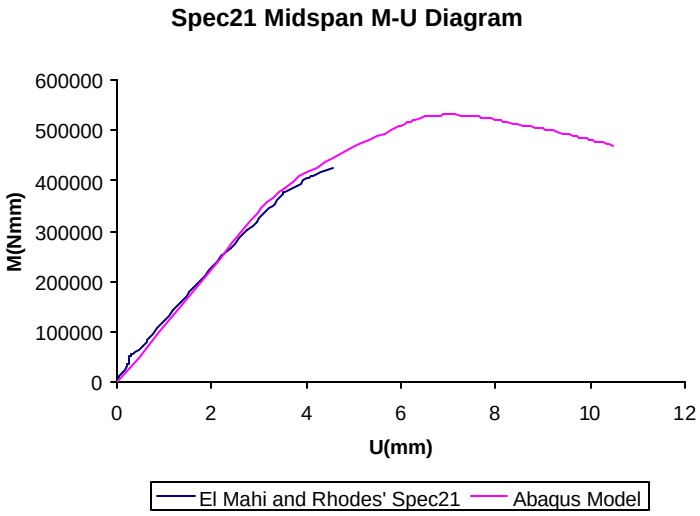

Figure 4.1.16 Study on Mesh Size

4.1.3.3.5 Geometric Imperfections

Two types of imperfections are found in existing measuring data: type I imperfection refers to the maximum local imperfection in a stiffened element; while type II imperfection refers to the maximum deviation from straightness for an unstiffened flange. It is found that type I and type II imperfections do not have strong linear relationship and that type I imperfection is less important. Further study shows that type II imperfection is function of flange slenderness. The magnitude of the normalized type II imperfection (d_2/t) corresponding to cdf25 (cumulative distribution function is at 25% level, or imperfection magnitude of 75% probability of exceedance), cdf50 and cdf75 can be calculated as follows.

cdf25: $[0.039(bf/t) - 0.1638]+(-0.8617)[0.0174(bf/t) - 0.2063]$

cdf50: $[0.039(bf/t) - 0.1638]+(0.0643)[0.0174(bf/t) - 0.2063]$

cdf75: $[0.039(bf/t) - 0.1638]+(0.7698)[0.0174(bf/t) - 0.2063]$

where, d_2 is the maximum magnitude of Type II imperfection; t is the plate thickness; bf is the flange width. Details of the imperfection studies can be found in Appendix B.

The lowest eigenmode is selected for the imperfection distribution. Two maximum type II imperfection magnitudes, one at the 25% CDF level (cumulative distribution function is at 25% level, or imperfection magnitude of 75% probability of exceedance) and the other at the 75% CDF level are used to evaluate ultimate strength.

4.1.3.3.6 Model Cross-Sections

A survey of cross sections commonly used by the industry indicated the following dimension:

(a: width of flanges; b: width of web; t: plate thickness; Fy: yield strength)

I. a is 2.25", 3.25", 3.75",
   b is 1",1.5", 2", 2.5"
   t is 0.064", 0.067", 0.083", 0.1"
   Fy: 1) 36ksi; 2) rolled

II. only has two standard braked shapes
   a=8.75", b=3.25", t=0.088" Fy=55ksi
   a=10.25", b=3.1875", t=0.092", Fy=55ksi

III. a=2.25"-3.30", t=0.060"-0.064", 0.081"
   b/t=16-26, Fy=51-59ksi

Based on the above data, web width of 2.25", 3.25", 3.75" are chosen for parameter studies. In parametric studies, thickness varies from 0.064", 0.067" to 0.083"; flange slenderness changes from 10 to 54.7. The flange over web

ratio is chosen to be less than 1 such that the cross sections are practical sections in industry. F_y equal to 36ksi($248N/mm^2$) and 55ksi($379N/mm^2$) respectively are selected for study.

4.1.3.3.7 Stress Strain Curve

Fy=$248N/mm^2$, E= 205000Mpa; and Fy=$379N/mm^2$, E= 205000Mpa are chosen for this parameter study. Stress strain curve is presented in Figure 4.1.17.

4.1.3.3.8 Parameter Study Results and Discussion

Imperfection sensitivity is shown in Figure 4.1.18. Ultimate load obtained from Abaqus is compared with that from my proposed method and M_{abaqus}/M_{ns} is plotted against l in Figure 4.1.19, where l refers to flange slenderness, which is $\sqrt{\frac{f_y}{f_{cr}}}$.

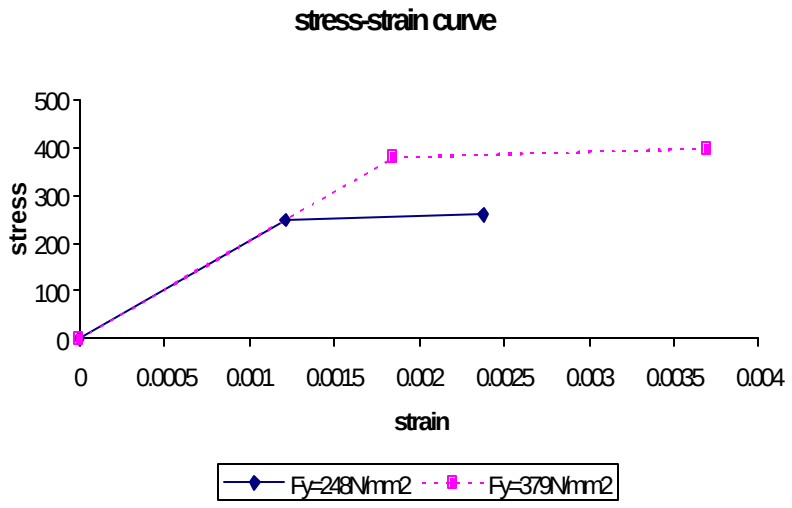

Figure 4.1.17 Stress Strain Curve

4.1.3.3.9 Summaries and Conclusions:

1) It is obvious in Figure 4.1.18 that the ultimate load corresponding to cdf25 is not much different from that corresponds to cdf75. Thus it can be concluded that plain channel sections are not imperfection sensitive cross sections.

2) Based on the observation of Figure 4.1.19, it is concluded that the amount of imperfection magnitude in proposed design formulations in Part 5.1.1 is accurately considered.

3) From Figure 4.1.19, it is seen that results from the proposed design formulations have good agreement with Abaqus results.

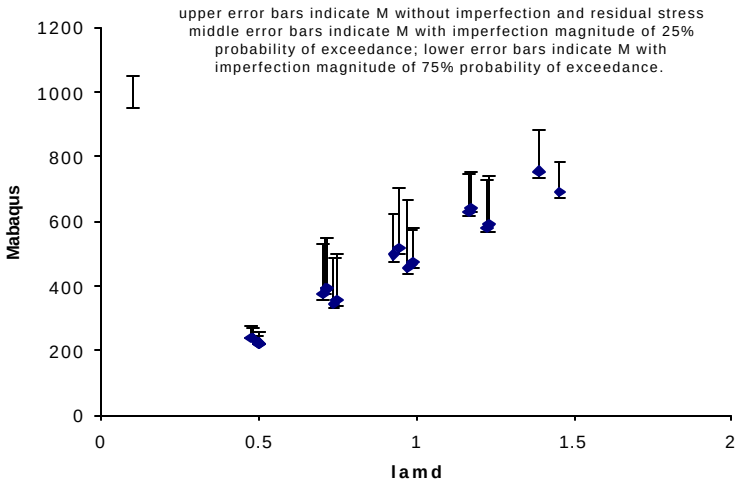

Figure 4.1.18 Imperfection Sensitivity Study

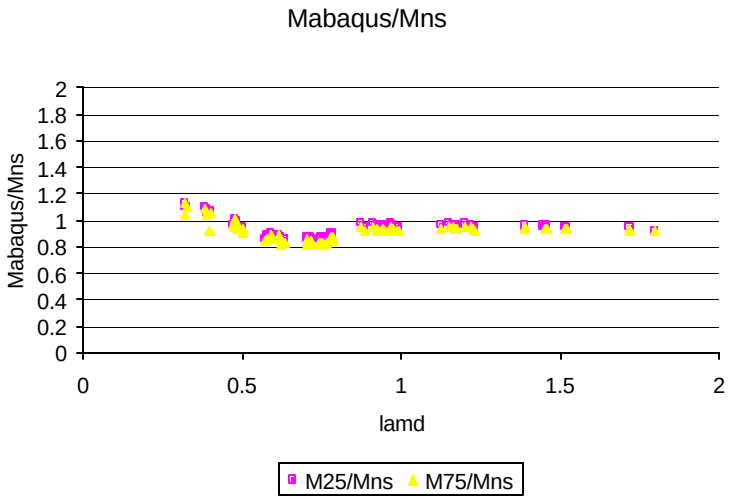

Figure 4.1.19 M_{abaqus} / M_{ns} vs. $\sqrt{\frac{f_y}{f_{cr}}}$

4.2 Flat-ended and Pin-ended Columns

Ben Young's experimental work at University of Sydney is evaluated by Finite Element Program ABAQUS in Part 4.2.1 and reasons for unsatisfactory results of pin-ended columns are investigated; hence possible reasons for discrepancies are listed in Part 4.2.3. Based on these studies, design recommendations are therefore presented in Part 5.2.

4.2.1 Verification Studies using Abaqus

Verification studies to evaluate Ben Young's test results are important, because their experimental investigation (especially for pin-ended column test) is used as the basis for the design recommendations. Finite element study using Abaqus is carried out to verify the experimental work.

4.2.1.1 Finite Element Model of Ben Young's Experiements

--Fix-ended conditions are to restrain both minor and major axis rotations as well as twisting rotations and warping;
--Pin-ended conditions are to allow rotation about minor axis, while restraining major axis rotations as well as twisting rotations and warping;
--Two thick end plates are introduced to restrain warping.
--Element Type: shell element S9R5
--Aspect ratio: 1.02~1.21
--Imperfection distribution: the lowest eigenmode is selected
--Imperfection magnitude: maximum type II imperfection magnitudes at the cdf50 (imperfection magnitude of 50% probability of exceedance) are used to evaluate ultimate strength based on the imperfection model discussed in Appendix B
--Residual Stress: residual stress and distribution and magnitude in Figure 4.1.10 are introduced.

4.2.1.2 Abaqus Study Results and Conclusions

Specimen P36F0280, P36F3000, P36P0280, P36P1315 in Series P36 and P48F0300, P48F3500, P48P0300, P48P1565 in Series P48 of Ben Young's experiments are selected for Verification Study. The Abaqus results are listed in Table 4.1. It can be found in Table 4.1 that Abaqus results have good agreement with Ben Young's test results.

Table 4.1 Abaqus Results for Ben Young's Experiments

Specimen	Pt N	cdf50 Pabaqus N	Pabaqus / Pt
P36F0280	65000	70000	1.077
P36F3000	24700	25795	1.044
P36P0280	55200	60250	1.091
P36P1315	27000	27225	1.008
P48F0300	66000	77550	1.175
P48F3500	29500	27456	0.931
P48P0300	45200	58938	1.304
P48P1565	31200	29832	0.956

Middle P denotes pin_ended conditions

Middle F denotes fix-ended conditions

4.2.2 Studies on Fix-ended Columns

Ben Young's experiments showed that shifting of the neutral axis after local buckling did not induce overall bending for the fixed-ended columns. (Figures 4.2.1 and 4.2.2)

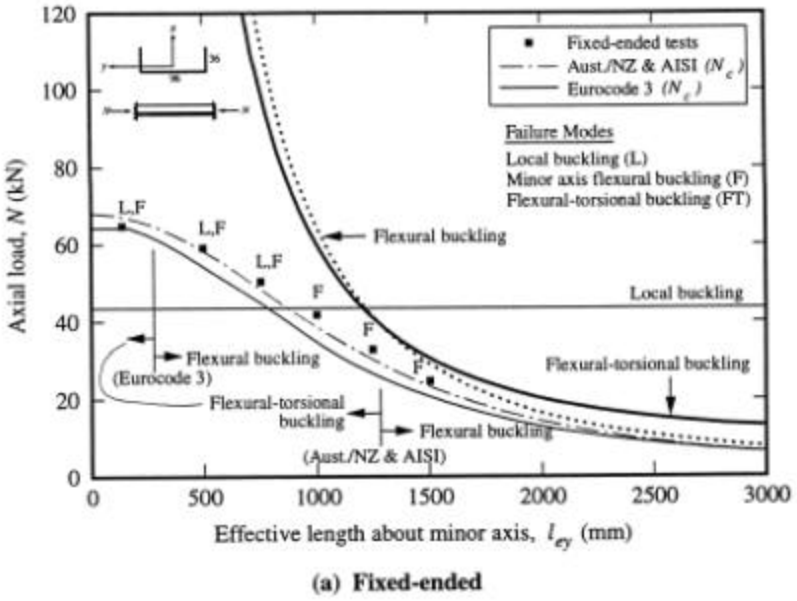

(a) Fixed-ended

Figure 4.2.1 Comparison of test strengths with design strengths for Series P36 (Taken from Ben Young's dissertation(1997))

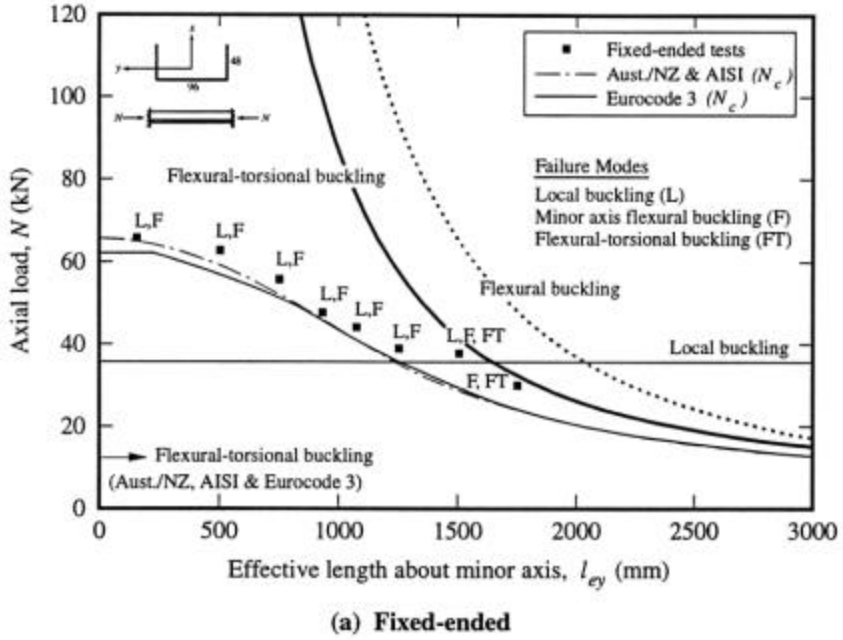

(a) Fixed-ended

Figure 4.2.2 Comparison of test strengths with design strengths for Series P48 (Taken from Ben Young's dissertation(1997))

4.2.3 Studies on Pin-ended Columns

For the pin-ended columns, shifting of the neutral axis after the local buckling is considered in Ben Young's work (1998), and therefore members have combined compressive axial load and bending. Ben Young's experimental studies have deepened the understanding of the pin-ended column behavior. However, his work using beam-column equations (the dark dash line -- Aust / NZ & AISI k=0.43) did not show satisfactory results for Series P48 in Figure 4.2.3.

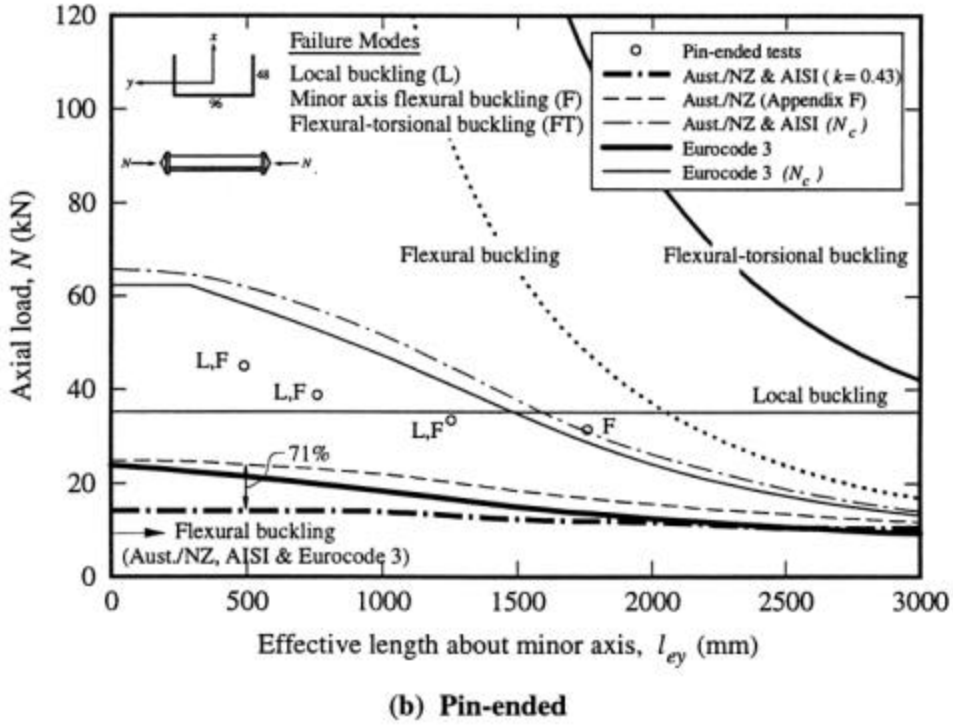

(b) Pin-ended

Figure 4.2.3 Comparison of test strengths with design strengths for Series P48 (Taken from Ben Young's Dissertation (1997))

Possible reasons for unsatisfactory results by using beam-column equations for pin-ended columns are discussed as follows:

1) For bending part, when calculating the effective width of the flanges, there is no provision for unstiffened elements under stress gradient. In Ben Young's study, the flanges were conservatively assumed to be in uniform compression. This assumption contributes to the poor prediction of Pult by AISI Specification.

2) Using beam-column equations for pin-ended columns, the same amount of eccentricity is taken along the entire length of the column for the entire load history. But actually when load is applied, the eccentricity varies along the

entire length of the column. These contribute to the discrepancies between test results and results from AISI Specifications.

Based on the observation of the lateral deflection graphs for the load history of these specimens, it is found that the global deflection shape is sine wave for pin-ended columns and that the average eccentricity is less than two thirds of the maximum magnitude of the lateral deflection. Thus the beam-column equation is improved for pin-ended columns by using 2/3 of the maximum of eccentricity instead of the maximum of eccentricity. The comparison results for Series P36 and Series P48 specimens in Ben Young's experiments are shown in Tables 4.2 and 4.3, respectively.

Table 4.2 Comparison results for Series P36

Specimen	Ptest	Pns	Pns/Ptest	Pns	Pns/Ptest
		(beam-column)-e		(beam-column)-2/3e	
P36P0280-	55.2	41.906	0.759	47.228	0.856
P36P0315-	52.1	40.329	0.774	45.471	0.873
P36P0815-	40.9	32.923	0.805	36.116	0.883
P36P1315-	27	22.64	0.839	23.722	0.879
		mean	0.794	mean	0.872
		Stedv	0.035	stedv.	0.012

Table 4.3 Comparison results for Series P48

Specimen	Ptest	Pns(BC)	Pns/Ptest	Pns	Pns/Ptest
		(beam-column)-e		(beam-column)-2/3e	
P48P0300+	45.2	35.938	0.795	41.666	0.922
P48P0565-	38.6	35.443	0.918	40.836	1.058
P48P1065	33.9	30.826	0.909	34.804	1.027
P48P1565-	31.2	24.713	0.792	26.912	0.863
		Mean	0.854	mean	0.967
		Stedv	0.069	Stedv.	0.091

5. ULTIMATE STRENGTH: PROPOSED PROCEDURES

The design procedures developed are applicable to cross-sections in the range of practical sections used in the industry, namely $b_2 / b_1 \leq 1$. The design procedures developed are consistent with AISI Specification for calculating the overall capacity of plain channels.

The formulations developed involve the use of effective widths for the component plate elements that are in the post-buckling. Using these effective widths effective section properties and hence the ultimate load carrying capacities are determined. The approach is thus in agreement with the frame work of the unified approach of Pekoz (1987) used in the AISI Specification (1996).

For members that exhibit inelastic reserve capacity, post yield strain reserve capacity expressed in terms of a ratio, C_y that is the ratio ultimate strain divided by the yield strain. The ultimate moment of a flexural member is determined by statics based on the ultimate strain capacity as is done in the AISI Specification (1996). The details of the equations developed are given below.

5.1 Beams

5.1.1 Minor Axis Bending with Stiffened Element in Tension

Effective Width Model for Flanges

$l = 1.052(b_2 / t)\sqrt{f_y / Ek_f}$ or $l = \sqrt{f_y / f_{cr}}$

$k_f = 0.1451(b_2 / b_1) + 1.2555$

if $l > 0.859$

$$r = 0.925\left(f_{cr} / f_y \right)^{1/3.9}$$

if $l \le 0.859$

$r = 1$

$b_e = r b_2$

$M_{ns} = f_y S_e$

Post-yield Strain Reserve Capacity Model

$C_y = 3.0$ for $l \le 0.535$

$C_y = 0.5877 / (l - 0.0924)^2$ for $0.535 < l < 0.859$

$C_y = 1$ for $l \ge 0.859$

The nominal moment capacity is determined as described in AISI Specification (1996) Section C3.1.1 b.

5.1.2 Minor Axis Bending with Stiffened Element in Compression

Effective Width Model

For stiffened elements in uniform compression:

The effective width, b, is to be determined using AISI Specification Section B2.1 $f = F_y$, $k = k_w$. The value of k_w is to be determined by the equations given in Part 3.

For unstiffened elements under a stress gradient:

For the post-buckling behavior of unstiffened elements a consistent effective width shown in Figure 5.1 as suggested by Schafer (1997) is used.

When $y = \frac{f_2}{f_1}$,

$b_{1o} = bw / (1 - y)$

$b_{2o} = (b / (1 - y))\sqrt{w^2 - 2w + r}$

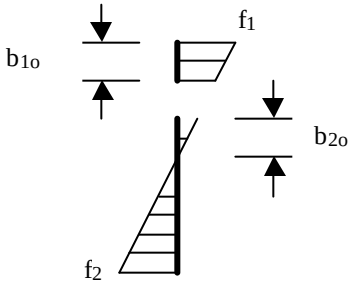

where

$0 \le r < 0.77 \quad w = 0.30 r$

$0.77 \le r < 0.95 \quad w = 0.23$

$0.95 \le r \le 1.00 \quad w = -4.6 r + 4.6$

in which,

$r = 1$ when $l \le 0.673$

$r = (1 - 0.22/\lambda)/\lambda$ when $\lambda > 0.673$

$\lambda = \sqrt{f_1/f_{cr}}$

$M_{ns} = F_y S_e$

Figure 5.1 Consistent Effective Width

When unstiffened elements does not undergo local buckling, the nominal moment capacity is determined based on initiation of yielding or its ultimate moment. The ultimate is determined based on the ultimate (post-yield) strain capacity.

Post-yield Strain Reserve Capacity Model

$C_y = 3$ for $\lambda \leq 0.46$

$C_y = 3 - 2*(\lambda - 0.46)/(0.673 - 0.46)$ for $0.46 < \lambda < 0.673$

$C_y = 1$ for $\lambda \geq 0.673$

The nominal moment capacity is determined as described in AISI Specification (1996) Section C3.1.1 b.

5.1.3 Major Axis Bending

Effective Width Model

Reduction factor for distortional buckling stress, suggested by Schafer (1997), is obtained as follows.

$R_d = 1$ when $\lambda \leq 0.673$

$R_d = \frac{1.17}{\lambda + 1} + 0.3$ when $\lambda > 0.673$

where, $\lambda = \sqrt{f_y / f_{cr}}$

$f_{cr} = \min[f_{cr}, R_d f_{cr}]$

For unstiffened element in uniform compression, the effective widths are determined as described in AISI Specification Section B3.2 with $f = F_y$, and using the plate buckling coefficient as given in Part 3, namely k= k_f

For stiffened element under a stress gradient, the consistent effective width described above is used $M_{ns} = F_y S_e$.

Post-yield Strain Reserve Capacity Model

Post-yield Strain Reserve Capacity Model needs further study when more experimental data are available.

5.2 Flat-ended and Pin-ended Columns

Flat-ended columns: assuming loading through the effective centroid, column equation is to be used to design flat-ended columns.

Pin-ended columns: assuming loading through the effective centroid, beam-column equation is to be used to design pin-ended columns. Two thirds of the maximum eccentricity is selected for the beam-column equation because the eccentricity varies along the length of the column.

5.3 Beam-Columns

Strength of plain channel beam columns can be determined by the interaction equations (AISI Specification Section C5.2.2) with the improved plate buckling coefficient k described in Part 3.

The parameters for the column part of the beam-column equations, flat-ended columns are to be treated as concentrically loaded columns; while pin-ended columns are treated as beam-columns. The eccentricity of the load should be determined on the basis of the location of the load and the average deflections of the beam column instead of the maximum deflections. The parameters for the beam part of the beam-column equations, the formulations developed above are to be used.

6. ULTIMATE STRENGTH: EXPERIMENTAL INVESTIGATION

6.1 Experiments of Minor Axis Beam Bending with Stiffened Elements in Tension

Tests were performed on two plain channel beams, the dimensions of which are common in industry. The purpose of the test is firstly, to study the behavior of plain channel cross sections of minor axis beam bending with stiffened elements in tension, and secondly, to evaluate the proposed design procedure. Geometric imperfections were measured before testing. Details of the imperfection measurement are discussed in Appendix A.

6.1.1 Test Specimens

Two plain channel beams with end plates were tested. The measured cross-section dimensions, as well as material properties, were listed in Table 6.1, where t is thickness; L is the beam span of the pure bending part shown in Figures 6.1 and 6.2. Thickness was measured with a metric micrometer, and web and flange width were measured with a vernier calliper. All these measurements were taken as the average value of three readings at different locations.

Table 6.1 Cross-section Dimensions and Material Properties

	b1(in)	b2(in)	t(in)	L(in)	Fy(kips)
Specimen1	2.237	1.0265	0.0648	35.25	58.4
Specimen2	2.3055	1.567	0.0758	59.25	58.4

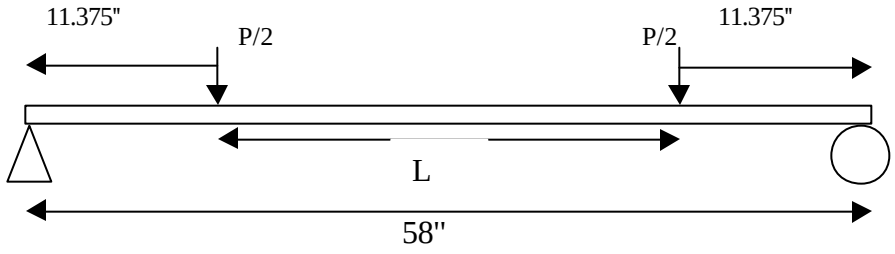

Figure 6.1 Dimensions of Beam Specimen1

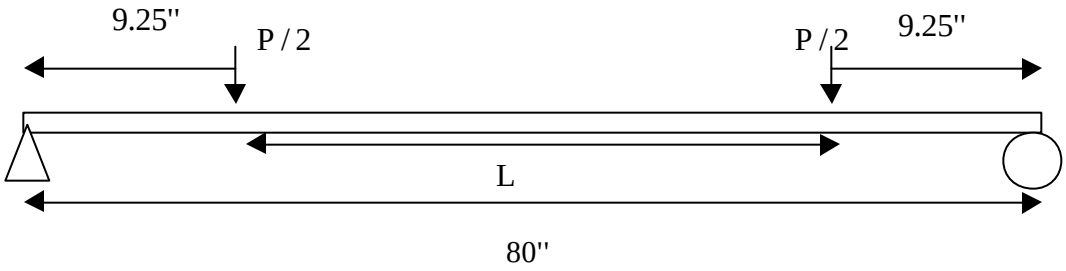

Figure 6.2 Dimensions of Beam Specimen2

6.1.2 Test Setup

Beams were tested on the flat table of the test machine. The test machine was a Baldwin 400kip open loop load frame. The magnitude and speed of loading were controlled by adjusting the loading and unloading valves of the control panel. Load was measured with a pressure sensor working in parallel with the test machine force measuring system. Displacement was measured with DC-DC Linear Variable Differential Transformers mounted between the table of the test machine and appropriate points on the bottom of the deflecting beam. Measurements were made with an HP3497 data acquisition system controlled by an IBM PC clone computer.

During the test, a load vs. displacement curve was plotted on the computer screen and individual measurement values were printed on the computer screen. All data was stored on the computer disk drive for later analysis.

Two very stiff arms of C cross-section were firmly attached to the two end plates of each beam in order to ensure the application of pure moment in plain channel beam. Load was applied through a load spreading beam onto plates outside of the pure bending range. The test setup is sketched in Figure 6.3.

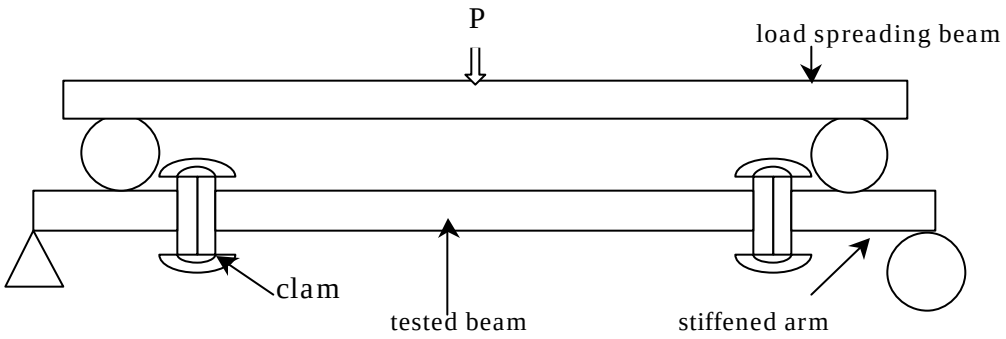

Figure 6.3 Beam Test Setup

6.1.3 Beam Test Results

Load vs. Displacement Curves for specimen1 and specimen 2 are plotted in Figures 6.4 and 6.5. The displacement refers to the difference between mid-span deformation and end plates deformation. The evaluation of the proposed design procedure is presented in Table 6.2.

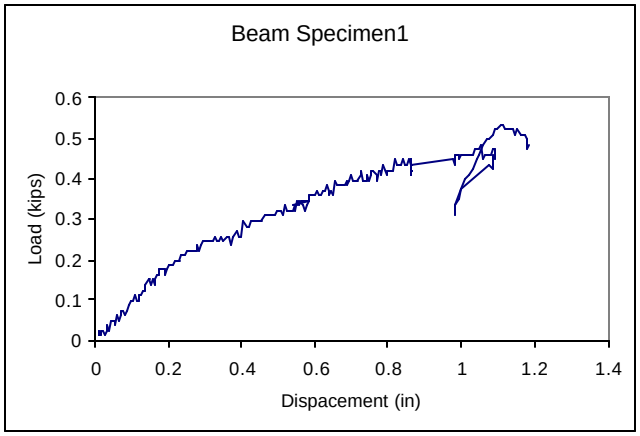

Figure 6.4 Load vs. Displacement curve of Beam Specimen1

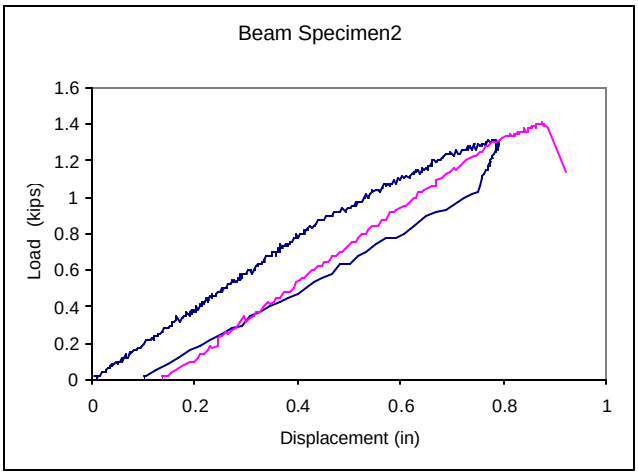

Figure 6.5 Load vs. Displacement curve of Beam Specimen2

The unstiffened components in compression almost buckled simultaneously at the two ends of the beam in Specimen 1, shown in Figure 6.6.

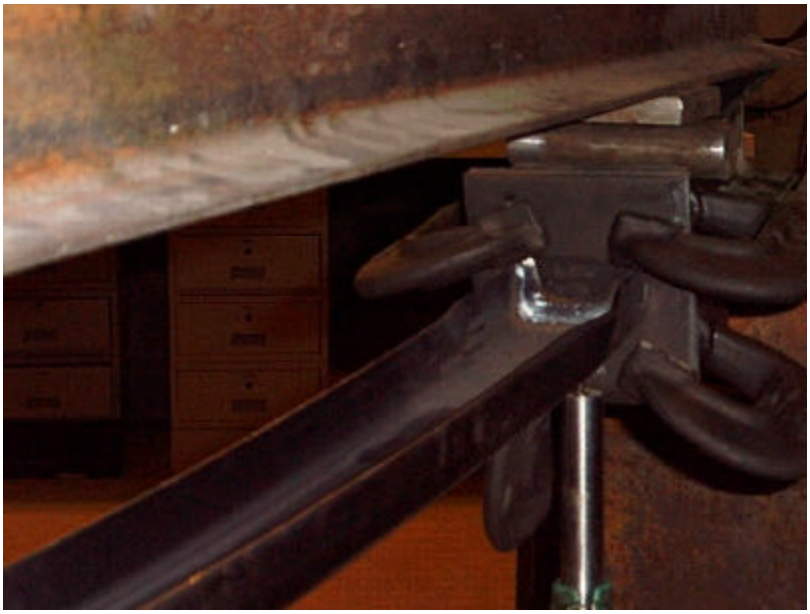

Figure 6.6 Beam Specimen1

The buckling of one of the unstiffened components followed by the buckling of the other unstiffened components and twisting are observed in Specimen 2, shown in Figure 6.7.

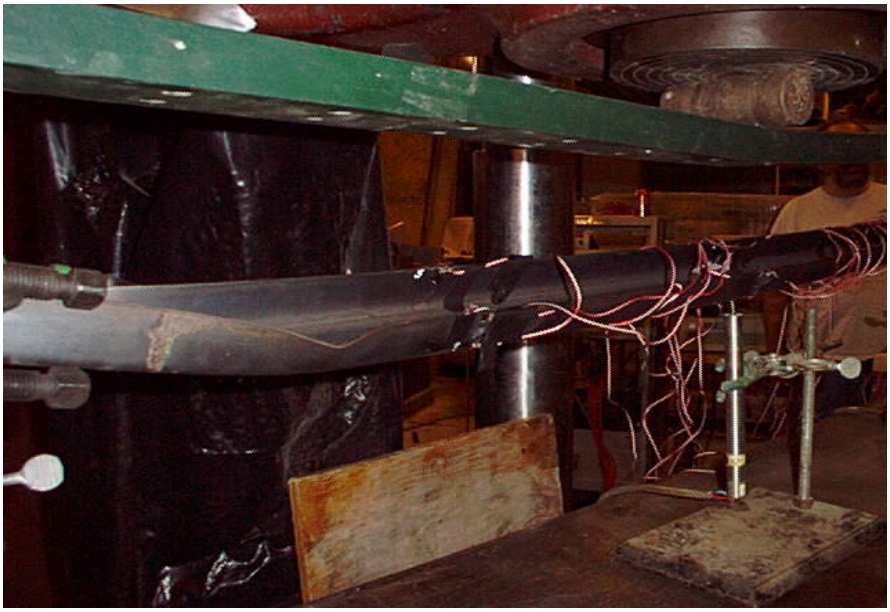

Figure 6.7 Beam Specimen 2

Table 6.2 Evaluation of Proposed Design Procedure

	l	M_{test} (KNmm)	M_{ns} (KNmm)	M_{ns}/M_{test}
Specimen1	0.6379	342.22	364.1	1.064
Specimen2	0.8236	735.132	703.4	0.957

6.2 Experiments on Beam-Columns

6.2.1 Introduction

The following three load cases shown in Figure 6.8 are of interest:

Case 1: Axial Loading with Bending about Symmetry Axis

Case2: Axial Loading with Bending about the Centroidal Axis Perpendicular to the Symmetry Axis

Case 3: Axial Loading with Biaxial Bending

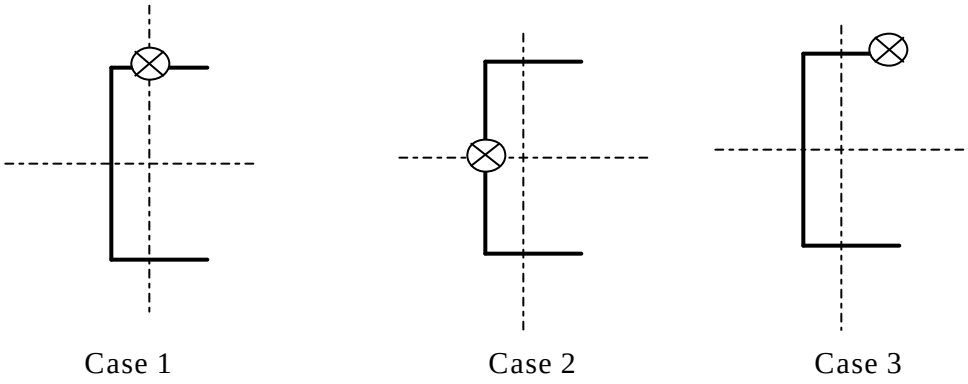

Figure 6.8 Load Conditions

As substantial experimental data are available from Jayabalan and Srinivasa's Experiments for Case 2, experiments on Case 1 and Case 3 will be conducted.

6.2.2 Test Specimens

Four beam-column tests were performed: two on short columns and two on long columns. The cross section is shown in Figure 6.9. The measured dimensions and material properties are listed in Table 6.3.

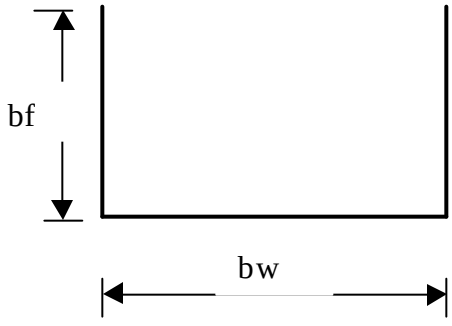

Figure 6.9 Cross-Section Geometry
of Beam-Column Test

Table 6.3 Cross Section Dimensions and Material Properties

	bf(in)	bw(in)	t(in)	L(in)	Fy(kips)
BC1_30	1.979	3.271	0.0666	30.00	36
BC2_30	2.036	3.277	0.0750	30.75	36
BC1_65	2.028	3.278	0.0650	65.00	36
BC2_65	2.075	3.278	0.0630	64.75	36

6.2.3 Test Setup

The end conditions of beam-columns were pin-ended which allowed rotations about x-x and y-y axis with restraining twist rotations and warping. The effective length coefficients were $K_x = K_y = 1.0$ and $K_t = 0.5$. End plates were welded to the column. Thus, cross sectional warping at the ends were restrained by the end plates. Hence, the eccentric load did not produce a bimoment at the ends. As it was eccentric loading in these experiments, twisting at the ends were prevented as a result of cross sectional warping being restrained. The test setup is sketched in Figure 6.10.

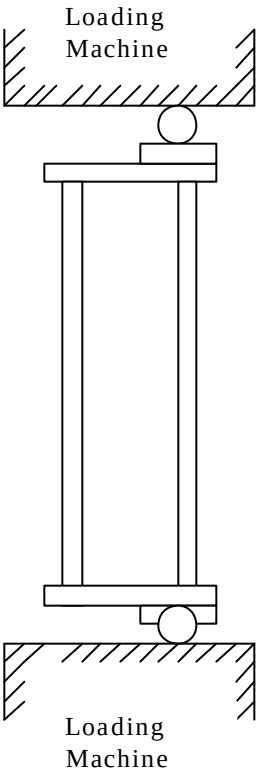

Figure 6.10 Test Setup

The steel plate was used to transfer the

load into the column. The hinge at the supports was accomplished by a steel ball. The load was applied to the column through a steel ball. Circular dimples were machined on the end plates so that the steel balls rested on a particular position with respect to the specimen throughout the test. Washers were welded onto the end plates to prevent the steel balls from accidentally dislodging from its positions. The column was loosely chained to the testing machine at the top and the bottom. A spirit level was used to ensure that the column is vertical.

Displacement transducers were mounted to measure the midheight deflections as well as the deflections at the supports. By this way, it was possible to compensate the midheight deflection from the possible movements of the steel ball at the supports when the applied load was increased. Twelve resistance strain gages were mounted around the cross-section at column midheight to monitor the subultimate strain variations.

6.2.4 Test Results:

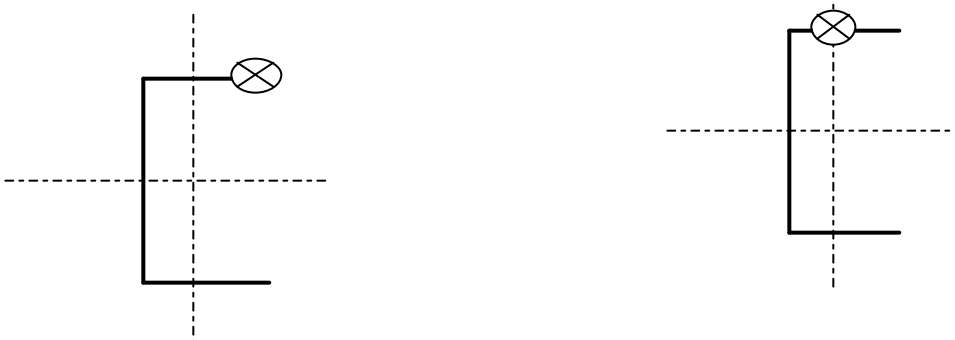

BC1-Axial Loading with Bending about Symmetry Axis

BC2-Axial Loading with Biaxial Bending

Figure 6.11 Load Conditions of Beam-Column Test

Four beam-column tests were evaluated and compared with finite element studies, as shown in Table 6.4. Test setup as well as failure modes are given in Figures 6.12, 6.13, 6.14, 6.15, 6.16 and 6.17.

Table 6.4 Cross-Section Dimensions and Test Results

	bf(in)	bw(in)	t(in)	L(in)	ex(in)	ey(in)	P(pound)		FEM / EXP
							EXP	FEM	
BC1_30	1.979	3.271	0.0666	30.00	1.437	1.636	2137.65	2520	1.179
BC2_30	2.036	3.277	0.0750	30.75	0	1.639	6434.65	6165	0.958
BC1_65	2.028	3.278	0.0650	65.00	1.467	1.639	1436.80	1599.8	1.113
BC2_65	2.075	3.278	0.0630	64.75	0	1.639	4186.53	4860	1.161

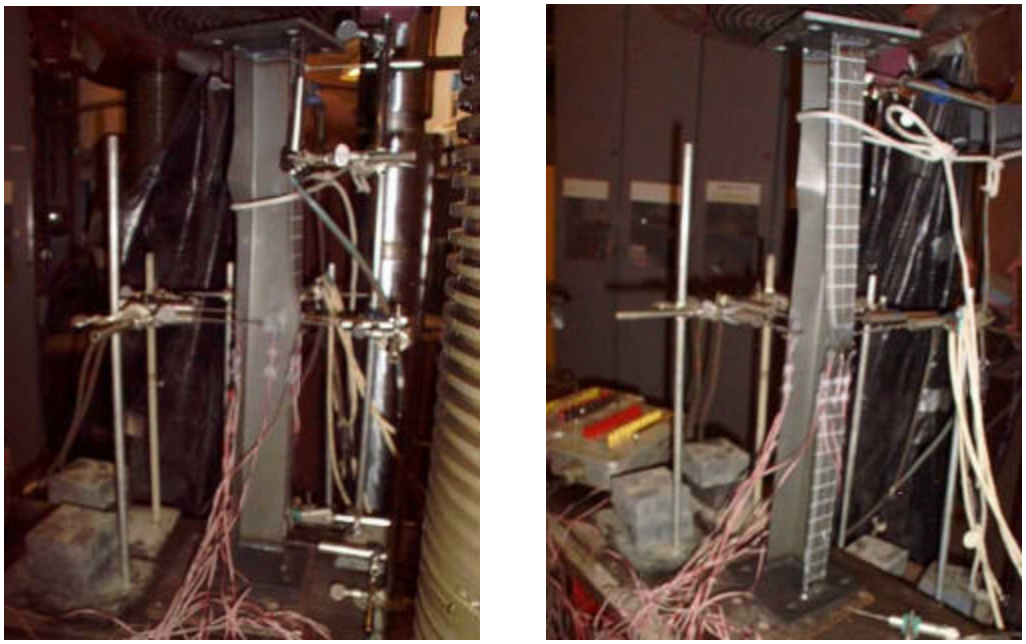

Figure 6.12 BC1_30 Setup and Failure Mode

Figure 6.13 BC2_30 Setup and Failure

Figure 6.14 BC1_65 Failure Mode

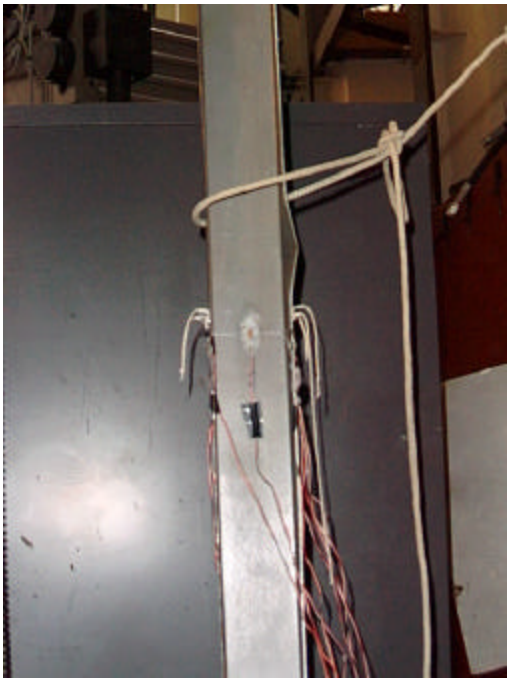

Figure 6.15 BC1_65 Close-

Figure 6.16 BC2_65 Failure Mode

Figure 6.17 BC2_65 Close-up

7. EVALUATION OF PROPOSED ULTIMATE STRENGTH PROCEDURES

Details of the experimental, analytical and numerical studies of plain channels subjected to axial load, bending and combined axial load and bending were discussed. In Part 2, previous research is reviewed. In Part 3, simple equations for plate buckling coefficients are obtained. Based on finite element studies in Part 4, design procedures of channels are proposed in Part 5. Experiment investigation is presented in Part 6. The results of the proposed design procedures are compared with the experimental results in this part. The possible reasons for discrepancies between test data and proposed design procedures are also discussed.

7.1 Evaluation of Experimental Results of Beams

7.1.1 Minor Axis Bending with Stiffened Element in Tension

7.1.1.1 Comparison with Available Experimental Data

1) Comparison with Enjiky's Data (Table 7.1)

Table 7.1 Evaluation of All Enjiky's Data

	l	Mns / Mtest	Cy
Group1:1	0.15569	0.965904	3
2	0.30984	0.853825	3
3	0.46362	0.851136	3
4	0.61726	0.966837	2.1334
5	0.77082	1.058123	1.2769
6	0.92433	1.042927	1
7	1.0778	1.108672	1
8	1.2313	1.133222	1
9	1.3636	1.004066	1
10	1.7897	0.990688	1
11	2.0453	1.073457	1
12	2.301	1.022192	1
13	2.5567	0.984931	1
group2	0.95666	1.096539	1
	0.95666	1.134919	1
	0.95666	1.108377	1
	0.95666	1.118431	1
	0.95666	0.810898	1
	0.95666	0.857118	1
group3:1	0.15569	0.915583	3
2	0.30984	0.802439	3
3	0.46362	0.890313	3
4	0.61726	1.005561	2.1334
5	0.77082	1.077099	1.2769
6	0.92433	1.028595	1
7	1.0778	1.118093	1
8	1.2313	1.182103	1
9	1.3636	1.023301	1
10	1.7897	1.007597	1
11	2.0453	1.032482	1
12	2.301	1.282742	1
13	2.5567	1.339029	1

Enjiky has extensive test data which are organized into three groups. Group1 and group 3 have the same dimensions of plain channels except the

different span in test setup, shown in Figure 7.1 and 7.2. Experiments within group2 were identical in virtually every respect with only the varying loading time intervals (ie 3, 4, 6 and 8 minutes). Time interval of 3 minutes was adopted for groups 1 and 3 experiments.

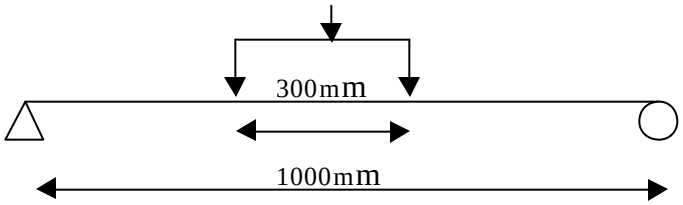

Figure 7.1 Test Setup for Group1 for Enjiky's Experiment

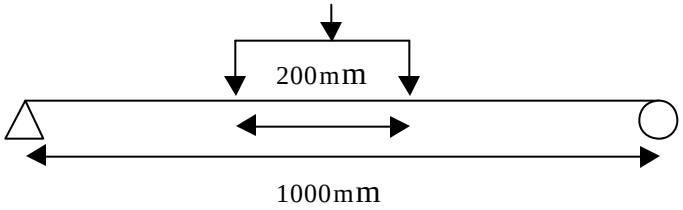

Figure 7.2 Test Setup for Group 3 for Enjiky's Experiment

The comparison results of Enjiky's three groups of data are plotted in Figure 7.3. It is found that the results from group1 and group3 are very close, except the last two data. In order to investigate the span effect on these two data, the load factor and its corresponding half wavelength obtained from CUFSM are presented in Table 7.2.

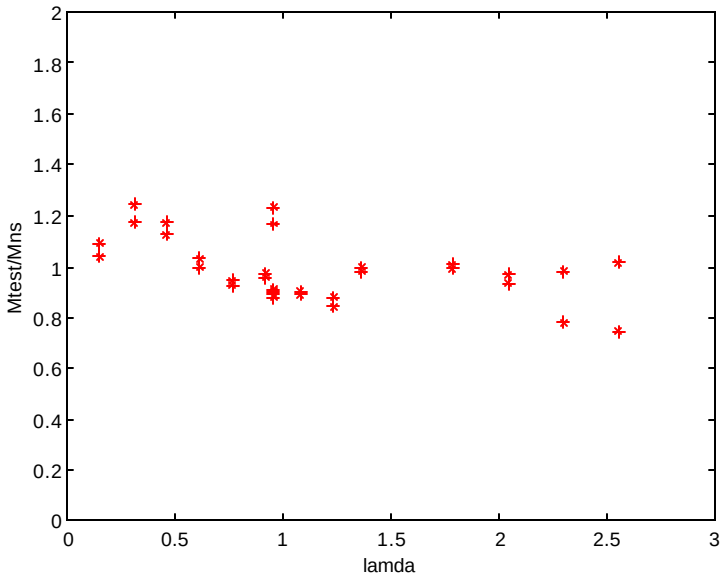

Figure 7.3 Comparison Study of Enjiky's Three Groups of Data

Table 7.2 CUFSM study of Enjiky's Cross Sections

Unstiffened Element in Compression			
No	Type	Half Wavelength(mm)	Load Factor
1	30x8x1.6	27	55.16
2	45x16x1.6	36	20.95
3	60x24x1.6	47	10.92
4	75x32x1.6	59	6.70
5	90x40x1.6	71	4.53
6	105x48x1.6	81	3.26
7	120x56x1.6	96	2.46
8	135x64x1.6	106	1.93
9	160x80x1.6	126	1.68
10	210x105x1.6	166	0.97
11	240x120x1.6	191	0.75
12	270x135x1.6	210	0.59
13	300x150x1.6	235	0.48

The plate buckling coefficient k is based on the minimal load factor obtained from CUFSM parameter study. In specimen No12 and No13, the load factor reached its lowest value at 210mm and 235mm, respectively. But

the span in Group 3 is only 200mm, which is too short to reach its minimal load factor. Thus, Group 1 is chosen as a better set of data between group1 and group3 and the comparison results are listed in Table 7.3.

Table 7.3 Evaluation of Enjiky's Data

	l	Mns / Mtest	Cy
1	0.15569	0.965904	3
2	0.30984	0.853825	3
3	0.46362	0.851136	3
4	0.61726	0.966837	2.1334
5	0.77082	1.058123	1.2769
6	0.92433	1.042927	1
7	1.0778	1.108672	1
8	1.2313	1.133222	1
9	1.3636	1.004066	1
10	1.7897	0.990688	1
11	2.0453	1.073457	1
12	2.301	1.022192	1
13	2.5567	0.984931	1
	mean	1.004306	
	stedv	0.084924	

2) Comparison with P. Jayabalan's Data (Table 7.4)

Table 7.4 Evaluation of P. Jayabalan's Data

	l	Mns / Mtest	Cy
1	1.5491	1.016436	1
2	1.8475	1.0662	1
3	2.7525	1.056758	1
4	1.4913	0.838856	1
5	1.8349	0.843028	1
6	2.868	0.983865	1
	Mean	0.967524	
	Stedv	0.102385	

3) Comparison with El Mahi and Rhodes' Data (for right-angled cross section only) (Table 7.5)

Table 7.5 Evaluation of El Mahi and Rhodes' Data

	l	Mns / Mtest	Cy
1	0.26824	0.808146	3
2	0.54921	0.807037	2.8164
3	0.76156	0.883392	1.3125
4	1.0668	0.871384	1
5	0.37498	0.884251	3
6	0.70894	1.015187	1.5461
7	1.0777	0.983478	1
8	1.4113	1.016229	1
9	0.39854	1.054107	3
10	0.7375	0.956206	1.4122
11	1.1167	1.119207	1
12	1.4346	1.09565	1
13	0.29177	0.915919	3
14	0.53382	0.833403	3
15	0.80389	0.88199	1.1609
16	1.0536	0.929282	1
17	0.76372	1.016425	1.3041
18	1.5538	0.893975	1
19	2.2472	0.963484	1
20	3.0494	1.005328	1
21	2.3775	0.939055	1
22	1.7958	0.938615	1
23	1.2127	0.917936	1
24	2.3767	0.891186	1
25	2.3229	1.287465	1
26	1.2313	0.948947	1
27	0.87776	0.910415	1
28	1.1128	1.081362	1
29	1.365	1.088838	1
30	1.4982	1.211152	1
31	1.7009	1.30373	1
32	1.4982	1.211152	1
33	1.7009	1.165311	1
34	0.70789	0.911245	1.5514
35	0.90444	0.845952	1
36	1.2219	0.954745	1
37	1.0899	0.932227	1
38	1.3543	1.164185	1
39	1.3431	1.062011	1
	mean	0.992298	
	stedv	0.127991	

4) Comparison with Fang Yiu and Pekoz' Data (Table 7.6)

Two experiments were conducted in Cornell University. Details of these two tests are in Part 6.1.

Table 7.6 Evaluation of Fang Yiu and Pekoz' Data

	l	Mns / Mtest	Cy
1	0.63788	1.064068	1.9751
2	0.82358	0.956846	1.0993
	mean	1.010457	
	stedv	0.075817	

7.1.1.2 Evaluation Data and Resistance Factor f

Experimental result of El Mahi and Rhodes (1985), Enjiky (1985), Jayabalan (1989), and the tests carried out at Cornell University in 1999 by Fang Yiu and Teoman Pekoz were used to formulate the provisions for the case of minor axis bending with stiffened element in tension.

The mean value of M_{ns} over M_{test} ratio (excluding the results for plain channels where the flanges are not at right angles to the web) is 0.993; the sample standard deviation is 0.114; resistance factor f is 0.718 in probability model. For specimens with post-yield reserve capacity, that is, Cy>1, f is 0.690; When Cy=1, f is 0.740. The comparison results are shown in Figure 7.4.

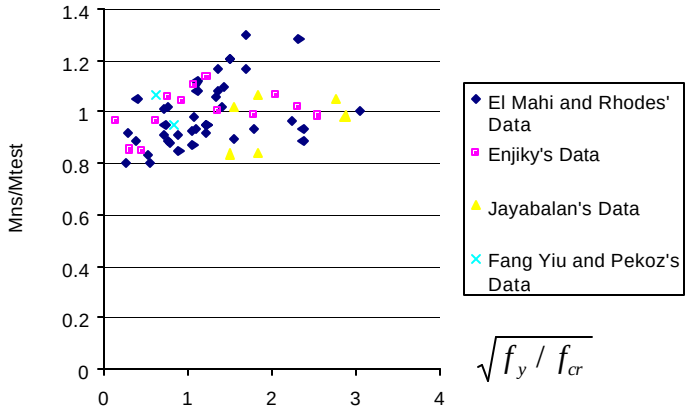

Figure 7.4 Comparative Study of Minor Axis Bending with Stiffened Element in Tension

7.1.2 Minor Axis Bending with Stiffened Element in Compression

7.1.2.1 Comparison with Available Experimental Data

1) Comparison with Enjiky's Data (Table 7.7)

Table 7.7 Evaluation of All Enjiky's Data

	l	Mns / Mtest	Cy
group1	0.12998	0.91152	3
	0.21609	0.81576	3
	0.30037	0.8585	3
	0.38406	0.63041	3
	0.46746	0.35104	2.9299
	0.55072	0.95206	2.1482
	0.63389	1.1805	1.3672
	0.717	1.3896	1
	0.76777	1.1835	1
	1.0077	1.2849	1
	1.1517	1.1291	1
	1.2956	1.461	1
	1.4396	1.5261	1
group2	0.12998	0.68364	3
	0.21609	0.83532	3
	0.30037	0.90635	3
	0.38406	0.91264	3
	0.46746	0.93598	2.9299
	0.55072	1.011	2.1482
	0.63389	1.3277	1.3672
	0.717	1.6453	1
	0.76777	1.4494	1
	1.0077	1.7365	1
	1.1517	2.0596	1
	1.2956	2.2483	1
	1.4396	2.5629	1
group3	0.28547	0.82314	3
	0.365	0.87998	3
	0.44427	0.92337	3
	0.52339	0.91732	2.4048
	0.60244	0.93811	1.6626
	0.68142	1.0575	1
	0.82247	1.0467	1
	1.0795	1.021	1
	1.2337	1.0272	1
	1.3879	0.9828	1
	1.5421	1.042	1

Enjiky has extensive test data which are organized into three groups. Group1 and group 2 have the same dimensions of plain channels except the different span in test setup, shown in Figure 7.5 and 7.6. In group 1 and group 2, load was applied as shown in Figure 7.7, which caused local crushing besides local buckling. Improved load condition in Figure 7.8 is adopted to avoid local crushing in group 3. Therefore, group 3 is selected for comparison study and the comparison results are shown in Table 7.8.

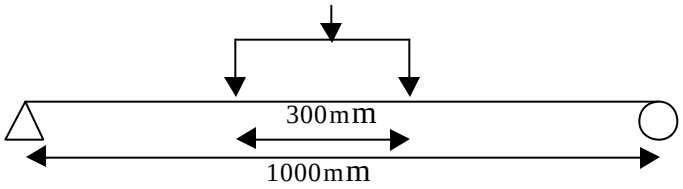

Figure 7.5 Test Setup for Group1

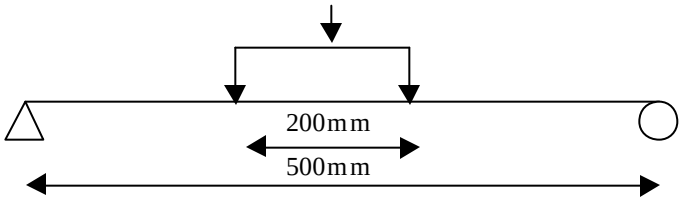

Figure 7.6 Test Setup for Group2

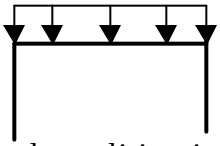

Figure 7.7 Load condition in Group1 and Group2

Figure 7.8 Load condition in Group 3

Table 7.8 Evaluation of Enjiky's Data

	l	Mns / Mtest	Cy
1	0.28547	0.82314	3
2	0.365	0.87998	3
3	0.44427	0.92337	3
4	0.52339	0.91732	2.4048
5	0.60244	0.93811	1.6626
6	0.68142	1.0575	1
7	0.82247	1.0467	1
8	1.0795	1.021	1
9	1.2337	1.0272	1
10	1.3879	0.9828	1
11	1.5421	1.042	1
	mean	0.969011	
	stedv	0.077709	

2) Comparison with P. Jayabalan's Data (Table 7.9)

Table 7.9 Evaluation of P. Jayabalan's Data

	l	Mns / Mtest	Cy
1	0.33074	0.98847	3
2	0.43754	2.405	3
3	0.35765	1.2985	3

It is reported in Jayabalan's experiments that local crushing and local buckling both contribute to the failure, while local crushing is not considered in AISI equation, which causes the discrepancies in test data and design equations.

7.1.2.2 Evaluation Data and Resistance Factor f

Test results of Enjiky (1985) are used for minor axis bending with stiffened element in compression. The mean value of M_{ns} over M_{test} ratio is 0.9690; the sample standard deviation is 0.0777; resistance factor f = 0.7253 in probability model. The comparison results are shown in Figure 7.9.

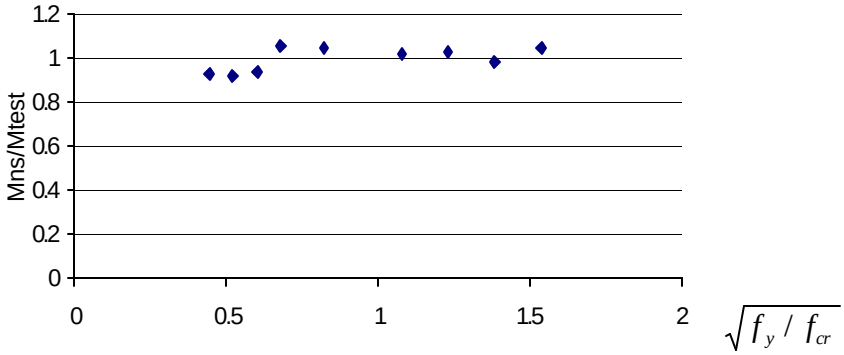

Figure 7.9 Comparative Study of Minor Axis Bending with Stiffened Element in Compression

7.1.3 Major Axis Bending

7.1.3.1 Comparison with Available Experimental Data

1) Comparison with Reck's Data (Table 7.10)

Table 7.10 Evaluation of Reck's Data

	Reck's Specimen		
	Mtest	Mns	Mns / Mtest
	(in-K)	(in-K)	
UP-9	36.9	34.5541	0.9364
UP-10	14.3	12.7170	0.8893
UP-11	15.5	12.1074	0.7811
		mean	0.868933
		stedv	0.079628

2) Comparison with Asko Talja 's Data (Table 7.11)

Table 7.11 Evaluation of Asko Talja's Data

Test Name	Mtest(kNm)	Mns	Mns / Mtest	failure mode
UU1 / MR1	56.88	48.428	0.8514	Yielding
UU1 / MR2	39.75	48.428	1.2183	lateral buckling

The underestimation of Specimen UU1 / MR2 was due to the imprecise boundary conditions in the experiments, which was observed by Asko. Asko type cross section shown in Figure 7.10 was supposed to act separately as two

individual plain channels, while the sections rotate together under force during the experiment. These contribute to the discrepancies between test data and design equations.

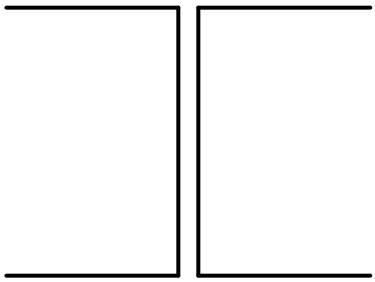

Figure 7.10 Asko Type Cross Section

7.1.3.2 Evaluation Data

Test results of Reck reported by Kalyanaraman (1976) and Talja (1992) provided the basis for the design procedure. For the relevant test data from these references the mean value of M_{ns} over M_{test} ratio is 0.8646 and the sample standard deviation is 0.0656. Resistance factor f = 0.6318 in probability model. The comparison results are shown in Figure 7.11.

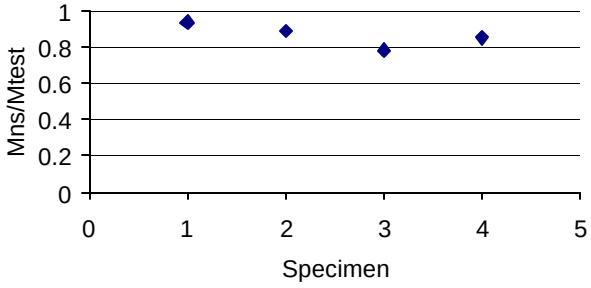

Figure 7.11 Comparative Study of Major Axis Bending

7.2 Evaluation of Experimental Results of Columns

7.2.1 Flat-ended Columns

7.2.1.1 Comparison with Available Experimental Data

1) Comparison with Asko Talja's data--fixed-ended column with uniform compression (Table 7.12)

Table 7.12 Evaluation of Asko Talja's data

Asko Talja (flat ended column)			
Specimen	**Ptest(KN)**	**Pns**	**Pns/Ptest**
		(Column)	
U-127x40x6: 1	770	672.7	0.874
2	640	617.7	0.965
3	475	539.6	1.136
4	305	431	1.413
U-186x80x6: 1	980	964.1	0.984
2	1020	913.6	0.896
3	900	810.4	0.900
4	640	679.3	1.061
U-286x80x6: 1	1020	1066.7	1.046
2	940	1001	1.065
3	945	894.5	0.947
4	750	738.8	0.985
		mean	1.023
		stedv.	0.146

2) Comparison with Ben Young's data -- fixed-ended column with uniform compression (Table 7.13, 7.14)

Table 7.13 Evaluation of Ben Young's Data Series P36

Series P36- flat-ended column			
Specimen	**Ptest**	**Pns**	**Pns/Ptest**
		(column)	
P36F0280	65	64.786	0.997
P36F1000	59	56.824	0.963
P36F1500	50.1	46.31	0.924
P36F2000	41.7	37.257	0.893
P36F2500	32.8	29.186	0.890
P36F3000	24.7	22.629	0.916
		mean	0.931
		stedv.	0.042

Table 7.14 Evaluation of Ben Young's Data Series P48

Series P48- flat-ended column

Specimen	Ptest	Pns(C)	Pns/Ptest
		(column)	
P48F0300	66	62.992	0.954
P48F1000	62.7	57.139	0.911
P48F1500	55.5	49.613	0.894
P48F1850	47.2	45.697	0.968
P48F2150	43.6	39.785	0.913
P48F2500	38.5	33.978	0.883
P48F3000	37.4	27.739	0.742
P48F3500	29.5	23.332	0.791
		mean	0.882
		stedv.	0.078

3) Comparison with Mulligan's data -- fixed-ended stub-column with uniform compression (Table 7.15)

Table 7.15 Evaluation of Mulligan's Data

Mulligan Stub Column Specimens

Specimen		Ptest	Pns	Pns/Ptest
SC/1	60x30	7.40	6.47	0.874
SC/1	90x30	7.35	6.58	0.895
SC/1	120x30	7.80	6.77	0.868
SC/2	120x30	7.10	7.01	0.988
SC/1	40x60	7.88	7.30	0.927
SC/2	40x60	7.89	7.36	0.933
SC/1	60x60	9.16	7.81	0.853
SC/1	100x60	9.20	8.79	0.955
SC/1	120x60	8.20	6.71	0.819
SC/1	180x60	8.52	6.98	0.819
SC/2	180x60	8.50	6.98	0.821
			mean	0.886
			stedv	0.058

4) Comparison with Pekoz's data -- fixed-ended column with uniform compression (Table 7.16)

Table 7.16 Evaluation of Pekoz's data

Pekoz Stub Column Specimens

Specimen	Ptest	Pns	Pns/Ptest
		column	
1	4.70	6.007	1.278
2	4.00	3.622	0.906
3	4.10	5.841	1.425
4	4.00	5.371	1.343
5	6.90	7.984	1.157
6	14.60	16.203	1.110
7	5.20	6.767	1.301
		mean	1.217
		stev.	0.174

It is reported in Pekoz's data (1998) that Specimen 3, 4, 6 and 7 have crippling of flange in the failure mode. Crippling of flange is not considered in column equation, which contributes some discrepancies in test data and design equations.

7.2.1.2 Evaluation Data and Resistance Factor *f*

Data from Talja (1990), Young (1997), Mulligan & Pekoz (1983) provided the basis for the procedures for flat-ended columns. The mean value of M_{ns} over M_{test} ratio for the data is 0.950; the sample standard deviation is 0.126; resistance factor *f* is 0.670 in probability model for fixed-ended columns. The results are illustrated in Figure 7.12.

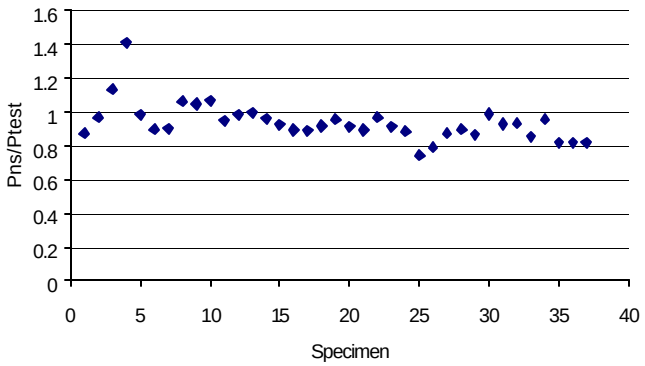

Figure 7.12 Comparative Study of
Flat-ended Columns

7.2.2 Pin-ended Columns

7.2.2.1 Comparison with Available Experimental Data

1) Comparison with Ben Young's data -- pin-ended column with uniform compression (Table 7.17, 7.18)

Table 7.17 Evaluation of Ben Young's data SeriesP36

Specimen	Pt	Pns	Pns/Pt
		(beam-column)	
P36P0280-	55.2	47.228	0.856
P36P0315-	52.1	45.471	0.873
P36P0815-	40.9	36.116	0.883
P36P1315-	27	23.722	0.879
		mean	0.872
		stedv.	0.012

Table 7.18 Evaluation of Ben Young's data SeriesP48

Specimen	Pt	Pns	Pns/Pt
		(beam-column)	
P48P0300+	45.2	41.666	0.922
P48P0565-	38.6	40.836	1.058
P48P1065	33.9	34.804	1.027
P48P1565-	31.2	26.912	0.863
		mean	0.967
		Stedv.	0.091

7.2.2.2 Evaluation Data and Resistance Factor f

Test results from Young (1997) for two series of pin-ended column test Series P36 and P48 were used in the development of the design procedures. The mean value of M_{ns} over M_{test} ratio is 0.920; the sample standard deviation is 0.078; resistance factor f is 0.675 in probability model. The results are illustrated in Figure 7.13.

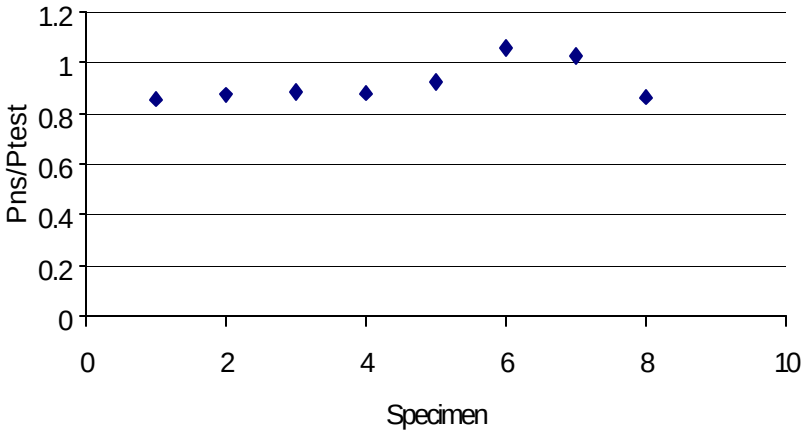

Figure 7.13 Comparative Study of Pin-ended Columns

7.3 Evaluation of Experimental Results of Beam - Columns

7.3.1 Evaluation Methods using Interaction Equations

Beam-Column Interaction Equations:

$$\frac{P_u}{P_n}+\frac{C_{mx}M_{ux}}{M_{nx}(1-\frac{P_u}{P_{Ex}})}+\frac{C_{my}M_{uy}}{M_{my}(1-\frac{P_u}{P_{Ey}})}\le 1.0$$

$$\frac{P_u}{P_{no}}+\frac{M_{ux}}{M_{nx}}+\frac{M_{uy}}{M_{ny}}\le 1.0$$

where,

$$P_{Ex}=\frac{p^2EI_x}{(K_xL_x)^2}$$

$$P_{Ey} = \frac{p^2 E I_y}{(K_y L_y)^2}$$

Ultimate loads are computed based on four methods described as follows.

Method 1

1) in beam-column interaction equations, for beam part and column part, use improved plate buckling coefficients obtained from CUFSM (in Part 3). For those not practical cross-sections, use improved plate buckling coefficients from CUFSM, instead of the kf equations in Part 3;

2) in beam-column equations, for the case of flat-ended column, the shift of neutral axis caused by local buckling does not induce overall bending, as is discussed in Part 5.2; for the case of pin-ended column, column itself is treated as a beam-column with the average deflection instead of the maximum deflection, as is suggested in Part 5.2;

3) in beam-column equations, for beam part, when stiffened elements are in tension, the proposed design equations described in Part 5.1.1 are used; when stiffened element is in compression, consistent effective width equation described in Part 5.1.2, is used to decide the effective width; when unstiffened element is in uniform compression, the proposed design equations described in Part 5.1.3 are used.

Method 2

1) in beam-column interaction equations, for beam part and column part, use improved plate buckling coefficient k obtained from CUFSM (in Part 3); For

those not practical cross-sections, using improved plate buckling coefficients from CUFSM, instead of the kf equations in Part 3.

2) in beam-column equations, for the case of pin-ended column, pin-ended column itself is roughly treated as a column.

3) in beam-column equations, for beam part, when stiffened elements are in tension, the proposed design equations described in Part 5.1.1 are used; when stiffened element is in compression, consistent effective width in Part 5.1.2, is used to decide the effective width; when unstiffened element is in uniform compression, the proposed design equations described in Part 5.1.3 are used.

Method 3

1) in beam-column interaction equation, for beam part and column part, use plate buckling coefficient k according to AISI specification, except for minor axis bending with stiffened element in tension, as there is no accurate provisions in the Specification;

2) in beam-column equations, for beam part, when unstiffened element is in uniform compression, AISI Part V B2.3 is used.

Method 4

Beam-Column interaction equation using gross cross-sections.

7.3.2 Load Condition -- Eccentricity of the Load in the Plane of Symmetry

7.3.2.1 Evaluation of Available Experimental Data

1) the load position is on the same side as the shear center with respect to centroid along the x axis in the plane of symmetry (Figure 7.14)

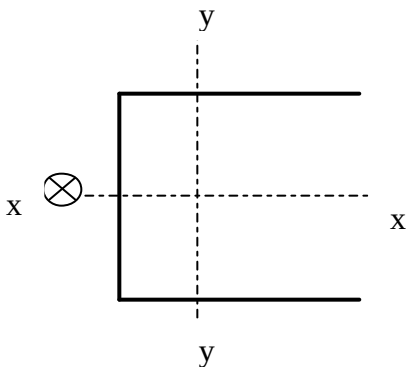

Figure 7.14:
Load Condition

- Evaluation of Jayabalan's Experiments

As it is flat-ended beam-column test, methods 1 and 4 are used to evaluate the experimental data, as shown in Tables 7.21 and 7.22

- Evaluation of Srinivasa's Experiments

As it is pin-ended beam-column test, methods 1, 2 and 4 are used to evaluate the experimental data, as shown in Table 7.23.

2) the load position is on the other side as the shear center with respect to centroid along the x axis in the plane of symmetry (Figure 7.15)

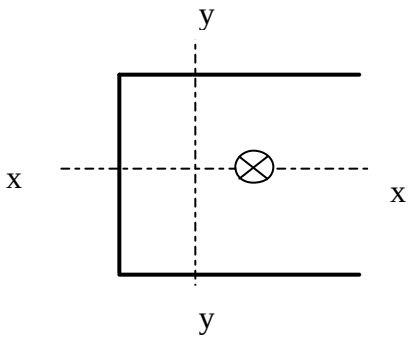

Figure 7.15
Load Condition

- Evaluation of Jayabalan's Experiments

As it is flat-ended beam-column test, methods 1 and 4 are used to evaluate the experimental data, as shown in Tables 7.25 and 7.26

- Evaluation of Srinivasa's Experiments

As it is pin-ended beam-column test, methods 1, 2 and 4 are used to evaluate the experimental data, as shown in Tables 7.27 and 7.28

7.3.2.2 Discussions

Observations and Discussions

a) In Jayabalan's Experiments , the theoretical value of the non-uniform stress coefficient a_{th} which relates to the position of the column in the loading frame and depth of the section as well as $a_{\exp}$ which relates to the experimental edge stresses are chosen for further calculation.
b) The data in shaded cells correspond to industrial practical cross-sections with D/L close to and around less than 1.

c) The un-shadowed cells from Table 7.21 to Table 7.28, which correspond to not practical sections, are not studied by the current research. As in beam-column interaction equations, for beam part, the proposed design equations described in Part 4 is applicable only to beams undergoing local buckling.

Table 7.21 Evaluation of Jayabalan's Data Based on non-uniform stress coefficient a_{exp}

NO	D(mm)	D/t	W(mm)	D/W	t(mm)	L(mm)	e0x(mm)	Method1	N1/Ntest	Method2	N2/Ntest	Jay test
C2	96.8	49.90	50	1.94	1.94	943.3	3.395	28494.74	0.385	86580.84	1.17	74000
C4	89.8	51.31	59	1.52	1.75	312.3	4.351	21857.82	0.377	62127.99	1.07	58000
C6	97.4	49.69	50.7	1.92	1.96	183.3	9.326	38459.3	0.476	98939.66	1.22	80800
C8	120.2	66.41	57.7	2.08	1.81	1027.3	2.184	12750.36	0.264	65599.1	1.36	48300
C10	119.4	68.62	56.8	2.10	1.74	353.3	7.741	17846.13	0.362	63970.65	1.30	49300
C12	119.7	70.00	59.4	2.02	1.71	203.3	8.585	20384.42	0.345	74111.79	1.25	59100
C14	59.4	34.34	61	0.97	1.73	571.3	1.489	31051.14	0.699	41954.15	0.94	44400
C16	61.1	34.13	56.9	1.07	1.79	273.3	2.184	35836.86	0.734	47482.88	0.97	48800
C18	184.7	87.12	53.1	3.48	2.12	1007.3	6.894	24633.27	0.175	177796.5	1.26	140780
C20	184.2	85.67	49.1	3.75	2.15	335.3	12.675	16496.24	0.161	162377.2	1.58	102720

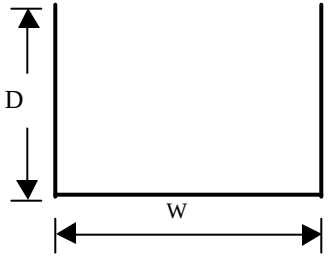

Figure 7.16 Jayabalan's Cross Section

Table 7.22 Evaluation of Jayabalan's Data Based on non-uniform stress coefficient a_{th}

NO	D(mm)	D/t	W(mm)	D/W	t(mm)	L(mm)	e0x(mm)	Method1	N1/Ntest	Method2	N2/Ntest	Jay test
C2	96.8	49.90	50	1.94	1.94	943.3	1.079	29106.89	0.393	93218.73	1.26	74000
C4	89.8	51.31	59	1.52	1.75	312.3	2.708	22293.05	0.384	66039.33	1.14	58000
C6	97.4	49.69	50.7	1.92	1.96	183.3	5.257	40123.44	0.497	112571.7	1.39	80800
C8	120.2	66.41	57.7	2.08	1.81	1027.3	1.470	12807.53	0.265	66972.01	1.39	48300
C10	119.4	68.62	56.8	2.10	1.74	353.3	4.162	18345.27	0.372	70786.07	1.44	49300
C12	119.7	70.00	59.4	2.02	1.71	203.3	7.004	20627.25	0.349	77322.05	1.31	59100
C14	59.4	34.34	61	0.97	1.73	571.3	0.683	32051.56	0.722	43933.22	0.99	44400
C16	61.1	34.13	56.9	1.07	1.79	273.3	1.456	36825.62	0.755	49377.11	1.01	48800
C18	184.7	87.12	53.1	3.48	2.12	1007.3	3.403	24889.43	0.177	188746	1.34	140780
C20	184.2	85.67	49.1	3.75	2.15	335.3	9.724	16632.94	0.162	171781.6	1.67	102720

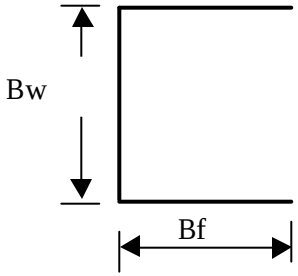

Figure 7.17 Srinivasa's Cross Section

Tables 7.23 Dimensions of Srinivasa's Cross Section

Specimen	Bf(mm)	Bf / t	Bw(mm)	Bf / Bw	t(mm)	L(mm)	ex(mm)
LPCI-11	50.20	33.92	42.91	1.17	1.48	598.00	-1.61
LPCI-12	50.58	33.95	41.53	1.22	1.49	902.00	-2.17
LPCI-31	49.61	33.52	43.98	1.13	1.48	1193.00	-11.80
LPCII-31	90.83	61.37	38.43	2.36	1.48	1100	-8.26
LPCII-32	89.37	59.98	42.05	2.13	1.49	1498	-19.34
LPCIII-33	89.93	60.36	42.92	2.10	1.49	2205	-45.32

Tables 7.24 Evaluation of Srinivasa's Data

Specimen	Method 1	N1 / Ntest	N1 / Nfem	Method 2	N2 / Ntest	N2 / Nfem	Method3	N3 / Ntest	N3 / Nfem	Ntest	Nfem
LPCI-11	20569.97	0.595	0.556	24266.05	0.702	0.656	37398.26	1.081	1.011	34580	37000.6
LPCI-12	17794.62	0.683	0.574	20861.33	0.801	0.673	30500.76	1.171	0.984	26046	30994.74
LPCI-31	13442.75	0.442	0.614	14917.4	0.491	0.681	17448.34	0.574	0.797	30411	21895.92

LPCII-31	8599.87	0.347	0.336	9765.9	0.393	0.382	33783.61	1.361	1.322	24819	25563.57
LPCII-32	7893.36	0.227	0.214	8809.17	0.254	0.239	22213.92	0.639	0.603	34737	36821.22
LPCIII-33	5144.84	0.189	0.217	5572.94	0.204	0.235	10757.37	0.394	0.453	27282	23735.34

Table 7.25 Evaluation of Jayabalan's Experiments Based on non-uniform stress coefficient a_{exp}

NO	D(mm)	D/t	W(mm)	D/W	t(mm)	L(mm)	e0x(mm)	Method1	N1/ Ntest	Method2	N2/ Ntest	Jay test
C1	89.4	49.67	59.1	1.513	1.8	940.3	1.9817	24798.19	0.55	61180.17	1.35	45200
C3	89.3	50.17	59.3	1.506	1.78	312.3	3.7539	20934.86	0.51	52541.07	1.29	40800
C5	89.7	50.39	57.7	1.555	1.78	183.3	9.6153	17491.54	0.28	41566.21	0.67	62400
C7	120.3	69.54	56.8	2.118	1.73	1030.3	1.5017	16472.21	0.37	69232.8	1.54	44900
C9	120.3	65.03	58.9	2.042	1.85	344.3	7.6475	16357.22	0.42	58515.59	1.49	39400
C11	120	66.3	57.4	2.091	1.81	201.3	9.3401	16438.7	0.52	58228.15	1.84	31700
C13	61.5	34.75	58	1.06	1.77	568.3	1.6654	28032.38	0.72	40100.01	1.03	39000
C15	62	34.25	59.8	1.037	1.81	271.3	1.8691	27507.16	0.68	43809.82	1.08	40400
C17	184.4	88.23	53.1	3.473	2.09	1003.3	6.1507	17826.42	0.17	183812.91	1.74	105400
C19	184.7	87.54	50.7	3.643	2.11	337.3	14.2734	15324.24	0.17	177590.28	1.92	92700

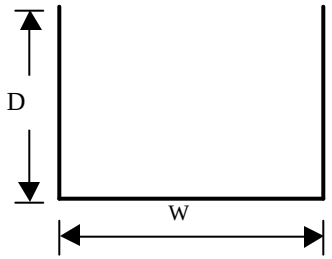

Figure 7.16 Jayabalan's Cross Section

Table 7.26Evaluation of Jayabalan's Experiments Based on non-uniform stress coefficient a_{th}

NO	D(mm)	D/t	W(mm)	D/W	t(mm)	L(mm)	e0x(mm)	Method1	N1/ Ntest	Method2	N2/ Ntest	Jay test
C1	89.4	49.67	59.1	1.513	1.8	940.3	0.9318	26004.6	0.58	64733.03	1.43	45200
C3	89.3	50.17	59.3	1.506	1.78	312.3	2.8929	21947.9	0.54	54961.87	1.35	40800
C5	89.7	50.39	57.7	1.555	1.78	183.3	5.0376	20653.05	0.33	50702.41	0.81	62400
C7	120.3	69.54	56.8	2.118	1.73	1030.3	1.5017	16472.21	0.37	69232.8	1.54	44900
C9	120.3	65.03	58.9	2.042	1.85	344.3	4.6819	17615.36	0.45	65116.54	1.65	39400
C11	120	66.3	57.4	2.091	1.81	201.3	8.0782	16802.79	0.53	60711.86	1.92	31700
C13	61.5	34.75	58	1.06	1.77	568.3	0.7314	31120.69	0.80	43427.21	1.11	39000
C15	62	34.25	59.8	1.037	1.81	271.3	1.6803	28295.3	0.70	44495.89	1.10	40400
C17	184.4	88.23	53.1	3.473	2.09	1003.3	3.4787	18414.13	0.17	194214.1	1.84	105400
C19	184.7	87.54	50.7	3.643	2.11	337.3	10.4429	16419.52	0.18	192892.68	2.08	92700

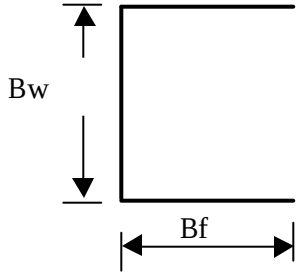

Figure 7.17 Srinivasa's Cross Section

Tables 7.27 Dimensions of Srinivasa's Cross Section

Specimen	Bf(mm)	Bf/t	Bw(mm)	Bf/Bw	t(mm)	L(mm)	ex(mm)	NAISI/Ntest
LPCI-21	49.57	33.49	43.72	1.134	1.48	1503	10.5	0.29
LPCII-11	90.76	60.91	38.12	2.381	1.49	797	1.3	0.13
LPCII-12	90.65	61.25	38.89	2.331	1.48	1503	3.78	0.2
LPCII-21	91.34	61.3	37.15	2.459	1.49	1099	9.97	0.2
LPCII-22	89.36	59.97	42.02	2.127	1.49	1499	28.88	0.15
LPCII-23	88.86	60.45	42.62	2.085	1.47	2200	43.68	0.19
LPCIII-11	155.5	105.1	48.85	3.183	1.48	1097	1.92	0.12

Tables 7.28 Evaluation of Srinivasa's Data

Specimen	Method1	N1/Ntest	N1/N(FE)	Method2	N2/Ntest	N2/N(FE)	Method3	N3/Ntest	N3/N(FE)	Rao test	N(FE)/ Ntest	Failure Mode
LPCI-21	9841	0.68	0.72	10448	0.72	0.76	12525	0.87	0.91	14470	0.95	TF
LPCII-11	15741	0.67	0.79	23114	0.98	1.16	51107	2.17	2.55	23544	0.85	TF
LPCII-12	10847	0.69	0.73	13282	0.85	0.89	24181	1.54	1.62	15696	0.95	TF
LPCII-21	11655	0.87	0.81	14753	1.10	1.03	29603	2.20	2.06	13440	1.07	TF
LPCII-22	7842	0.63	0.84	9068	0.73	0.97	16628	1.34	1.79	12410	0.75	TF
LPCII-23	4700	0.59	0.79	5048	0.63	0.85	8389.3	1.05	1.41	7956	0.75	TF
LPCIII-11	14090	0.81	1.07	24954	1.44	1.90	79627	4.60	6.05	17315	0.76	D

7.3.3 Load Condition -- Eccentricity of the Load in the Plane of Asymmetry

7.3.3.1 Evaluation of Available Experimental Data

1) Axial Loading with Bending about Symmetry Axis (Figure 7.18)

Evaluation of Fang Yiu and Pekoz's data: As it is pin-ended beam-column test, methods 1, 2, 3 and 4 are used to evaluate the experimental data, as shown in Tables 7.29.

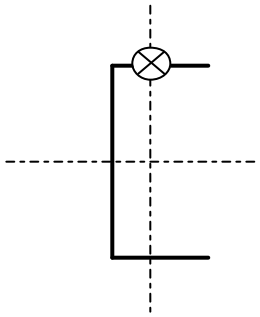

Figure 7.18 Case1 Load Condition

Table 7.29 Results of Axial Loading with Bending about Symmetry Axis

	Method 1	N1/Nabq	Method 2	N2/Nabq	Method 3	N3/Nabq	Method 4	N4/Nabq	Abaqus
B1_30	17810.90	0.64	20913.08	0.75	19819.8	0.71	29611.5	1.06	27900
B1_65	15760.21	0.71	17849.64	0.80	16947.2	0.76	23330.8	1.05	22200

2) Axial Loading with Biaxial Bending (Figure 7.19)

Evaluation of Fang Yiu and Pekoz's data: As it is pin-ended beam-column test, methods 1, 2, 3 and 4 are used to evaluate the experimental data, as shown in Tables 7.30.

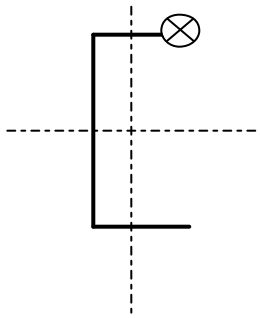

Figure 7.19 Case3 Load Condition

Table 7.30 Results of Axial Loading with Biaxial Bending

	Method 1	N1/Nabq	Method 2	N2/Nabq	Method 3	N3/Nabq	Method 4	N4/Nabq	Abaqus
B2_30	7593.88	0.64	8020.72	0.67	7944.99	0.67	9867.18	0.83	11900
B2_65	6808.69	0.64	7161.02	0.67	7397.83	0.69	8503.89	0.79	10700

7.3.3.2 Discussions

1) In the above-mentioned methods, Method 1 is a better description of beam-column behavior, while the results from Method1 are the least close to Abaqus results. This shows that the beam-column interaction equations are conservative.

2) Method 2 uses the plate buckling coefficients from Part 3, while Method 3 adopted the plate buckling coefficients from AISI Specification. The results from Method 2 and Method 3 are not too much different.

7.3.4 Evaluation Data

Jayabalan (1989) and Srinivasa (1998) provide results of beam-column experiments with eccentricity of the load in the plane of symmetry. Fang Yiu and Pekoz in 2000 tested beam-column with eccentricity of the load in the plane of asymmetry. Only the data corresponding to practical cross-sections are evaluated and plotted in Figure 7.20.

The correlation of the test results of C, channel, and hat section beam-columns with the use of interaction equations was plotted in Figure 7.3-1 of Pekoz (1987). This figure presented the results of all the tests with loads with uniaxial or biaxial eccentricities. Rp, Rx and Ry represent the first, second and the third terms of the AISI interaction equation. Ro equals 0.707(Rx+Ry). The projections of test points on the Rp-Ro plane was plotted. The results

that fell outside of the solid line in the Figure 7.20 on the right indicated that the interaction equation is conservative for those cases. Results from Jayabalan (1989) and Srinivasa (1998) and Fang Yiu and Pekoz are added to the Pekoz (1987) figure and given in Figure 7.20. It is seen that the interaction equation is also conservative for plain channel section.

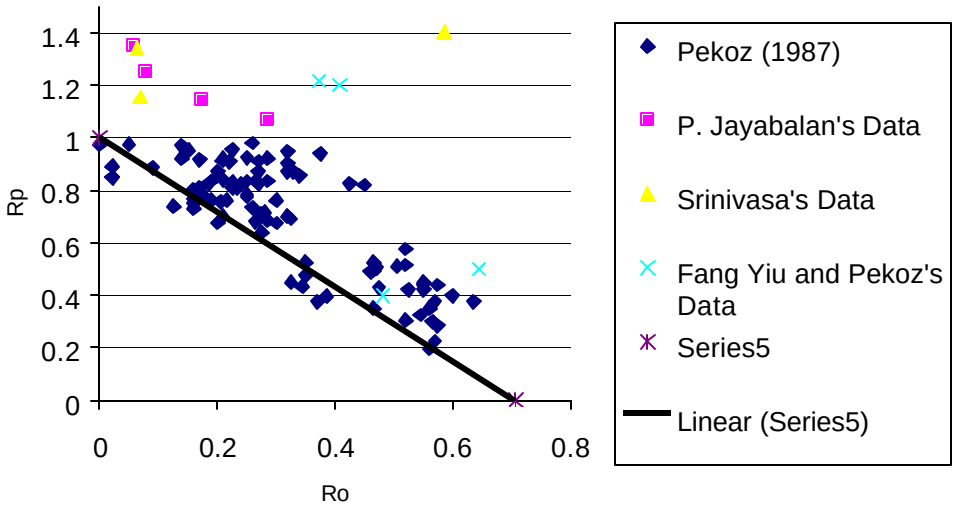

Figure 7.20 Beam-Column Interaction Plotting

8. CONCLUSIONS

Design recommendations for calculating the overall capacity of plain channel sections subjected to various types of stress gradients in the range of practical applications by the industry are presented. Comparison studies indicate good agreement with experimental results.

APPENDICES

Appendix A: Imperfection Measurements

Geometric imperfections in cold-formed steel members refer to the deviations of an actual member from a "perfect" geometry. These imperfections include bowing, warping, or twisting of a member, as well as local imperfections such as dents, and plate waviness. As a matter of fact, the strength of a cold-formed steel member is influenced by imperfections.

A milling machine and a lathe are used to take imperfection measurements of specimens with different lengths. There are rulers in vertical, lateral and longitudinal directions of the milling machine, which help locate the measuring positions. When the available milling machines is not long enough, specimens can be measured on a lathe or in several passes on the milling machine.

A.1.1 Imperfection Measurement Setup on a Milling Machine

Specimens were mounted on the table of a milling machine, which provided a flat reference surface for the imperfection measurements. The collet of the milling machine could move vertically, laterally, and longitudinally, which enabled the imperfection measurements of different lines along the length of the specimens. A DC-DC Linear Variable Differential Transformer with a measurement range of ± 0.05 inches was attached firmly to the collet of the milling machine. Imperfection data were recorded in a

computer at a constant interval. Figures A.1 shows the experimental setup.

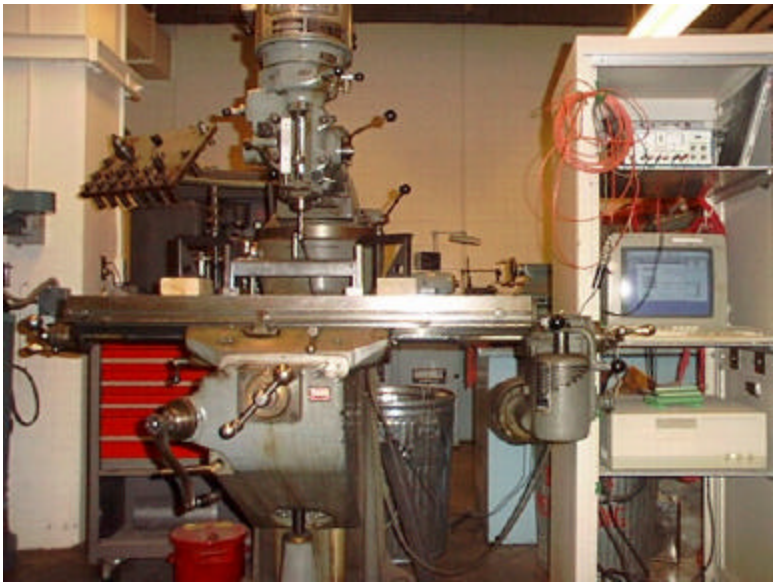

Figure A.1 Imperfection Experimental Setup

A.1.2 Imperfection Measurement Setup on a Lathe

Two end plates of specimens were clamped to the chuck end supports of a lathe. They were centered with respect to the centroid of the specimen cross section. Because there was no ruler in a lathe, grids need to be marked to locate measuring positions. A marker was attached to the tool support, which was moved horizontally to mark lines. In order to mark vertical lines to these horizontal lines, plastic rulers were stuck to the top of the specimen with tape. A center head of a combination square set was used to mark the vertical lines on two sides of the cross section with the alignment of the vertical lines on the top. Thus, a grid with the interval of 1 inch was marked before measuring the imperfections, as shown in Figure A.2. A DCDT (with $\pm 0.05''$ measuring range) was mounted on the tool support of the lathe. The tool support was moved horizontally to position the DCDT at 1 inch intervals

along each horizontal line. The DCDT can be adjusted up and down, back and forth to measure imperfection of different sides of the cross section. The measuring system, comprised of an IBM- PC clone computer, an NI-LPC 16 channel data acquisition card, and a power supply was monitored while the DCDT initial position was set. The horizontal positioner for the tool support was used to move the DCDT from position to position for measurements, as shown in Figures A.3. The data acquisition program stored the data in a file. Measurements were made at 1 inch increments horizontally along 3 lines on each outside surface of the specimen. With the lathe, imperfections of longer specimens can be measured. But when specimens are longer than the lathe, we can measure the specimen in several segments by measuring one segment and repositioning the specimen on the milling machine bed to measure the next segment.

A.1.3 Imperfection Measurement Setup on a Milling Machine for Long Specimens

As you can see from Figures A.4 and A.5 that specimens are much longer than the length of the moveable bed of the milling machine. Imperfections of two or more segments of the specimen can be measured. The specimen was put on top of two supports, which firmly stood on the milling machine. Four clamps were used to attach the specimen to the supports in A.6. There are also four alignment pins on the supports, with two on each support. When the one side of the specimen was measured, the other side of the specimen was leaning along the two alignment pins, shown in Figure A.7. After the imperfections of the first half were taken, the specimen slid

longitudinally along the four alignment pins. Thus, the twists and lateral movements of the specimens were prevented.

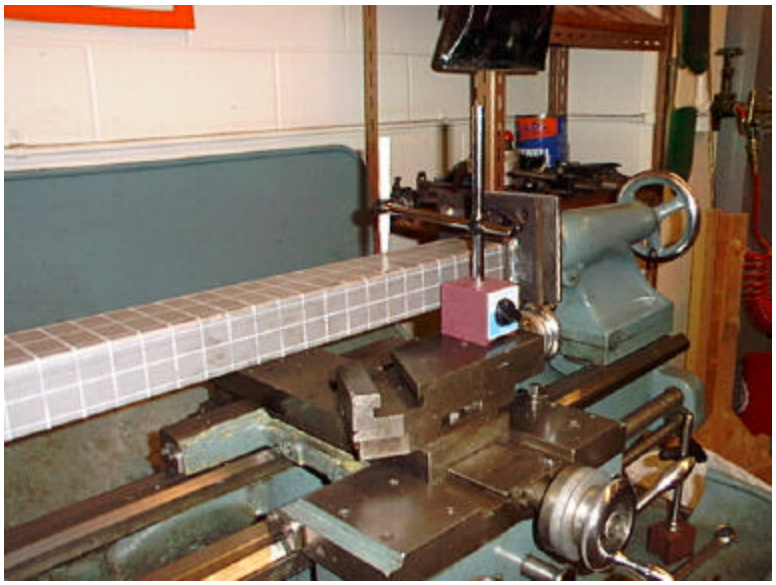

Figure A.2 Marking Grids

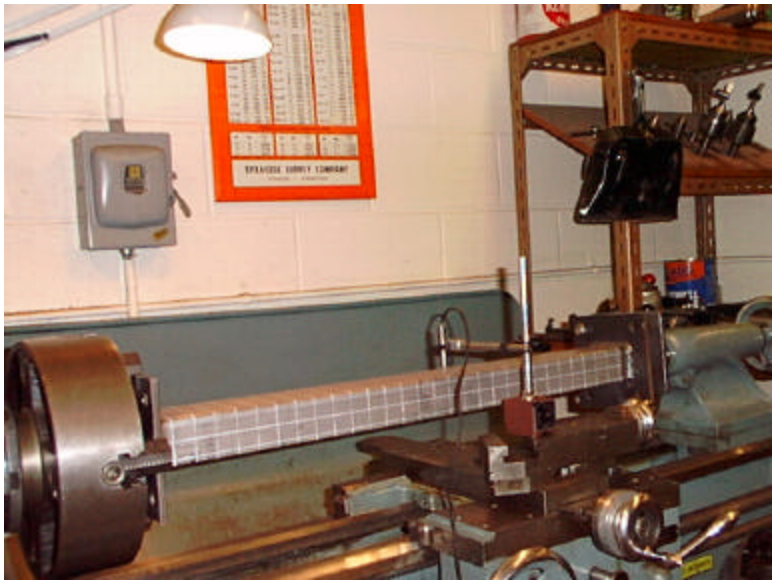

Figure A.3 Measuring Imperfections
in the Middle of the Specimen

Figure A.4 First Half of Imperfection Measuring

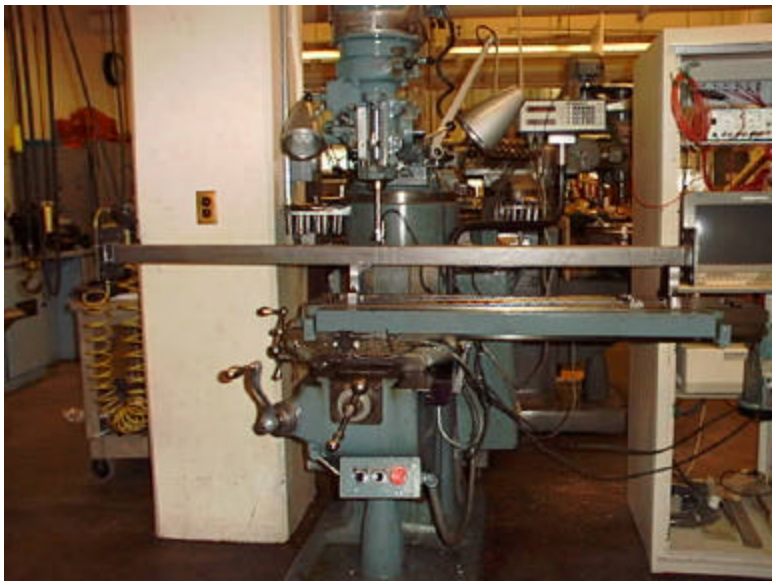

Figure A.5 Second Half of Imperfection Measuring

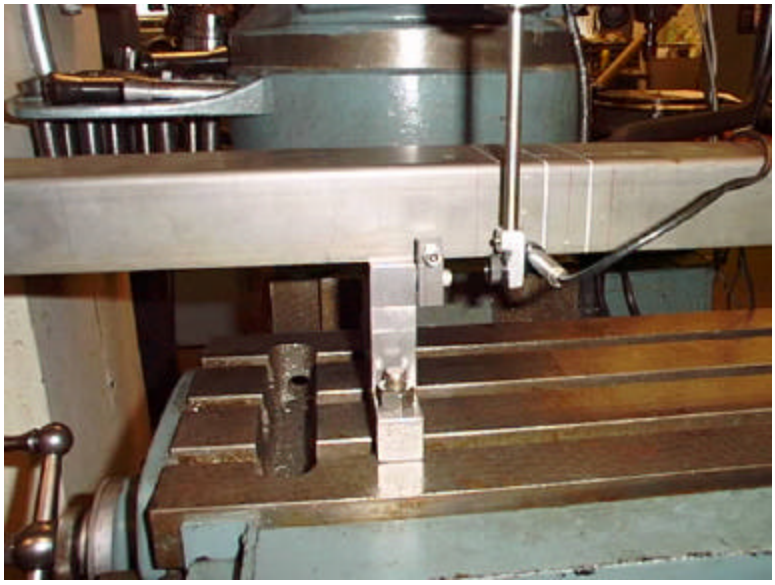

Figure A.6 One Side of the Specimen Imperfection Measuring with Clamps and Supports

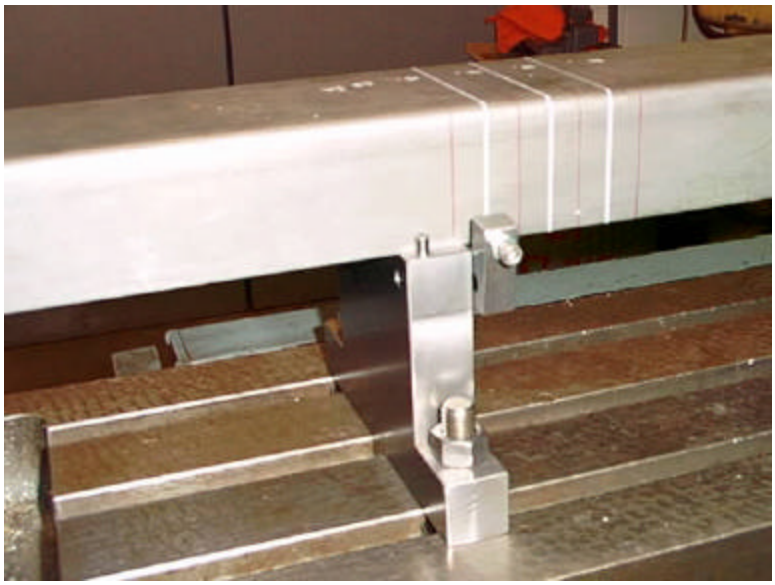

Figure A.7 The Other Side of the Specimen Imperfection Measuring with Alignment Pins, Clamps and Supports

Appendix B: Geometric Imperfection Studies

Several researchers have investigated geometric imperfections of cold-formed steel plain channels: Mulligan & Pekoz(1983), Ben Young(1998). All the researchers reported the maximum imperfections. These data are used in this study. Moreover, imperfections are measured before beam and beam-column tests by Fang Yiu & Pekoz(2000) to understand the magnitude of imperfections and the variation of plate imperfections in the cross section as well as along the length.

Two types of geometrical imperfections are found in the experimental data. In Part B.1.1 and B.1.2, random variable nature of the two types of the maximum imperfections are studied and the maximum imperfection models are established in Part B.1.3. The random process nature of the imperfection distribution is found in Part B.1.4 and the average imperfection spectrums for web and flanges are provided in Part B.1.5. Using the results from B.1.3 and B.1.5, random nature of the plain channel members subjected to three beam-column load conditions are studied in Part B.1.7.

B.1.1 Two Types of Maximum Geometrical Imperfections

Maximum imperfections can be used as upper bounds of imperfection magnitude. Two types of imperfections are found in existing measuring data, which are shown in Figure B.1.1. Type I imperfection refers to the maximum local imperfection in a stiffened element, while Type II imperfection refers to the maximum deviation from straightness for an unstiffened flange.

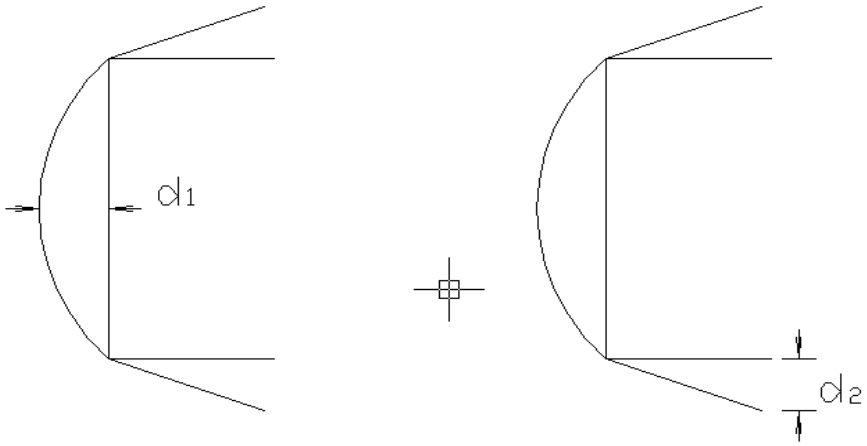

Type I Imperfection Type II Imperfection

Figure B.1.1 Two Types of Maximum Geometrical Imperfections

B.1.2 Correlation between Type I Imperfection and Type II Imperfection

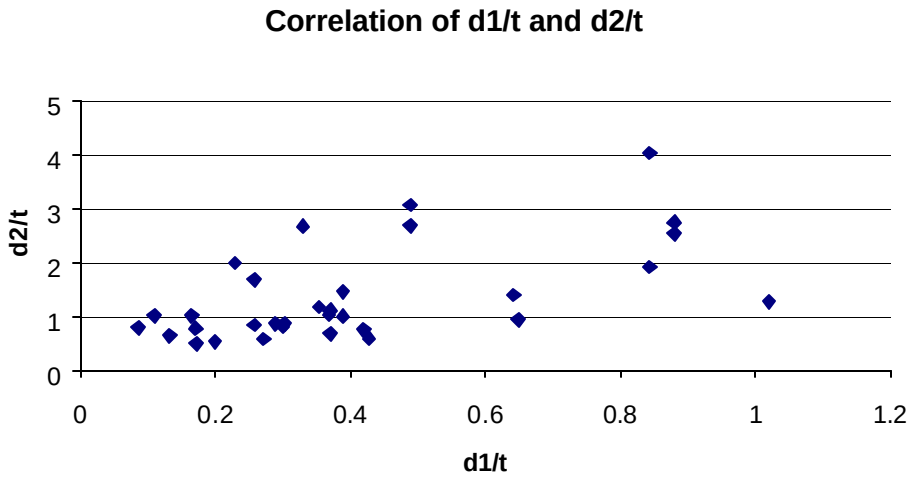

Figure B.1.2 Correlation between Type I and Type II Imperfection

Type I and II imperfection data from Mulligan & Pekoz, Ben Young, and Fang

Yiu & Pekoz are plotted in Figure B.1.2, which display the correlation between Type I and Type II imperfection. The correlation coefficient of d_1/t and d_2/t is

$$r_{d_1/t,d_2/t} = \frac{Cov(d_1/t, d_2/t)}{s_{d_1/t} s_{d_2/t}} = 0.5546$$

This shows that Type I and Type II imperfections do not have strong linear relationship.

B.1.3 Treat the Magnitude of Imperfections as a Random Variable

As imperfections are inevitably influenced by a variety of variables such as forming process and material handling, it is appropriate to treat imperfections as a random variable.

B.1.3.1 Prediction of Type I Imperfections as a Function of Thickness

Type I imperfection d_1 is normalized by the plate thickness t. The histograms of Type I imperfections are given in Figure B.1.3.

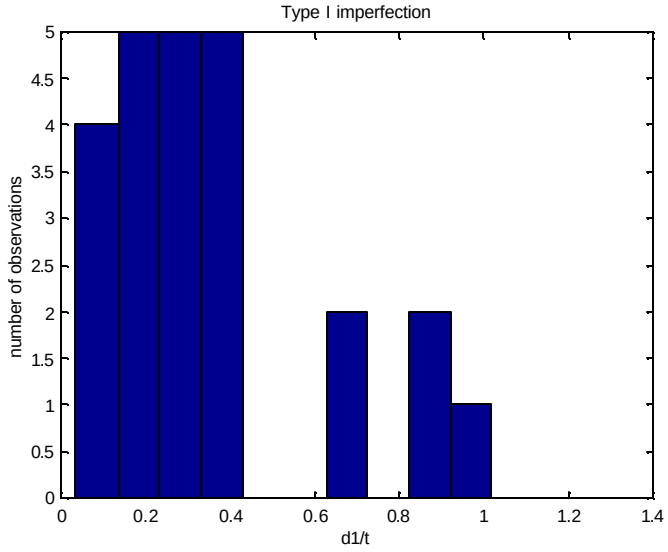

Figure B.1.3 Histograms of Type I Imperfection

Type I imperfections is assumed to be a function of the material thickness alone as it is of local imperfections. As only a few analyses can be performed, cumulative distribution function (CDF) is very useful. CDF 25 indicates cumulative distribution function is at 25% level, or imperfection magnitude of 75% probability of exceedance. The numerically estimated CDF for Type I imperfections is shown in Figure B.1.4.

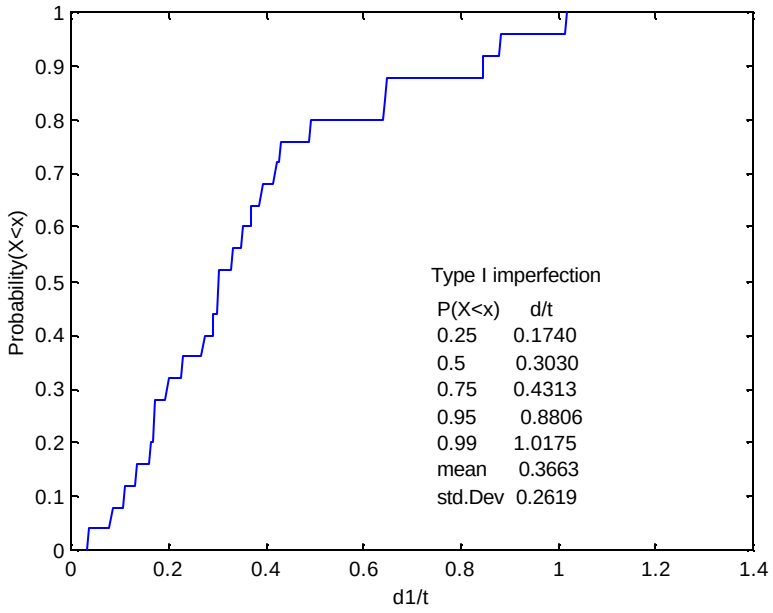

Figure B.1.4 Estimated CDF for Type I Imperfection

B.1.3.2 Prediction of Type II Imperfections a Function of Flange Slenderness

Type II imperfection d_1 is normalized by the plate thickness t and the histograms of Type II Imperfections are given in Figure B.1.5. The difference between the two types of imperfections is obvious in histograms.

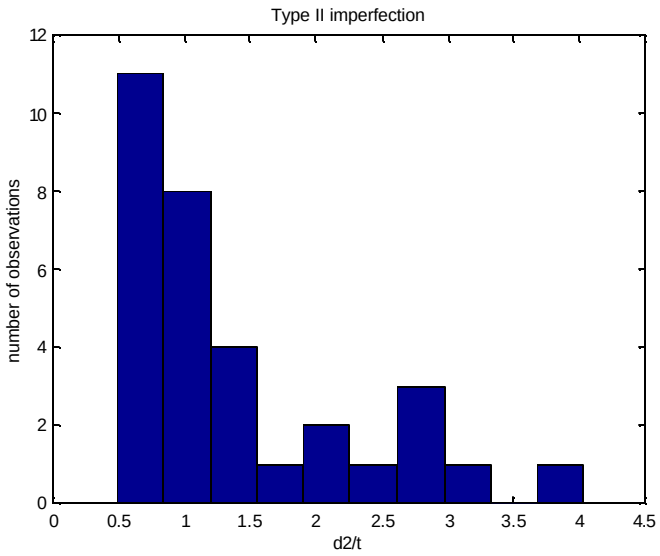

Figure B.1.5 Histograms of Type II Imperfection

Type II Imperfection in an unstiffened element is actually a function of flange slenderness and not only that of the thickness. The following is a brief description of the Type II imperfection model.

B.1.3.2.1 Description of Method

All available experimental measurements of Type II imperfection are plotted in Figure B.1.6. These data are grouped into four sets according to different flange slenderness. Histograms of four sets of $\frac{\frac{d_2}{t} - m}{s}$ with varying mean m and standard deviation s according to different flange slenderness can be obtained, where $\frac{\frac{d_2}{t} - m}{s}$ is a random variable with zero mean and unit variance. Combining these four histograms together, we get Figure B.1.7. The mean value and standard deviation of Type II imperfection are obtained by least-squares linear regression line in Figures B.1.8 and B.1.9, respectively.

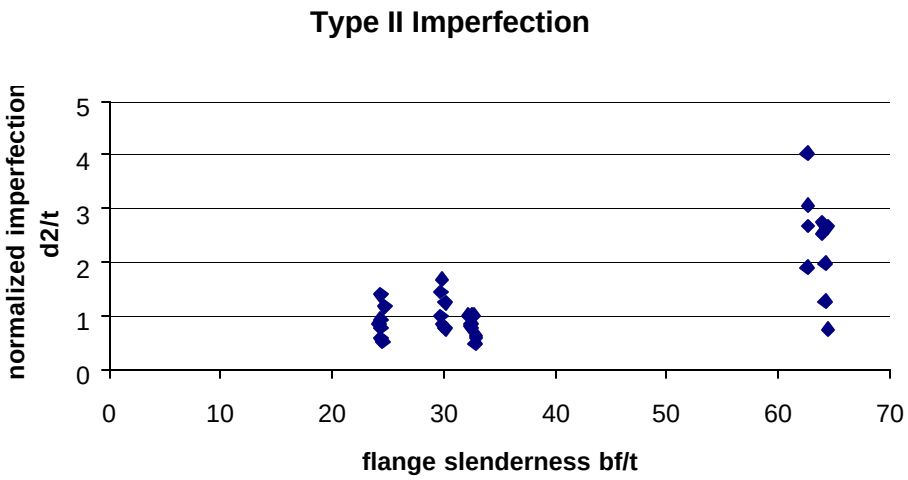

Figure B.1.6 All Available Experimental Measurement

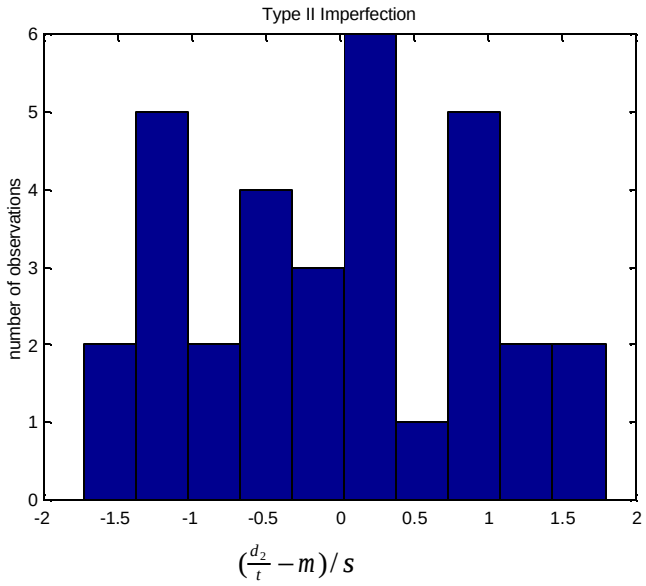

Figure B.1.7 Histogram of $\frac{\frac{d_2}{t}-m}{s}$ for

All Available Experimental Measurement

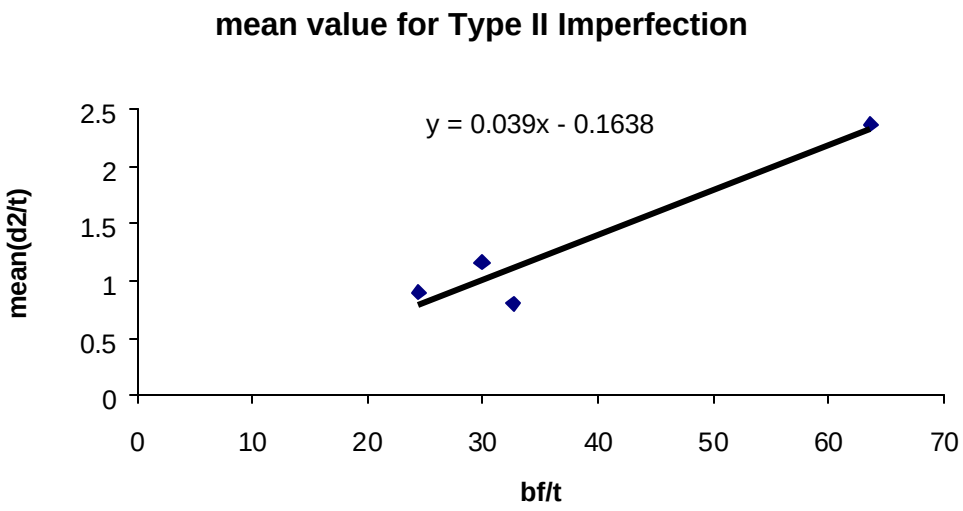

Figure B.1.8 Mean Value of Type II Imperfection

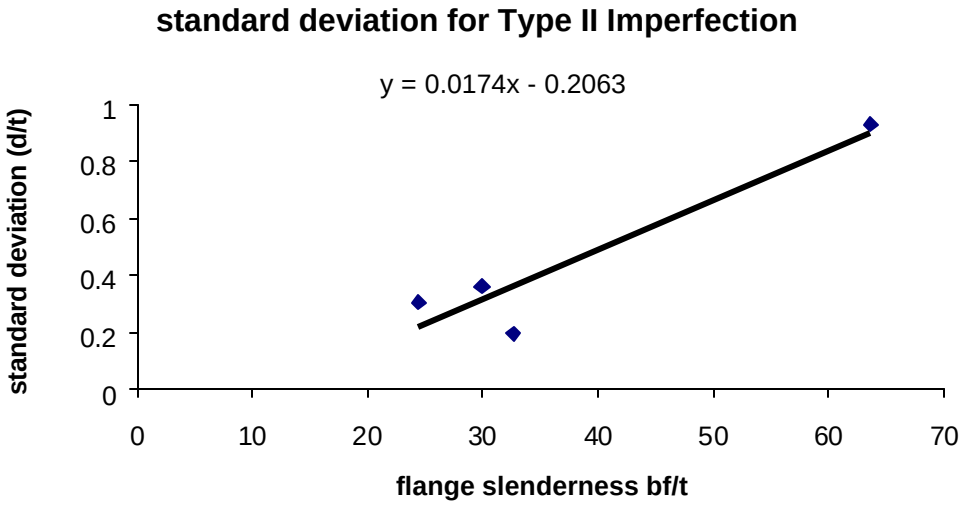

Figure B.1.9 Standard Deviation of Type II Imperfection

B.1.3.2.2 Type II Imperfection Model

The numerically estimated cumulative distribution function (CDF) for Type II Imperfections can be obtained and is shown in Figure B.1.10. Type II imperfection model d_2/t is therefore developed:

cdf25: $[0.039(bf/t) - 0.1638]+(-0.8617)[\ 0.0174(bf/t) - 0.2063]$

cdf50: $[0.039(bf/t) - 0.1638]+(\ 0.0643)[\ 0.0174(bf/t) - 0.2063]$

cdf75: $[0.039(bf/t) - 0.1638]+(\ 0.7698)[\ 0.0174(bf/t) - 0.2063]$

where, d_2 is the maximum magnitude of Type II imperfection; t is the plate thickness; bf is the flange width.

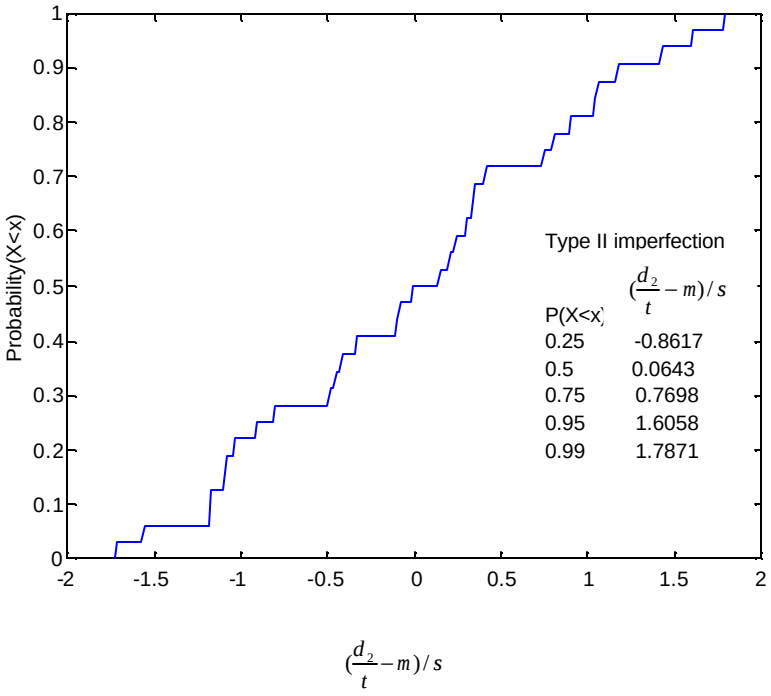

Figure B.1.10 Estimated CDF for Type II Imperfections

B.1.4 Treat the Distribution of Imperfections as a Random Process

Imperfections of three 30in long plain channel columns with the dimensions of 3.2x2.0x0.072 inch are measured. The spacing of the measurements is 1 inch for all three specimens. Nine lines along the length are measured starting from the same plane of cross section to understand the deviation of the imperfections in the cross sections as well as along the length, as shown in Figure B.1.11. These plain channel members are industry interested cross-sections. Thus the imperfection measurements represent the real imperfection pattern in practical cross sections.

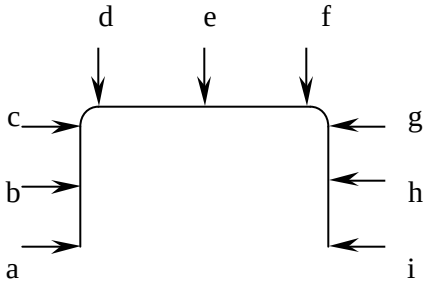

Figure B.1.11 Nine Measurements of a Cross Section

Local imperfections are deviations from a perfect geometry. In order to study local imperfections, the imperfection signals are obtained by subtracting a least-squares linear regression line from the raw imperfection data. The Fast Fourier transformation results of the imperfection signals are shown in Figures B.1.12, B.1.13 and B.1.14. These transforms plot the imperfection frequency(1/mm) versus the imperfection amplitude(mm). The transform reveals both the amplitude and frequency of the underlying sine curve.

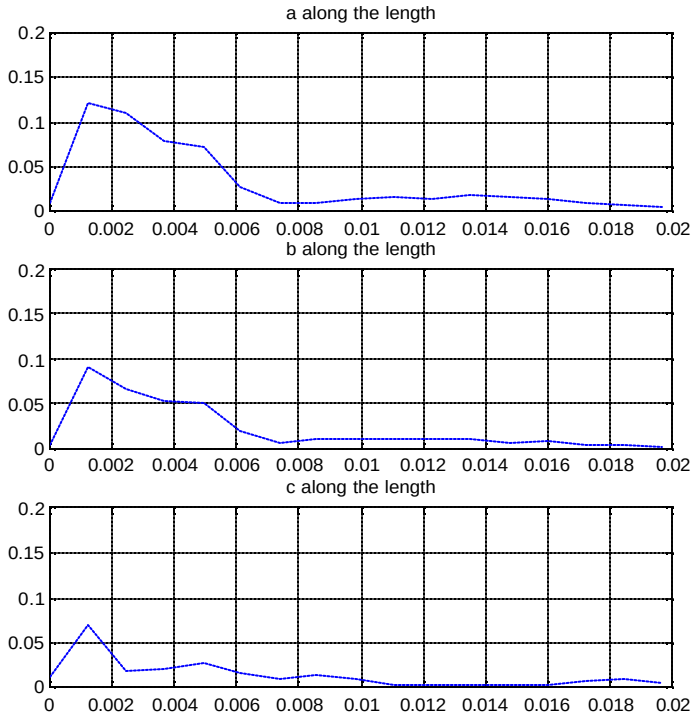

Figure B.1.12 Fourier Transform of Imperfections along Line a, b and c

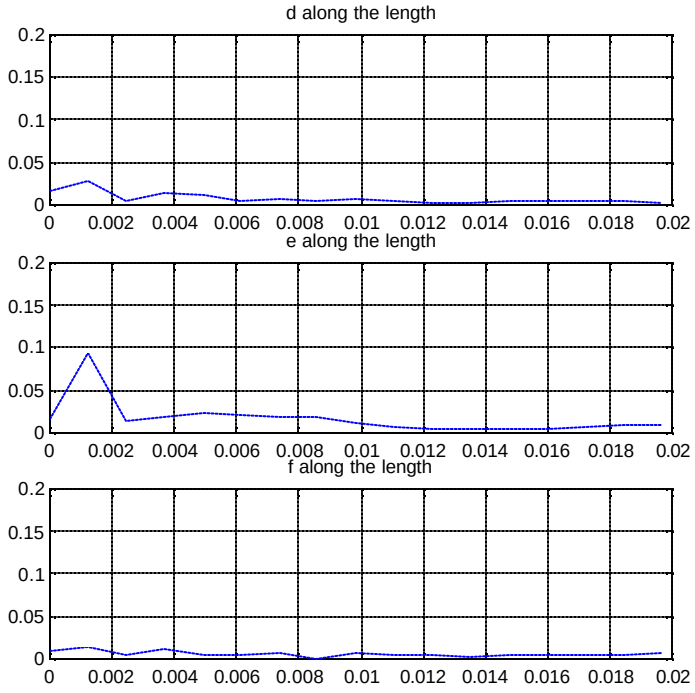

Figure 4.1.13 Fourier Transform of Imperfections along Line d,e, and f

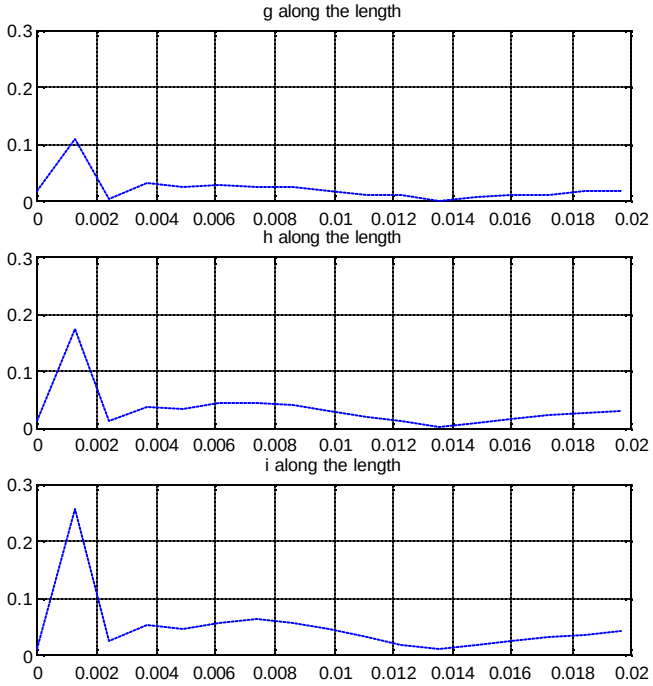

Figure B.1.14 Fourier Transform of Imperfections along Line g, h and i

From the above analysis, it is observed that:

1) Local imperfections of these members are summations of sine terms with an appropriate amplitudes, frequency, and phase shift. The imperfection signal can be expressed in: $X(t) = \sum_{k=1} s_k (A_k \cos w_k t + B_k \sin w_k t)$

2) Imperfections in web and flanges have different patterns. Imperfections in two flanges are not geometrically symmetric, shown in Figure B.1.15.

3) Imperfections in the flange can be assumed to be linear, as shown in Figure B.1.15.

4) Imperfections in the web can be assumed to be symmetric. Imperfections between the web junctions and the mid-height of the web can be assumed to

be linear, as shown in Figure B.1.15.

5) Global imperfections, such as overall twist are not considered.

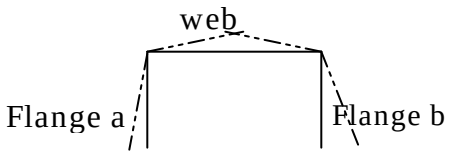

Figure B.1.15 Perfect Geometry and Deformed Shape

B.1.5 Average Imperfection Spectrum for Plain Channels

The imperfection spectrums characterizing imperfections of plain-channels specimens are created from actual imperfection measuring data. As imperfections in web and flanges have different distributions, average web imperfection spectrum and average flange imperfection spectrum are created in Figure B.1.16 and Figure B.1.17, respectively. Influential imperfections in web as well as in flange are listed in Tables B.1 and B.2, respectively.

B.1.5.1 Average Web Imperfection Spectrum

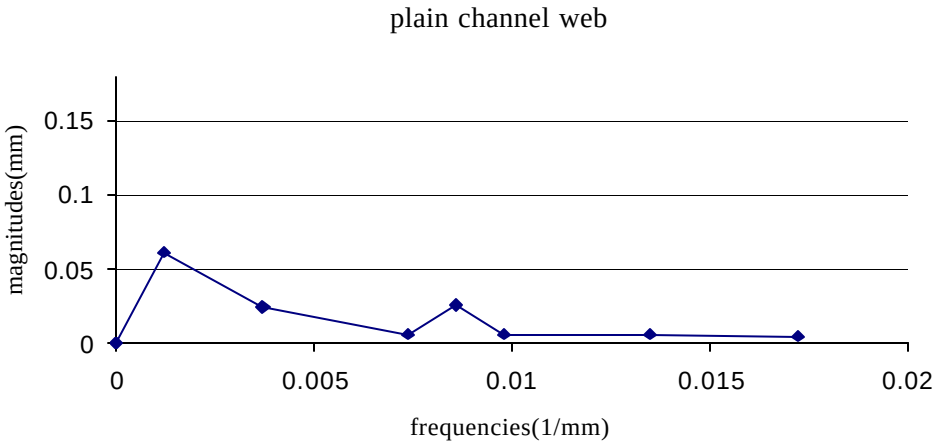

Figure B.1.16 Average Web Imperfection Spectrum

Table B.1 Web Influential Imperfections
in Web Imperfection Spectrum(Figure B.1.16)

Frequencies(1/mm)	Magnitudes(mm)
0.0012	0.0623
0.0037	0.0244
0.0074	0.0061
0.0086	0.0261
0.0098	0.0064
0.0135	0.0063
0.0172	0.0050

B.1.5.2 Average Flange Imperfection Spectrum

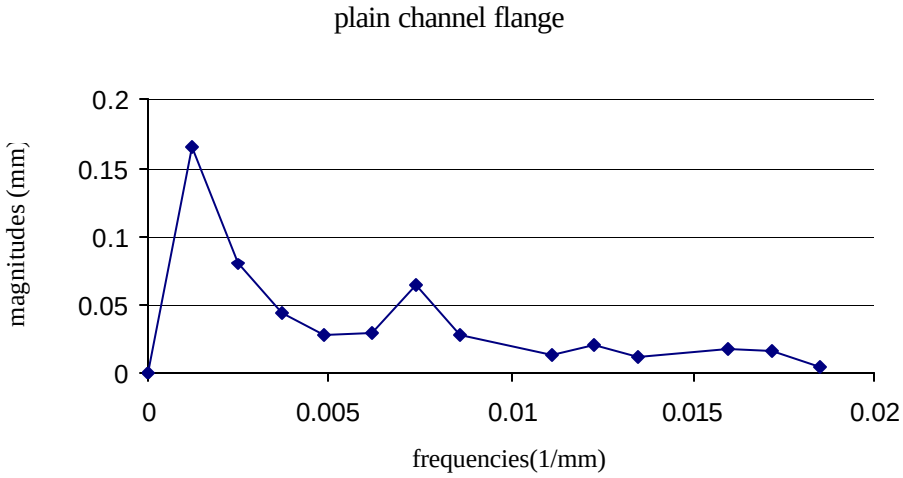

Figure B.1.17 Average Flange Imperfection Spectrum

Table B.2 Flange Influential Imperfections
in Flange Imperfection Spectrum(Figure B.1.17)

Frequencies(1/mm)	Magnitudes(mm)
0.0012	0.1646
0.0025	0.0798
0.0037	0.0442
0.0049	0.0270
0.0062	0.0293
0.0074	0.0644
0.0086	0.0282

0.0111	0.0135
0.0123	0.0200
0.0135	0.0121
0.0160	0.0168
0.0172	0.0163
0.0185	0.0038

The imperfection spectrums can be used to generate the imperfection signal, which is able to characterize the random process nature of the distribution.

B.1.6 Generating Imperfection Signal by Imperfection Spectrum

B.1.6.1 Probabilistic Model:

Longitudinal imperfection signal is assumed to be zero mean, real valued stationary Gaussian stochastic process. Imperfection signal has a one-sided spectral density, $G(w)$, where w is the circular frequency $w = 2pf$. In general the imperfection signal has a spectral representation that may be given as:

$$X(t) = \int_0^\infty [\cos wtdU(w) + \sin wtdV(w)]$$

where, $U(w)$ and $V(w)$ are zero-mean, real-valued, independent Gaussian process with the properties $E[dU^2(w)] = E[dV^2(w)] = G(w)dw$. For simulation we discretize to approximate this process with one-sided truncated power spectral density, $\tilde{G}(w) = \begin{cases} G(w), & 0 \le w \le \tilde{w} \\ 0, & w > \tilde{w} \end{cases}$, as shown in Figure B.1.18.

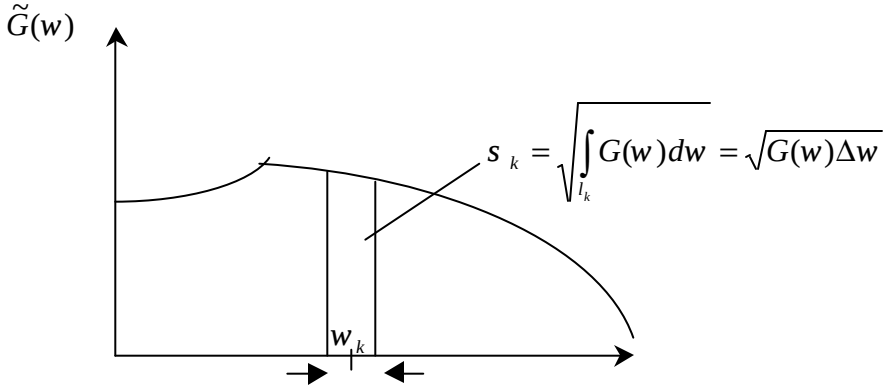

Figure B.1.18 Discretization of Imperfection Spectrum

The stochastic process X(t) can be approximated as

$$X(t) = \sum_{k=1}^{m} s_k (A_k \cos w_k t + B_k \sin w_k t)$$

where, A_k and B_k are independent Gaussian random variables with zero means and unit variance.

B.1.6.2 Generation of imperfection signal

Based on the obtained average imperfection spectrums in Part B.1.5, the imperfection signal $X(t) = \sum_{k=1}^{m} s_k (A_k \cos w_k t + B_k \sin w_k t)$ can be generated, in which the circular frequency $w = 2pf$, where f is the frequency (1/mm). Then truncate the spectrum and discretize it into m pieces. The area under each m piece is equal to s_k^2. m sets of A_k and B_k can be generated by randn.m in Matlab built-in function. By following this procedure, one realization of scaled Flange a imperfection signal, scaled Flange b imperfection signal and scaled web imperfection signal is shown in Figures B.1.19, B.1.20 and B.1.21, respectively.

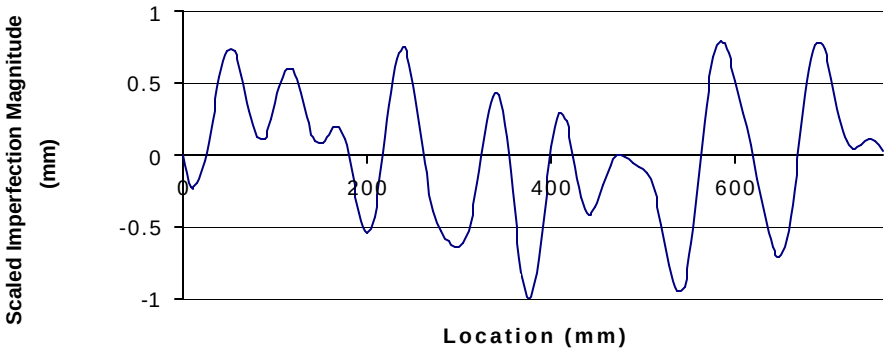

Figure B.1.19 Flange a Imperfection Signal

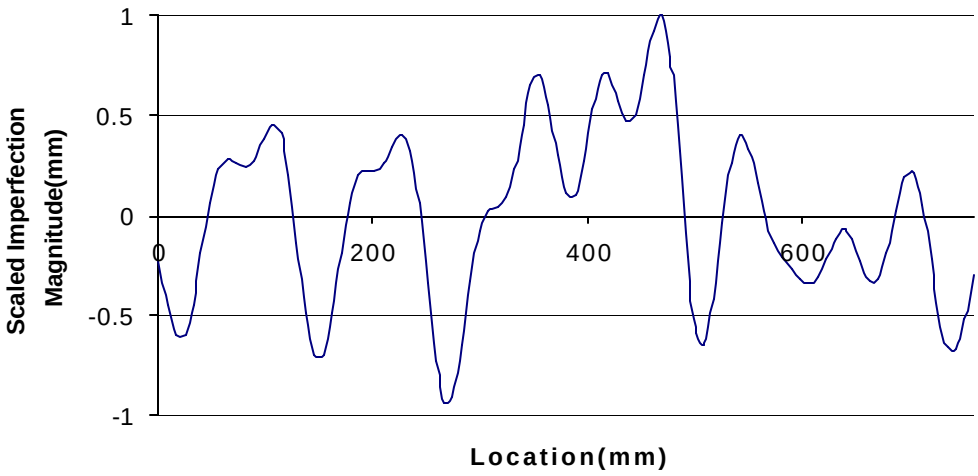

Figure B.1.20 Flange b Imperfection Signal

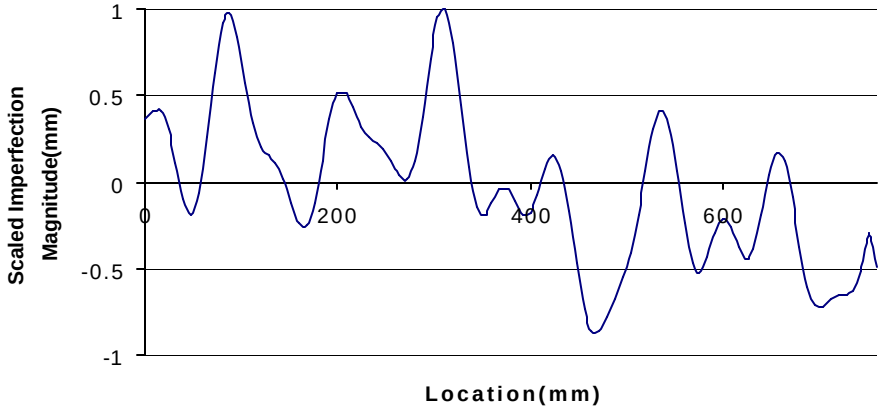

Figure B.1.21 Web Imperfection Signal

B.1.7 Imperfection Sensitivity Studies

For the above-mentioned three beam-column load cases, 30in long plain channel columns with the dimensions of 3.2x2.0x0.072 inch are selected for examining the influence of imperfection distribution and magnitude at the same time. A random imperfection signal can be generated from the obtained imperfection spectrums in Part B.1.5. The maximum of the web imperfection signal and the flange imperfection signal can be generated from the maximum type I and type II imperfections models in Part B.1.3. The spatial mapping of the variation of the imperfection distribution is shown in Figure B.1.15. Two different cumulated distribution functions (CDF value)-- cdf25 and cdf75 are used. Thus the strength loss due to imperfections can be systematically assessed. The ultimate strength (P_u / P_y) from the Abaqus analysis is listed in Tables B.3, B.4 and B.5. Imperfection sensitivity index is defined as:

$$\frac{2(P_{cdf25} - P_{cdf75})}{(P_{cdf25} + P_{cdf75})} \text{x}100\%$$

In order to study imperfection effect on the ultimate strength, three load cases shown in Figure B.1.22 are studied.

Case 1: Axial Loading with Bending about Symmetry Axis

Case 2: Axial Loading with Bending about the Centroidal Axis Perpendicular to the Symmetry Axis

Case 3: Axial Loading with Biaxial Bending

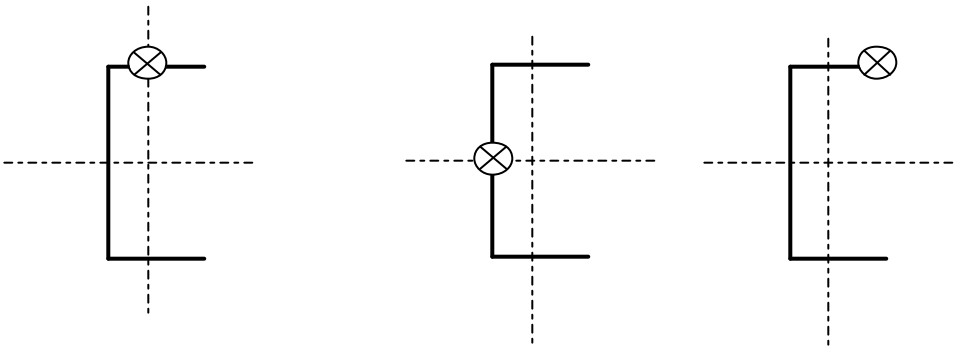

Load Case 1 Load Case 2 Load Case 3

Figure B.1.22 Load Cases

For each load case, 30 numbers of imperfection signals were generated. The loss in strength is more pronounced when the imperfection magnitude is increased. The numerically estimated cumulative distribution function (CDF) for the ultimate strength of three different load cases is shown in Figures B.1.23, B.1.24 and B.1.25. It is obvious from these figures that imperfection distribution and magnitude do result in different strength loss. Gaussian distribution is assumed for the ultimate load. For each load case, histograms, Gaussian distribution density function and imperfection sensitivity index are shown in Figures B.1.26, B.1.27 and B.1.28.

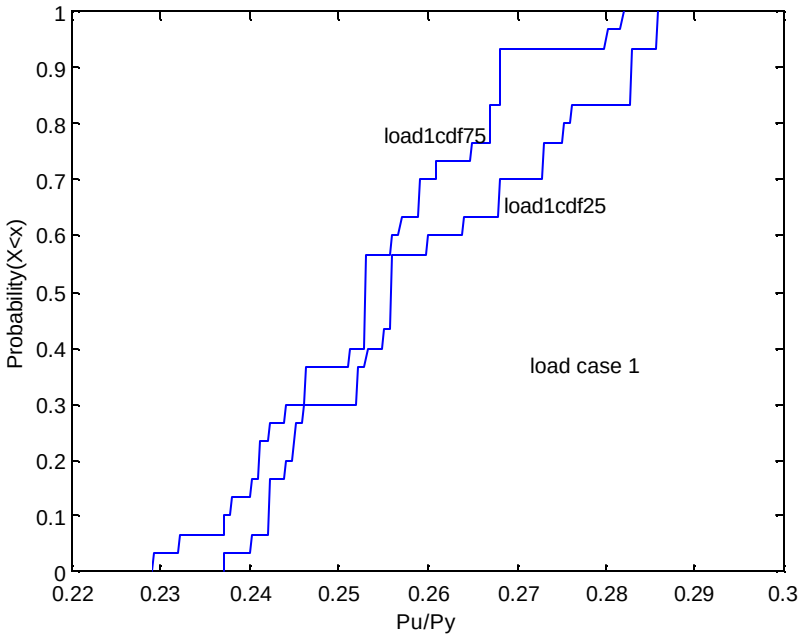

Figure B.1.23 CDF for Load Case 1

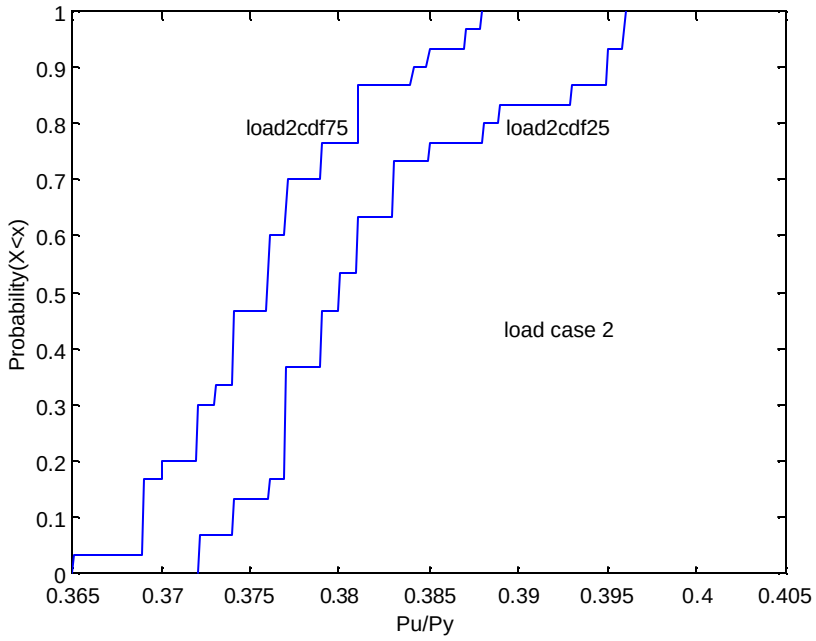

Figure B.1.24 CDF for Load Case 2

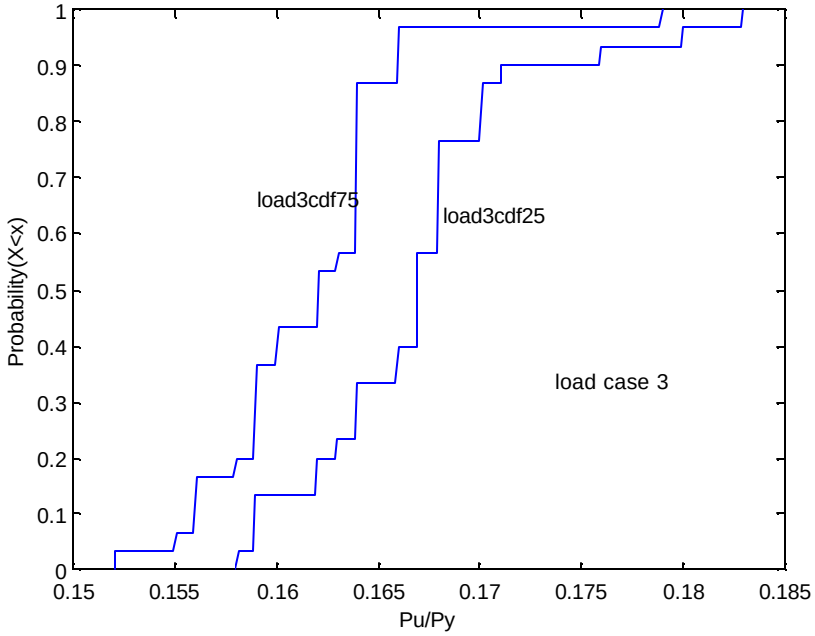

Figure B.1.25 CDF for Load Case 3

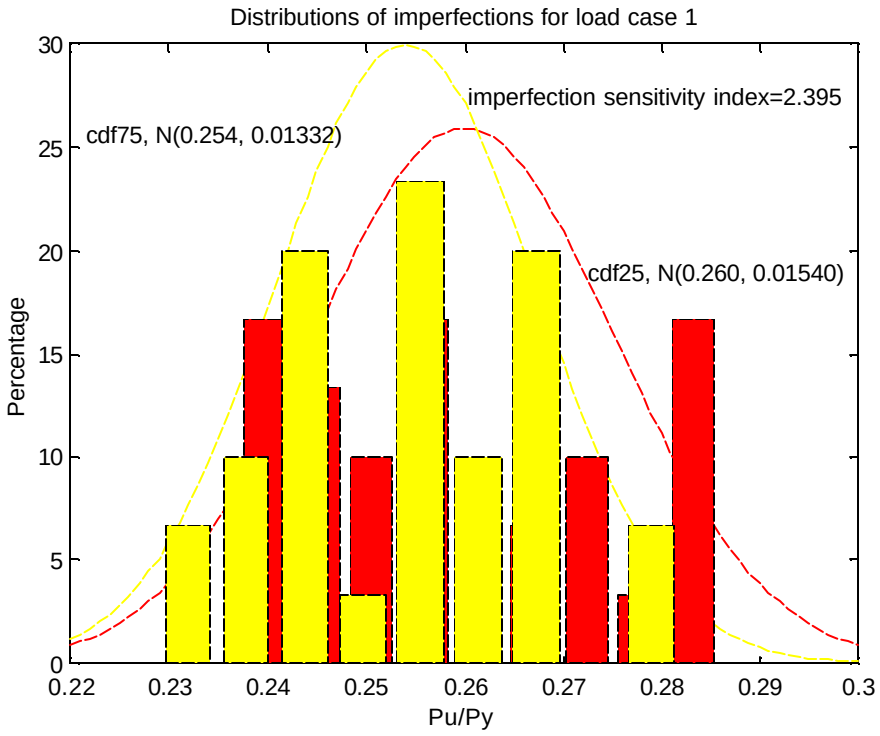

Figure B.1.26 Histogram, Gaussian Distribution Density Function and Imperfection Sensitivity Index for Load Case 1

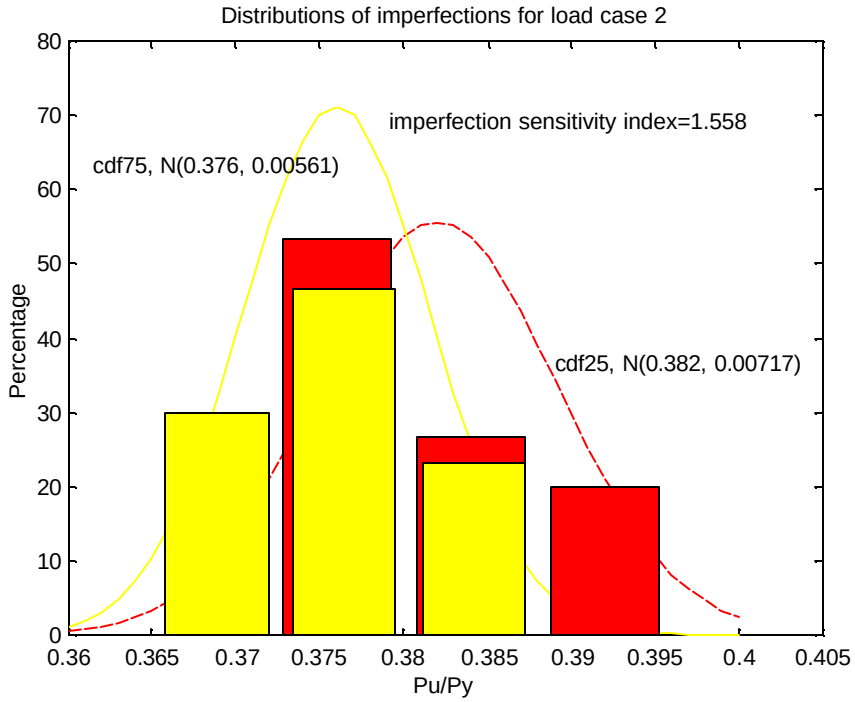

Figure 4.1.27 Histogram, Gaussian Distribution Density Function and Imperfection Sensitivity Index for Load Case 2

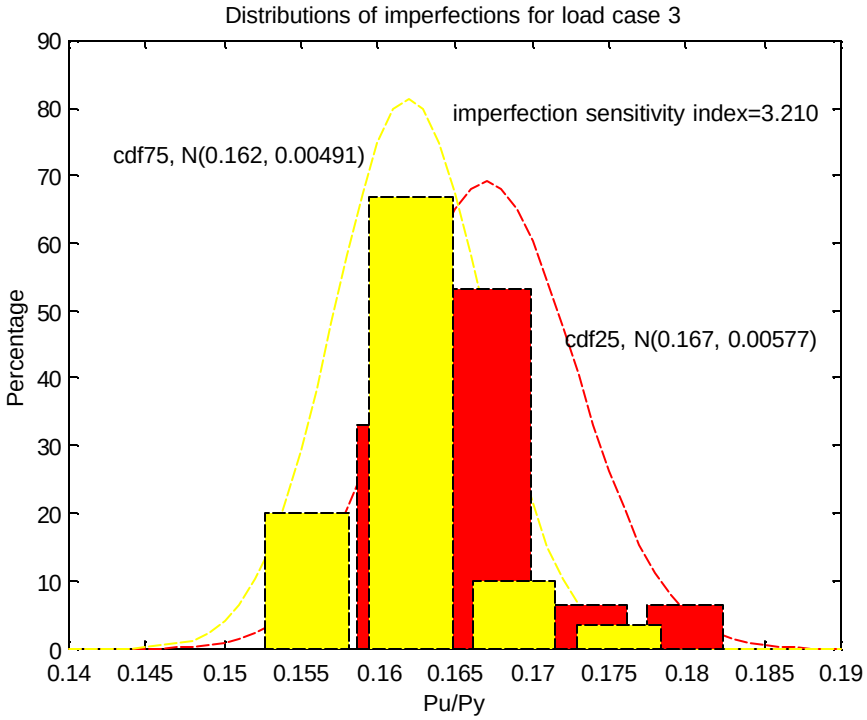

Figure B.1.28 Histogram, Gaussian Distribution Density Function and Imperfection Sensitivity Index for Load Case 3

The random process nature of the distribution and random variable nature of the maximum imperfection are considered at the same time to properly assess the importance of the imperfection sensitivity. From Figures B.1.26, B.1.27 and B.1.28, it is found that a member with large initial imperfections has a larger strength loss. Among these three load cases, load case 3-- axial loading with biaxial bending has the largest imperfection sensitivity index 3.210; load case 2-- axial loading with bending about the centroidal axis perpendicular to the symmetry axis has the least imperfection sensitivity index 1.558. However, all three load cases do not exhibit significant imperfection sensitivity. The ultimate strength is also influenced by imperfection distribution. Varying the imperfection distribution determines the scatter of resulting strength for a particular magnitude of imperfection. However, the most significant factor of strength is still the imperfection magnitude.

B.1.8 Conclusions

The imperfection magnitude is modeled using the maximum imperfection models in Part B.1.3. The imperfection distribution is modeled by the imperfection spectrum in Part B.1.5. The imperfection sensitivity of plain channel members subjected to three different beam-column load conditions is studied. It shows that plain channel sections are not imperfection-sensitive cross-sections and the use of the eigenmode imperfection pattern is sufficient. The lowest eigenmode is selected for the imperfection distribution. Maximum type II imperfection magnitude at the

cdf50 (imperfection magnitude of 50% probability of exceedance) is used for the imperfection magnitude.

d_2 / t at cdf50 is [0.039(bf / t) - 0.1638]+(0.0643)[0.0174(bf / t) - 0.2063],

where, d_2 is the maximum magnitude of Type II imperfection; t is the plate thickness; bf is the flange width.

Table B.3 Imperfection Studies on Load Case 1

Load Case 1	cdf25 Pu(N)	cdf75 Pu(N)	Imperfection Sensitivity Index	cdf25 Pu / Py	cdf75 Pu / Py
load1_input1	18000	17900	0.557	0.242	0.241
load1_input2	19000	18800	1.058	0.256	0.253
load1_input3	18000	17900	0.557	0.242	0.241
load1_input4	18800	18600	1.070	0.253	0.251
load1_input5	19900	19700	1.010	0.268	0.265
load1_input6	20400	19100	6.582	0.275	0.257
load1_input7	19000	18800	1.058	0.256	0.253
load1_input8	21000	19900	5.379	0.283	0.268
load1_input9	17600	17200	2.299	0.237	0.232
load1_input10	19300	19200	0.519	0.260	0.259
load1_input11	18000	17800	1.117	0.242	0.240
load1_input12	18700	18300	2.162	0.252	0.246
load1_input13	21200	20800	1.905	0.286	0.280
load1_input14	20300	19400	4.534	0.273	0.261
load1_input15	18300	18000	1.653	0.246	0.242
load1_input16	20500	19800	3.474	0.276	0.267
load1_input17	21000	19800	5.882	0.283	0.267
load1_input18	18200	17000	6.818	0.245	0.229
load1_input19	19000	18800	1.058	0.256	0.253
load1_input20	18200	18100	0.551	0.245	0.244
load1_input21	20300	19900	1.990	0.273	0.268
load1_input22	19900	19900	0.000	0.268	0.268
load1_input23	18900	18800	0.531	0.255	0.253
load1_input24	18700	18300	2.162	0.252	0.246
load1_input25	21000	19200	8.955	0.283	0.259

load1_input26	21200	20900	1.425	0.286	0.282
load1_input27	19000	18800	1.058	0.256	0.253
load1_input28	18100	17700	2.235	0.244	0.238
load1_input29	19600	19000	3.109	0.264	0.256
load1_input30	17800	17600	1.130	0.240	0.237

Table B.4 Imperfection Studies on Load Case 2

Load Case 2	cdf25 Pu(N)	cdf75 Pu(N)	Imperfection Sensitivity Index	cdf25 Pu / Py	cdf75 Pu / Py
load3_input1	28000	28000	0.000	0.377	0.377
load3_input2	28000	27700	1.077	0.377	0.373
load3_input3	27800	27600	0.722	0.374	0.372
load3_input4	28100	28000	0.357	0.379	0.377
load3_input5	27600	27400	0.727	0.372	0.369
load3_input6	27600	27100	1.828	0.372	0.365
load3_input7	28600	28600	0.000	0.385	0.385
load3_input8	28000	27400	2.166	0.377	0.369
load3_input9	27900	27800	0.359	0.376	0.374
load3_input10	28200	28000	0.712	0.380	0.377
load3_input11	28800	28500	1.047	0.388	0.384
load3_input12	28100	27900	0.714	0.379	0.376
load3_input13	28900	28300	2.098	0.389	0.381
load3_input14	28000	27900	0.358	0.377	0.376
load3_input15	29400	28800	2.062	0.396	0.388
load3_input16	28400	27500	3.220	0.383	0.370
load3_input17	28000	27800	0.717	0.377	0.374
load3_input18	28000	27400	2.166	0.377	0.369
load3_input19	29300	28100	4.181	0.395	0.379
load3_input20	28400	27800	2.135	0.383	0.374
load3_input21	29200	27900	4.553	0.393	0.376
load3_input22	28400	28300	0.353	0.383	0.381
load3_input23	28300	27900	1.423	0.381	0.376
load3_input24	28300	28300	0.000	0.381	0.381
load3_input25	28200	28100	0.355	0.380	0.379
load3_input26	27800	27400	1.449	0.374	0.369
load3_input27	28300	27800	1.783	0.381	0.374

load3_input28	29400	27600	6.316	0.396	0.372
load3_input29	29300	28700	2.069	0.395	0.387
load3_input30	28100	27600	1.795	0.379	0.372

Table B.5 Imperfection Studies on Load Case 3

Load Case 3	cdf25 Pu(N)	cdf75 Pu(N)	Imperfection Sensitivity Index	cdf25 Pu / Py	cdf75 Pu / Py
load2_input1	11800	11700	0.851	0.159	0.158
load2_input2	12200	11600	5.042	0.164	0.156
load2_input3	12200	11800	3.333	0.164	0.159
load2_input4	12600	12000	4.878	0.170	0.162
load2_input5	12500	12300	1.613	0.168	0.166
load2_input6	12600	11900	5.714	0.170	0.160
load2_input7	12700	11800	7.347	0.171	0.159
load2_input8	12300	12000	2.469	0.166	0.162
load2_input9	12400	12200	1.626	0.167	0.164
load2_input10	12300	11800	4.149	0.166	0.159
load2_input11	12500	12300	1.613	0.168	0.166
load2_input12	11800	11600	1.709	0.159	0.156
load2_input13	12500	12000	4.082	0.168	0.162
load2_input14	12400	12100	2.449	0.167	0.163
load2_input15	12000	11800	1.681	0.162	0.159
load2_input16	12500	12200	2.429	0.168	0.164
load2_input17	11700	11500	1.724	0.158	0.155
load2_input18	12400	12200	1.626	0.167	0.164
load2_input19	12200	11600	5.042	0.164	0.156
load2_input20	12600	12200	3.226	0.170	0.164
load2_input21	11800	11300	4.329	0.159	0.152
load2_input22	12400	12200	1.626	0.167	0.164
load2_input23	13400	13300	0.749	0.180	0.179
load2_input24	12400	12200	1.626	0.167	0.164
load2_input25	13600	12300	10.039	0.183	0.166

load2_input26	13100	12200	7.115	0.176	0.164
load2_input27	12500	12200	2.429	0.168	0.164
load2_input28	12100	11900	1.667	0.163	0.160
load2_input29	12000	11800	1.681	0.162	0.159
load2_input30	12500	12200	2.429	0.168	0.164

Appendix C: Design Recommendations

Design Recommendations for Plain Channels

The design recommendations for calculating the overall capacity of channel sections without lips (hereinafter-plain channels in Figure1) are applicable to cross-sections in the range of practical applications by the industry, namely $b_2 / b_1 \leq 1$.

The recommendations cover design of beams, columns and beam-columns. The recommendations treat members that are made up of elements that may or may not be in the post-buckling range. The failure mode for beams is local buckling. The recommendations consider the interaction between plates, and simple equations for plate buckling coefficients k are given for minor and major axis bending as well as for columns.

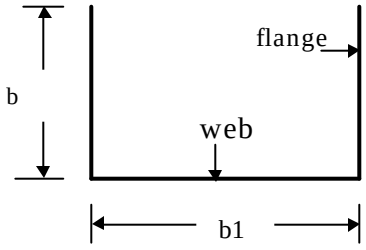

Figure 1

1.Notations

E = Modulus of Elasticity

u = Poisson's ratio

G = $\frac{E}{2(1+u)}$ = Shear Modulus

t = plate thickness

D = $\frac{Et^3}{12(1-u^2)}$ = plate rigidity

b_1 = Depth of web element

b_2 = Width of flange element

f_y = yield stress

f_{cr} = critical buckling stress of the cross-section

k_f = plate buckling coefficients considering interaction of plate elements in terms of flange width

k_w = plate buckling coefficients considering interaction of plate elements in terms of web depth

r = post-buckling reduction factor

l = slenderness factor

M_{ns} = nominal moment capacity

S_e = elastic section modulus of the effective section

C_y = compression strain factor

f_1 = maximum compressive (+) stress on an element under a stress gradient

f_2 = tension (-) stress for an element under a stress gradient

$y = \frac{f_2}{f_1}$

1. Elastic Buckling

1.1 Minor Axis Bending with Stiffened Element in Tension

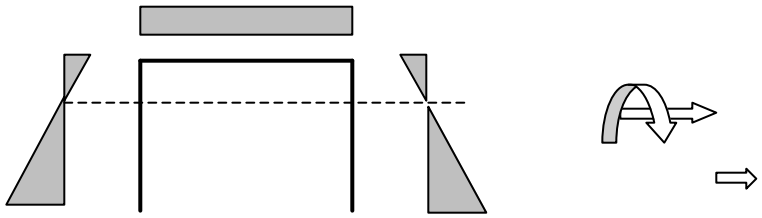

$$k_f = 0.1451\left(\frac{b_2}{b_1}\right) + 1.2555$$

1.2 Minor Axis Bending with Stiffened Element in Compression

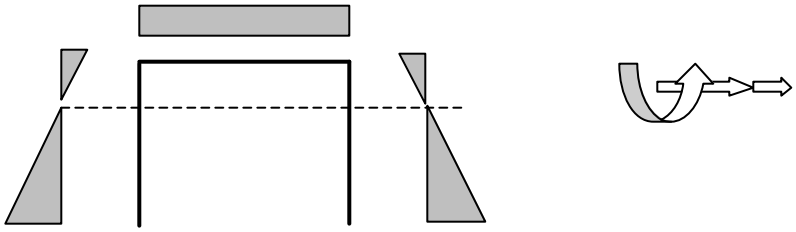

$$k_f = 4.5119\left(\frac{b_2}{b_1}\right)^2 + 6.5345\left(\frac{b_2}{b_1}\right) - 0.2064$$

$$\underline{k_w = (b_1 / b_2)^2 k_f}$$

1.3 Major Axis Bending with Unstiffened Element in Uniform Compression

Type a)

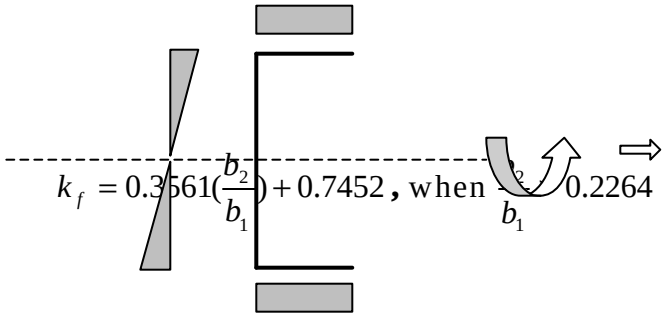

$$k_f = 0.3561(\frac{b_2}{b_1}) + 0.7452 \text{, when } \frac{b_2}{b_1} \le 0.2264$$

$$k_f = 4.2346(\frac{b_2}{b_1}) - 0.1329 \text{, when } \frac{b_2}{b_1} \le 0.2264$$

$$k_w = (b_1 / b_2)^2 k_f$$

Type b)

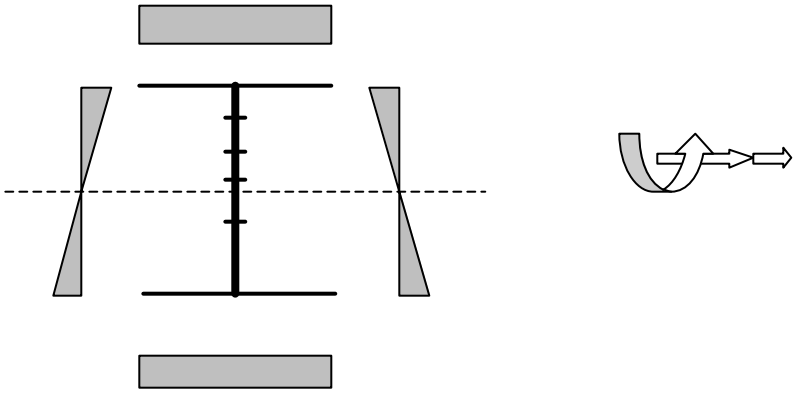

$$k_f = 0.0348(\frac{b_2}{b_1}) + 1.1246$$

$$k_w = (b_1 / b_2)^2 k_f$$

2.4 Columns

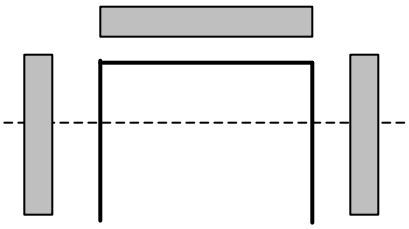

$$k_f = 1.2851(\frac{b_2}{b_1}) - 0.0237 \text{, when } \frac{b_2}{b_1} \le 0.7201$$

$$k_f = 0.0556(\frac{b_2}{b_1}) + 0.8617 \text{, when } \frac{b_2}{b_1} > 0.7201$$

3. Ultimate Strength

3.1 MINOR AXIS BENDING WITH STIFFENED ELEMENT IN TENSION

3.1.1 Effective Width Model for Flanges

$l = 1.052(b_2/t)\sqrt{f_y / Ek_f}$ or $l = \sqrt{f_y / f_{cr}}$

$k_f = 0.1451(b_2/b_1) + 1.2555$

if $l > 0.859$

$$r = 0.925\left(f_{cr} \Big/ f_y \right)^{1/3.9}$$

if $l \le 0.859$

$r = 1$

$b_e = rb_2$

$M_{ns} = f_y S_e$

The nominal moment capacity is determined by Eq.C 3.1.1-1 in AISI Specification PartV-45.

3.1.2 Post-yield Strain Reserve Capacity Model

$C_y = 3.0$ for $l \le 0.535$

$C_y = 0.5877 \Big/ (l - 0.0924)^2$ for $0.535 < l < 0.859$

$C_y = 1$ for $l \ge 0.859$

The nominal moment capacity is determined as in AISI Specification C3.1.1 b) on page V-46.

3.2 MINOR AXIS BENDING WITH STIFFENED ELEMENT IN

COMPRESSION

3.2.1 Effective Width Model

For stiffened element in uniform compression:
The effective width, b, shall be determined from AISI Specification B2.1 in Page V-35,
$f = F_y$, k= k_w
For unstiffened elements under a stress gradient:
When unstiffened elements undergo local buckling, consistent effective width shown in Figure 2 as suggested by Ben Schafer (1997) is used.

When $y = \frac{f_2}{f_1}$,

$$b_{1o} = bw / (1 - y)$$

$$b_{2o} = (b / (1 - y))\sqrt{w^2 - 2w + r}$$

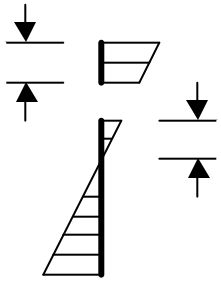

Figure 2

where

$0 \le r < 0.77 \quad w = 0.30r$

$0.77 \le r < 0.95 \quad w = 0.23$

$0.95 \le r \le 1.00 \quad w = -4.6r + 4.6$

in which,

$r = 1$ when $l \le 0.673$

$r = (1 - 0.22/l)/l$ when $l > 0.673$

$l = \sqrt{f_1 / f_{cr}}$

$M_{ns} = F_y S_e$

The moment capacity is determined by Eq.C 3.1.1-1 in AISI Specification PartV-45.

When unstiffened elements does not undergo local buckling, the nominal moment capacity is determined based on initiation of yielding or its ultimate load.

3.2.2 Post-yield Strain Capacity Model

$C_y = 3$ for $l \le 0.46$

$C_y = 3 - 2 * (l - 0.46)/(0.673 - 0.46)$ for $0.46 < l < 0.673$

$C_y = 1$ for $l \ge 0.673$

The nominal moment capacity is determined as in AISI Specification C3.1.1 b) on page V-

46.

3.3 MAJOR AXIS BENDING

Effective Width Model

Reduction factor for distortional buckling stress, suggested by Schafer (1997), is obtained as follows.

$R_d = 1$ when $l \leq 0.673$

$R_d = \frac{1.17}{l + 1} + 0.3$ when $l > 0.673$

where, $l = \sqrt{f_y / f_{cr}}$

$f_{cr} = \min [f_{cr}, R_d f_{cr}]$

For unstiffened element in uniform compression, the effective widths are determined as described in AISI Specification Section B3.2 with $f = F_y$, and using the plate buckling coefficient as given in Part 3, namely k= k_f

For stiffened element under a stress gradient, the consistent effective width described above is used $M_{ns} = F_y S_e$.

The moment capacity is determined by Eq.C 3.1.1-1 in AISI Specification PartV-45.

Post-yield Strain Reserve Capacity Model

Post-yield Strain Reserve Capacity Model needs further study when more experimental data are available.

3.4 FLAT-ENDED AND PIN-ENDED COLUMNS

Improved plate buckling coefficients k described in Part 2.4 are used.

Flat-ended columns: assuming loading through the effective centroid, column equation is to be used to design flat-ended columns.

Pin-ended columns: assuming loading through the effective centroid, beam-column equation is to be used to design pin-ended columns. Two thirds of the maximum eccentricity is selected for the beam-column equation because the eccentricity varies along the length of the column.

3.5 BEAM-COLUMN

1) using beam-column interaction equations (AISI Specification V-62 C5.2.2) with the improved plate buckling coefficient k described in Part 2

2) in column part of the beam-column equations , flat-ended column is treated as a column;

while pin-ended column itself is treated as a beam-column with the average deflection instead of the maximum deflection.
3) in beam part of the beam-column equations, when minor axis bending with stiffened element in tension or in compression, the design equations described in Part3.1 and in Part3.2 are used, respectively; when major axis bending, the design equations described in Part3.3 are used.

Appendix D: Sample Examples

1. Minor Axis Bending with Stiffened Element in Tension:

Given:
1.steel: f_y = 270MPa; E = 205000Mpa
2.section: Specimen 7 in El Mahi and Rhodes Experiment, M_{test} = 201.95Nm
centerline dimensions: t = 1.17mm; b_1 = 51.20mm; b_2 = 38.59mm
3.span L = 500mm

Required: flexural capacity using LRFD method

Solution:

$$k_f = 0.1451*(b_2/b_1)+1.2555 = 0.1451*38.59/51.20+1.2555 = 1.3649$$

$$D = \frac{Et^3}{12(1-u^2)} = \frac{205000*(1.17)^3}{12(1-0.3^2)} = 3.0067\text{x}10^4$$

$$f_{cr} = \frac{p^2 k_f D}{b_2^2 t} = \frac{p^2 *1.3649*30067}{(38.59)^2(1.17)} = 232.4638\text{MPa}$$

$$l = \sqrt{\frac{f_y}{f_{cr}}} = \sqrt{\frac{270}{232.4568}} = 1.0777 > 0.859$$

if $l > 0.859$

$$r = 0.925\left(f_{cr}/f_y\right)^{1/3.9} = 0.925*(232.4638/270)^{1/3.9} = 0.8902$$

the effective flange width $b_e = rb_2$ =0.8902*38.59=34.3528mm

$$I_e = \frac{b_e^3 t(2b_1 + b_e)}{3(2b_e + b_1)} = \frac{(34.3528)^3 * 1.17 * (2 * 51.20 + 34.3528)}{3(2 * 34.3528 + 51.20)} = 1.8032 \text{x} 10^4 \text{mm}^4$$

$$y_e = \frac{b_e^2}{(2b_e + b_1)} = \frac{34.3528 * 34.3528}{(2 * 34.3528 + 51.20)} = 9.8420 \text{mm}$$

$$M_{ns} = \frac{f_y I_e}{b_e - y_e} = \frac{270 * 18032}{(34.3528 - 9.8420)} = 198632.4 \text{Nmm}$$

Therefore

$M_{ns} / M_{test} = 198632.4/201950 = 0.9836$

2. Nominal Strength Based on Inelastic Reserve Capacity for Minor Axis Bending with Stiffened Element in Tension:

Given:

1.steel: f_y = 270Mpa; E = 205000Mpa

2.section: Specimen 6 in El Mahi and Rhodes Experiment, M_{test} =144.63Nm

centerline dimensions: t = 1.17mm; b_1 = 50.80mm; b_2 = 25.03mm

3.span L = 500mm

Required: flexural capacity using LRFD method based on inelastic reserve capacity

Solution:

$k_f = 0.1451 * b_2 / b_1 + 1.2555 = 0.1451 * 25.03/50.80 + 1.2555 = 1.3270$

$$D = \frac{Et^3}{12(1 - u^2)} = \frac{205000 * (1.17)^3}{12(1 - 0.3^2)} = 3.0067 \text{x} 10^4$$

$$f_{cr} = \frac{p^2 kD}{b_2^2 t} = \frac{p^2 * 1.3270 * 3.0067 x 10^4}{(25.03)^2 (1.17)} = 537.2213 \text{MPa}$$

$$l = \sqrt{\frac{f_y}{f_{cr}}} = \sqrt{\frac{270}{537.2169}} = 0.7089 < 0.859$$

if $l < 0.859$

$r = 1.0$

if $0.535 < l < 0.859$

$C_y = 0.5877 / (l - 0.0924)^2 = 0.5877 / (0.7089 - 0.0924)^2 = 1.5463 > 1$

Using equations from Reck, Pekoz and Winter, "Inelastic Strength of Cold-Formed Steel Beams", Journal of the Structural Division, November 1975, ASCE.

Approximate distance from neutral axis to the outer comprssion fiber, y_c (not considering the effect of radiused corners):

$$y_c = \{-(b_1 + 2b_2)C_y + \sqrt{(b_1 + 2b_2)^2 C_y^2 + 4(2 - 1/C_y - C_y)C_y(b_1 + b_2)b_2}\ \}/2/(2 - 1/C_y - C_y)$$
$$= \{-(50.80 + 2*25.03)*1.5463$$
$$+ \sqrt{(50.80 + 2*25.03)^2 1.5463^2 + 4*(2 - 1/1.5463 - 1.5463)*1.5463*(50.80 + 25.03)*25.03}\ \}$$
$$*1/2/(2 - 1/1.5463 - 1.5463)$$
$$= 19.2783$$
$$y_t = b_2 - y_c = 25.03 - 19.2783 = 5.7517 \text{ mm}$$
$$y_p = y_c / C_y = 19.2783/1.5461 = 12.4690 \text{ mm}$$
$$f_t = f_y y_t / y_p = 270*5.7517/12.4690 = 124.5456 \text{ MPa}$$
$$y_{cp} = y_c - y_p = 19.2783 - 12.4690 = 6.8093 \text{ mm}$$

Summing moments of stresses in component plates:

$$M_{ns} = f_y t[2/3 f_t y_t^2 / f_y + 2/3 y_p^2 + 2y_{cp}(y_p + y_{cp}/2) + f_t / f_y b_1 y_t]$$
$$= 270*1.17*[2/3*124.5456*5.7517^2/270 + 2/3*12.4690^2$$
$$+ 2*6.8093*(12.4690 + 6.8093/2) + 124.5456/270*50.80*5.7517]$$
$$= 146824.1915 \text{Nmm}$$

Therefore

$$M_{ns} / M_{test} = 146824.1915/144630 = 1.01517$$

3. Minor Axis Bending with Stiffened Element in Compression

Given:

1. steel: f_y = 210N/mm^2, E = 205000Mpa
2. section: Specimen 8 in Enjiky's Experiment Group 3, M_{test} =3430Nm
   centerline dimensions: t = 1.60mm; b_1 = 210mm; b_2 = 105mm
3. span: L = 300mm

Required: flexural capacity using LRFD method

Solution:

For stiffened element in uniform compression:

$$k_f = 4.5119(\frac{b_2}{b_1})^2 + 6.5345(\frac{b_2}{b_1}) - 0.2064 = 4.1888$$

$$k_w = (b_1 / b_2)^2 k_f = (210/105)^2 * 4.1888 = 16.7552$$

$$D = \frac{Et^3}{12(1-u^2)} = \frac{205000*(1.60)^3}{12(1-0.3^2)} = 7.6894\text{x}10^4$$

$$f_{cr} = \frac{p^2 k_w D}{b_1^2 t} = \frac{p^2 * 16.7552 * 7.6894x10^4}{(210)^2(1.60)} = 180.2118\text{MPa}$$

$$l = \sqrt{\frac{f_y}{f_{cr}}} = \sqrt{\frac{210}{180.2118}} = 1.0795 > 0.673$$

if $l > 0.673$

$r = (1 - 0.22/l)/l$ =(1-0.22/1.0795)/1.0795 = 0.7376

the effective web width $b_{1e} = rb_1$ =0.7376*210 = 154.896mm

For unstiffened element under a stress gradient:

if $0 \le (r = 0.7376) < 0.77$,

$w = 0.30r = 0.2213$

$y = -1$

$y_c = b_2^2/(2b_2 + b_{1e}) = 30.2141$ mm (see Figure 3)

$y_t = b_2 - y_c = 105 - 30.2141 = 74.7859$ mm

$y_p = y_c = 30.2141$ mm

$y_{tp} = y_t - y_p = 44.5718$ mm

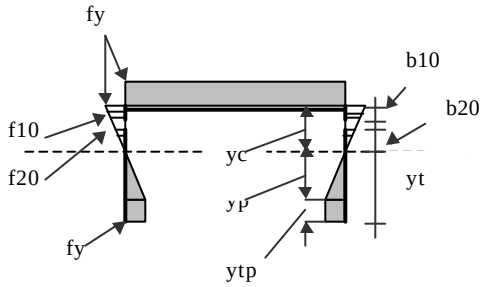

Fig.3 Stress Distribution

$b_{10} = (y_c + y_p)w/(1-y) = (30.2141 + 30.2141) * 0.2213/2 = 6.6864$ mm

$b_{20} = [(y_c + y_p)/(1-y)]\sqrt{w^2 - 2w + r}$

$= (30.2141 + 30.2141)/2 * \sqrt{0.2213^2 - 2*0.2213 + 0.7376} = 17.7210$ mm

Element	L(mm)	y from top fiber(mm)	Ly(mm^2)
Top stiffened Element	154.896	0	0
$2b_{10}$	2*6.6864	3.3432	2*22.3540
$2b_{20}$	2*17.7210	30.2141-17.7210/2=21.3536	2*378.4071
2yt	2*74.7859	30.2141+74.7859/2=67.6071	2*5056.0578
Total area sum $\sum$	353.2826		2*5456.819

Compute the neutral axis: $y_c = \frac{2*5456.819}{353.2826} = 30.8921$

$y_t = b_2 - y_c = 105 - 30.8921 = 74.1079$ mm

$y_p = y_c = 30.8921$ mm

$b_{10} = (y_c + y_p)w/(1-y) = (30.8921 + 30.8921) * 0.2213/2 = 6.8364$ mm

$b_{20} = [(y_c + y_p)/(1-y)]\sqrt{w^2 - 2w + r}$

$= (30.8921 + 30.8921)/2 * \sqrt{0.2213^2 - 2 * 0.2213 + 0.7376} = 18.1187$ mm

Element	L(mm)	y from top fiber(mm)	Ly(mm^2)
Top stiffened Element	154.896	0	0
$2b_{10}$	2*6.8364	3.4182	2*23.3682
$2b_{20}$	2*18.1187	30.8921-18.1187/2=21.83275	2*395.5810
2yt	2*74.1079	30.8921+74.1079/2=67.9461	2*5035.3428
Total area sum $\sum$	353.022		2*5454.292

Compute the neutral axis: $y_c = \dfrac{2 * 5454.292}{353.022} = 30.9006$ mm, which is very close to the result from last iteration 30.9006mm. Iteration stops here.

$y_t = b_2 - y_c = 105 - 30.9006 = 74.0994$ mm

$y_p = y_c = 30.9006$ mm

$y_{tp} = y_t - y_p = 43.1988$ mm

$b_{10} = (y_c + y_p)w/(1-y) = (30.9006 + 30.9006) * 0.2213/2 = 6.8383$ mm

$b_{20} = [(y_c + y_p)/(1-y)]\sqrt{w^2 - 2w + r}$

$= (30.9006 + 30.9006)/2 * \sqrt{0.2213^2 - 2 * 0.2213 + 0.7376} = 18.1237$ mm

$f_{20} = f_y b_{20}/y_c = 210 * 18.1237/30.9006 = 123.1684$ Mpa

$f_{10} = f_y (y_c - b_{10})/y_c = 210 * (30.9006 - 6.8383)/30.9006 = 163.5270$ Mpa

Summing moments of stresses in component plates:

$M_{ns} = f_y t[2y_{tp}(y_p + y_{tp}/2) + 2/3y_p^2] + f_{20} t(2/3)b_{20}^2$

$+ (f_{10} + f_y)tb_{10}[y_c - b_{10} + (f_{10} + 2f_y)b_{10}/3/(f_{10} + f_y)] + f_y b_{1e} t y_c$

M_{ns}=210*1.60*[2*43.1988*(30.9006+43.1988/2)+2/3*30.9006^2]+123.1684*1.60*

(2/3)*18.1237^2+(163.5270+210)*1.60*6.8383*[30.9006-6.8383+

(163.5270+2*210)*6.8383/3/(163.5270+210)]+210*154.896*1.60*30.9006

M_{ns}=3.5021e+006Nmm

Therefore

$M_{ns}/M_{test} = 3.5021\text{x}10^6/3430000 = 1.02$

4.Major Axis Bending with Unstiffened Element in Uniform Compression

Given:

1. steel: f_y =36ksi, E = 29500ksi
2. section: Specimen UP-10 in Reck's Experiment, M_{test} =14.3 in-K

   centerline dimensions: t = 0.0350in; b_1 = 3.978in; b_2 = 1.220in; type b) in Part 2.3)
3. span: L = 60 inch

Required: flexural capacity using LRFD method

Solution:

For unstiffened element in uniform compression:

$$k_f = 0.0348(\frac{b_2}{b_1}) + 1.1246 = 1.1353$$

$$D = \frac{Et^3}{12(1-u^2)} = \frac{29500*(0.035)^3}{12(1-0.3^2)} = 0.1158$$

$$f_{cr} = \frac{p^2 k_f D}{b_2^2 t} = \frac{p^2 *1.1353*0.1158}{(1.220)^2(0.0350)} = 24.9076\text{ksi}$$

$$l = \sqrt{\frac{f_y}{f_{cr}}} = \sqrt{\frac{36}{24.9076}} = 1.2022 > 0.673$$

$$R_d = \frac{1.17}{1+l} + 0.3 = \frac{1.17}{2.2022} + 0.3 = 0.8313$$

$$f_{cr} = R_d f_{cr} = 0.8313* 24.9076 = 20.7057$$

$$l = \sqrt{\frac{f_y}{f_{cr}}} = \sqrt{\frac{36}{20.7057}} = 1.3186 > 0.673$$

if $l > 0.673$

$r = (1-0.22/l)/l$ =(1-0.22/1.3186)/1.3186 = 0.6318

the effective width $b_{2e} = rb_2$ =0.6318*1.220 = 0.7708in

For Web:

if $0 \le r < 0.77$

$w = 0.30r$ =0.30*0.6318=0.18954

$$y = \frac{f_2}{f_1} = -1$$

$$b_{1o} = b_1 w / (1-y) = \frac{3.978*0.18954}{2} = 0.3770$$

$$b_{2o} = (b_1 / (1-y))\sqrt{w^2 - 2w + r}$$

$$= \frac{3.978}{2}\sqrt{0.18954^2 - 2*0.18954 + 0.6318}$$

= 1.0685

Element	L(in)	y from bottom fiber(in)	Ly (in^2)
Top Flange	0.7708	3.978	3.0662
Bottom Flange	1.2200	0	0
b_{10}	0.3770	3.978-0.3770/2=3.7895	1.4286
b_{20}	1.0685	1.989+1.0685/2=2.5233	2.6961
Negative Web Element	1.989	1.989/2=0.9945	1.9781
Sum $\sum$	5.4253		9.169

Compute the netrual axis: $y_{10} = \frac{9.169}{5.4253}$ =1.690

$$y_0 = b_1 - y_{01} = 3.978 - 1.690 = 2.2880$$

$$y = \frac{f_2}{f_1} = -\frac{y_{01}}{y_0} = -\frac{1.690}{2.2880}$$ =-0.7386

$$b_{1o} = b_1 w / (1-y) = \frac{3.978*0.18954}{1+0.7386}$$ =0.4337in

$$b_{2o} = (b_1 / (1-y))\sqrt{w^2 - 2w + r}$$

$$= \frac{3.978}{1.7386}\sqrt{0.18954^2 - 2*0.18954 + 0.6318}$$

=1.2292in

Element	L(in)	y from bottom fiber(in)	Ly (in^2)
Top Flange	0.7708	3.978	3.0662
Bottom Flange	1.2200	0	0
b_{10}	0.4337	3.978-0.4337/2=3.76115	1.6312
b_{20}	1.2292	1.690+1.2292/2=2.3046	2.8328
Negative Web Element	1.690	1.690/2=0.845	1.42805
Sum $\sum$	5.3437		8.9583

Compute the neutral axis: $y_{10} = \frac{8.9583}{5.3437}$=1.6764, which is very close to the result from last iteration 1.690. Iteration stops here.

$y_0 = b_1 - y_{01}$=3.978-1.6764=2.3016in

$y = \frac{f_2}{f_1} = -\frac{y_{01}}{y_0} = -\frac{1.6764}{2.3016}$=-0.7284

$b_{1o} = b_1 w \big/ (1-y) = \frac{3.978 * 0.18954}{1+0.7284}$=0.4362in

$b_{2o} = (b_1 \big/ (1-y))\sqrt{w^2 - 2w + r}$

$= \frac{3.978}{1.7284}\sqrt{0.18954^2 - 2*0.18954 + 0.6318}$

=1.2364in

For stiffened element under a stress gradient:

$f_1 = f_y$=36ksi

$f_2 = \frac{y_{01}}{y_0} f_y = \frac{1.6764}{2.3016} * 36 = 26.2211$ksi

$f_3 = \frac{y_0 - b_{10}}{y_0} f_y = \frac{2.3016 - 0.4362}{2.3016} * 36 = 29.1773$ksi

$f_4 = f_y \frac{b_{20}}{y_0} = 36 * \frac{1.2364}{2.3016} = 19.3389$ksi

dist= $\frac{(3y_0 - b_{10})b_{10}}{3(2y_0 - b_{10})} = \frac{(3*2.3016 - 0.4362)*0.4362}{3*(2*2.3016 - 0.4362)}$=0.2257in

Summing moments of stresses in component plates:

$M_{nx} = 2*[f_y t y_0 b_{2e} + f_2 t y_{01} b_2 + f_2 t y_{01}^2/3 + f_4 b_{20}^2 t/3 + (f_3 + f_y) b_{10} t (y_0 - b_{10} + \text{dist})/2]$

$M_{nx} = 2*[36*0.035*2.3016*0.7708 + 26.2211*0.035*1.6764*1.220 +$

$26.2211*0.035*1.6764^2/3 + 19.3389*1.2364^2*0.035/3 +$

$(29.1773+36)*0.4362*0.035*(2.3016 - 0.4362 + 0.2257)/2]$

M_{nx} = 12.7170in-k

Therefore

$M_{ns} / M_{test} = 12.7170/14.3 = 0.8893$

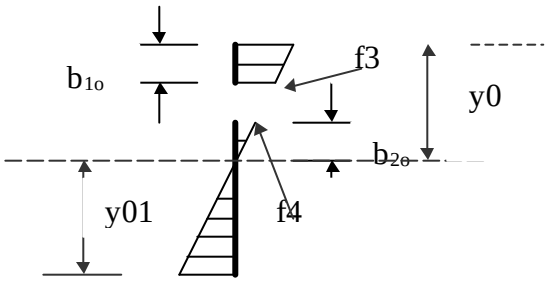

Figure 4.
Consistent Effective Width

5. Flat-ended Columns:

Given:
1. steel: f_y = 550MPa, E = 210000MPa, $u = 0.3$
2. section: in Ben Young's Experiment Series P36 specimen P36F3000, N_{test}=24700N $B_f = 36.8\,\text{mm}$; $B_w = 96.9\,\text{mm}$; small corner radii assumed $r_i = 0.85\,\text{mm}$; $t = 1.51\,\text{mm}$; base metal thickness $t_i = 1.47\,\text{mm}$
3. column length: $L = 3000.5\,\text{mm}$, the flat-ended bearings are designed to restrain both major axis and minor axis rotations as well as twist rotations and warping, K_x = 0.5; K_y = 0.5; K_t =0.5

Required: axial loading capacity using LRFD method

Solution:
1. calculate sectional properties of unreduced cross-section (see Figure 5)

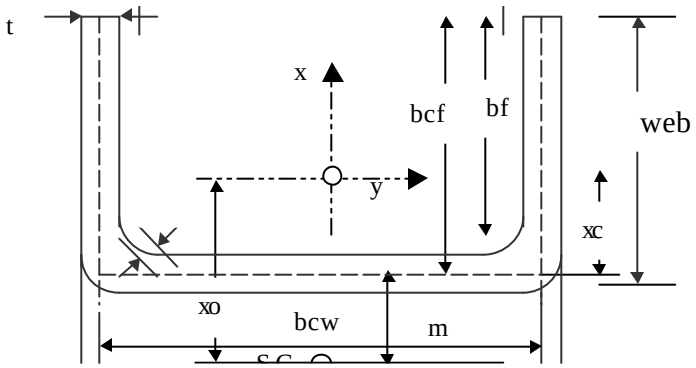

Figure 5 Ben Young's Cross Section

using Section 3.3.2 in Page I-31,
Flat width taken as the full centerline to centerline width element
Flat width of the web $b_w = B_w - 2(t + r_i) = 92.18$ mm; $b_{cw} = B_w - t = 95.39$mm

Flat width of the flange $b_f = B_f - (t + r_i) = 34.44$ mm; $b_{cf} = B_f - \frac{t}{2} = 36.045$mm

$r_c = r_i + t/2 = 1.605$ mm

Rounded corner length measured along centreline $u = \frac{p}{2} r_c = 2.521$ mm

Cross-Sectional area $A = t_i(b_w + 2b_f + 2u) = 244.17$ mm^2

Moment of inertia about x-axis:

$$I_x = \frac{t_i b_w^3}{12} + 2b_f t_i (\frac{b_w}{2} + r_c)^2 + 2\left\{(\frac{p^2 - 8}{4p}) t_i r_c^3 + u t_i (\frac{b_w}{2} + \frac{2}{p} r_c)^2\right\}$$

$= 3.427x10^5$ mm^4

Distance between the centroid and the centreline of the web (including corners)

$$x_c = \frac{t_i}{A}\left[2b_f (r_c + \frac{b_f}{2}) + 2u(1 - \frac{2}{p}) r_c\right] = 7.824 \text{ mm}$$

Moment of inertia about y-axis:

$$I_y = b_w t_i x_c^2 + 2[\frac{t_i b_f^3}{12} + b_f t_i (r_c + \frac{b_f}{2} - x_c)^2] + 2[(\frac{p^2 - 8}{4p}) t_i r_c^3 + u t_i (x_c - r_c + \frac{2}{p} r_c)^2]$$

$= 3.095x10^4$ mm^4

St. Venant torsion constant $J = \frac{t_i^3}{3}[b_w + 2b_f + 2u] = 175.876$ mm^4

Distance between shear center and web centerline $m = \frac{3b_{cf}}{(\frac{b_{cw}}{b_{cf}} + 6)} = 12.506$ mm

Distance between centroid and shear center $x_o = -(x_c + m) = -20.33$ mm

Warping constant $C_w = \frac{b_{cw}^2 b_{cf}^3 t_i}{12}\left(\frac{2\frac{b_{cw}}{b_{cf}}+3}{\frac{b_{cw}}{b_{cf}}+6}\right) = 5.007x10^7 \text{ mm}^6$

Calculate General Properties

Shear modulus $G = \frac{E}{2(1+u)} = 8.077x10^4 \text{ MPa}$

Radii of gyration about the x-axis $r_x = \sqrt{\frac{I_x}{A}} = 37.466 \text{ mm}$

Radii of gyration about the y-axis $r_y = \sqrt{\frac{I_y}{A}} = 11.258 \text{ mm}$

Polar radius of gyration about the shear center $r_{o1} = \sqrt{r_x^2 + r_y^2 + x_o^2} = 44.088 \text{ mm}$

$b = 1 - \left(\frac{x_o}{r_{o1}}\right)^2 = 0.787$

2. Determine the nominal axial strength in accordance with Section C4

According to Section C3.1.2:

$$s_x = \frac{p^2 E}{(\frac{K_x L_x}{r_x})^2} = \frac{p^2 * 210000}{(1500.25/37.466)^2} = 1292.607 \text{ MPa}$$

$$s_y = \frac{p^2 E}{(\frac{K_y L_y}{r_y})^2} = \frac{p^2 * 210000}{(1500.25/11.258)^2} = 116.711 \text{Mpa}$$

$$s_t = \frac{1}{Ar_{01}^2}(GJ + \frac{p^2 E C_w}{(K_t L_t)^2})$$

$$= \frac{1}{244.17*(44.088)^2}(80770*175.876 + \frac{p^2 * 210000 * 5.007x10^7}{1500.25^2}) = 127.080 \text{ MPa}$$

Compute the critical buckling stress:

$$F_{e1} = s_y = 116.711 \text{ MPa}$$

$$F_{e2} = \frac{1}{2b}[s_x + s_t - \sqrt{(s_x + s_t)^2 - 4b s_x s_t}]$$

$$= \frac{1}{2*0.787}[1292.607 + 127.080 - \sqrt{(1292.607+127.080)^2 - 4*0.787*1292.607*127.080}]$$

$$= 124.265 \text{ MPa}$$

$F_e = \min(F_{e1}, F_{e2}) = 116.711$ MPa

$l_c = \sqrt{\frac{f_y}{F_e}} = \sqrt{\frac{550}{116.711}} = 2.1708 > 1.5$

$F_n = [\frac{0.877}{l_c^2}] f_y = [\frac{0.877}{2.1708 * 2.1708}] * 550 = 102.358$ MPa

Compute the effective area A_e at the stress F_n:

$b_f / b_w = 34.44 / 92.18 = 0.3736 < 0.7201$

$k_f = 1.2851(b_f / b_w) - 0.0237 = 0.4564$

$l = \frac{1.052}{\sqrt{k_f}} \frac{b_f}{t_i} \sqrt{\frac{F_n}{E}} = \frac{1.052 * 34.44}{\sqrt{0.4564} * 1.47} \sqrt{\frac{102.358}{210000}} = 0.8054 > 0.673$

$r = (1 - 0.22 / l) / l = 0.9025$

$b_{we} = r b_w = 83.1924$ mm

$b_{fe} = r b_f = 31.0821$ mm

$A_e = (b_{we} + 2b_{fe} + 2u)t_i = (83.1924 + 2 * 31.0821 + 2 * 2.521) * 1.47 = 221.086$ mm ^{2}

$N_s = A_e F_n = 221.086 * 102.358 = 22629$ N

$N_{sn} / N_{test} = 22629 / 24700 = 0.916$

6. Pin-ended Columns:

Given:

1. steel: f_y = 550MPa, E = 210000Mpa, $u = 0.3$

2. section: in Ben Young's Experiment Series P36 specimenP36P0815, N_{test} =40900N

$B_f = 36.8$ mm; $B_w = 97.5$ mm; small corner radii assumed $r_i = 0.85$ mm; $t = 1.51$ mm; base metal thickness $t_i = 1.48$ mm

3. column length: $L = 814.9$ mm, the pin-ended bearings are designed to allow rotations about the minor y-axis, while restraining the major x-axis rotations as well as twist rotations and warping, $K_x = 0.5$; $K_y = 1$; $K_t = 0.5$;

Required: axial loading capacity using LRFD method

Solution:

1. Calculations of Dimensions and Properties:

using Section 3.3.2 in Page I-31,

Flat width taken as the full centerline to centerline width element

Flat width of the web $b_w = B_w - 2(t + r_i) = 92.78$ mm; $b_{cw} = B_w - t = 95.99$ mm

Flat width of the flange $b_f = B_f - (t + r_i) = 34.44$ mm; $b_{cf} = B_f - \frac{t}{2} = 36.045$ mm

$r_c = r_i + \frac{t}{2} = 1.605$ mm

Rounded corner length measured along centreline $u = \frac{p}{2} r_c = 2.521$ mm

Cross-Sectional area $A = t_i(b_w + 2b_f + 2u) = 246.719$ mm^2

Moment of inertia about x-axis:

$$I_x = \frac{t_i b_w^3}{12} + 2b_f t_i \left(\frac{b_w}{2} + r_c\right)^2 + 2\left\{\left(\frac{p^2 - 8}{4p}\right) t_i r_c^3 + u t_i \left(\frac{b_w}{2} + \frac{2}{p} r_c\right)^2\right\}$$

$= 3.501x10^5$ mm^4

Distance between the centroid and the centreline of the web (including corners)

$$x_c = \frac{t_i}{A}\left[2b_f\left(r_c + \frac{b_f}{2}\right) + 2u\left(1 - \frac{2}{p}\right) r_c\right] = 7.796 \text{ mm}$$

Moment of inertia about y-axis:

$$I_y = b_w t_i x_c^2 + 2\left[\frac{t_i b_f^3}{12} + b_f t_i \left(r_c + \frac{b_f}{2} - x_c\right)^2\right] + 2\left[\left(\frac{p^2 - 8}{4p}\right) t_i r_c^3 + u t_i \left(x_c - r_c + \frac{2}{p} r_c\right)^2\right]$$

$= 3.121x10^4$ mm^4

St. Venant torsion constant $J = \frac{t_i^3}{3}[b_w + 2b_f + 2u] = 180.138$ mm^4

Shear center $m = \frac{3b_{cf}}{\left(\frac{b_{cw}}{b_{cf}} + 6\right)} = 12.482$ mm

Distance between centroid and shear center $x_o = -(x_c + m) = -20.278$ mm

Warping constant $C_w = \frac{b_{cw}^2 b_{cf}^3 t_i}{12}\left(\frac{2\frac{b_{cw}}{b_{cf}} + 3}{\frac{b_{cw}}{b_{cf}} + 6}\right) = 5.115x10^7$ mm^6

Shear modulus $G = \frac{E}{2(1+u)} = 8.077x10^4$ MPa

Radii of gyration about the x-axis $r_x = \sqrt{\frac{I_x}{A}} = 37.670$ mm

Radii of gyration about the y-axis $r_y = \sqrt{\frac{I_y}{A}}$ =11.247 mm

Polar radius of gyration about the shear center $r_{o1} = \sqrt{r_x^2 + r_y^2 + x_o^2}$ = 44.235 mm

$$b = 1 - \left(\frac{x_o}{r_{o1}}\right)^2 = 0.790$$

2. Determine the nominal axial strength (P_{no}) in accordance with Section C4

Compute the effective area A_e at the yield stress f_y :

$b_f / b_w = 34.44 / 92.78 = 0.3712 < 0.7201$

$k_f = 1.2851 b_f / b_w - 0.0237 = 0.4533$

$$l = \frac{1.052}{\sqrt{k_f}} \frac{b_f}{t_i} \sqrt{\frac{f_y}{E}} = \frac{1.052 * 34.44}{\sqrt{0.4533} * 1.48} \sqrt{\frac{550}{210000}} = 1.861 > 0.673$$

$r = (1 - 0.22 / l) / l = 0.4738$

$b_{we} = r b_w = 43.959$ mm

$b_{fe} = r b_f = 16.318$ mm

$A_e = (b_{we} + 2b_{fe} + 2u)t_i = 120.823 \text{ mm}^2$

$P_{no} = A_e f_y = 66452.65$ N

Compute the centroid of effective section under axial force alone:

Distance between the effective centroid and centreline of the web (including corners)

$$x_{ce\_a} = t_i [2b_{fe}(r_c + b_{fe}/2) + 2u(r_c - \frac{\angle}{p} r_c)] / A_e = 3.939 \text{ mm}$$

Distance from the point of application of the load to the the centroid of the effective cross-section:

$$e_{s\_s} = x_{ce\_a} - x_c = -3.857 \text{ mm}$$

Because the eccentricity varies along the length of the column, two thirds of the maximum eccentricity is used

$$e_{s1} = \frac{2}{3} * \left| e_{s\_s} \right| = 2.571 \text{mm}$$

3. Determine the nominal axial strength (P_n) in accordance with Section C4

$$s_x = \frac{p^2 E}{(\frac{K_x L_x}{r_x})^2} = \frac{p^2 * 210000}{(0.5 * 814.9 / 37.670)^2} = 17715.835 \text{ MPa}$$

$$s_y = \frac{p^2 E}{(\frac{K_y L_y}{r_y})^2} = \frac{p^2 * 210000}{(1*814.9/11.247)^2} = 394.806 \text{ MPa}$$

$$s_t = \frac{GJ}{Ar_{01}^2}(1 + \frac{p^2 EC_w}{GJ(K_t L_t)^2}) = 1352.865 \text{ MPa}$$

Compute the critical buckling stress:

$$F_{e1} = s_y = 394.806 \text{ MPa}$$

$$F_{e2} = \frac{1}{2b}[s_x + s_t - \sqrt{(s_x + s_t)^2 - 4b s_x s_t}]$$

$$= \frac{1}{2*0.790}[17715.835 + 1352.865 - \sqrt{(17715.835 + 1352.865)^2 - 4*0.790*17715.835*1352.865}]$$

$$= 1330.188 \text{ MPa}$$

$$F_e = \min(F_{e1}, F_{e2}) = 394.806 \text{ MPa}$$

$$l_c = \sqrt{\frac{f_y}{F_e}} = \sqrt{\frac{550}{394.806}} = 1.1803 < 1.5$$

$$F_n = 0.658^{l_c^2} f_y = 307.009 \text{ MPa}$$

Compute the effective area A_e at the stress F_n:

$$b_f / b_w = 34.44/92.78 = 0.3712 < 0.7201$$

$$k_f = 1.2851 b_f / b_w - 0.0237 = 0.4533$$

$$l = \frac{1.052}{\sqrt{k_f}} \frac{b_f}{t_i} \sqrt{\frac{f_n}{E}} = \frac{1.052*34.44}{\sqrt{0.4533}*1.48} \sqrt{\frac{307.009}{210000}} = 1.3902 > 0.673$$

$$r = (1 - 0.22/l)/l = 0.6055$$

$$b_{we} = r b_w = 56.178 \text{ mm}$$

$$b_{fe} = r b_f = 20.853 \text{ mm}$$

$$A_e = (b_{we} + 2b_{fe} + 2u)t_i = 152.33 \text{ mm}^2$$

$$P_n = A_e F_n = 46766.68 \text{ N}$$

$$x_{ce\_a} = t_i[2b_{fe}(r_c + b_{fe}/2) + 2u(r_c - \frac{2}{p} r_c)]/A_e = 4.9038 \text{ mm}$$

$$e_{s\_m} = x_{ce\_a} - x_c = -2.892 \text{ mm}$$

Because the eccentricity varies along the length of the column, two thirds of the maximum eccentricity is used

$e_{s2} = \frac{2}{3} * |e_{s\_m}| = 1.928\text{mm}$

4.Determine the section moment capacity (M_{ny}) in accordance with Section C3

Compute the monosymmetry section constant about the y-axis j:

Assuming right corners

$b_{cw} = 95.99$ mm; $b_{cf} = 36.045$ mm;

Distance between the centroid of an unreduced cross-section and the centreline of the web

$$x_c' = \frac{{b_{cf}}^2}{b_{cw} + 2b_{cf}} = \frac{36.045^2}{95.99 + 2 * 36.045} = 7.730 \text{ mm}$$

$$x_o' = -(x_c' + \frac{3{b_{cf}}^2}{6b_{cf} + b_{cw}})$$

$$= -(7.730 + \frac{3 * 36.045^2}{6 * 36.045 + 95.99}) = -(7.730 + 12.482) = -20.212 \text{ mm}$$

$$\int_A x^3 dA = \frac{t_i}{2}[(b_{cf} - x_c')^4 - (x_c')^4] + \frac{b_{cw}^2 t_i}{4}[(b_{cf} - x_c')^2 - (x_c')^2]$$

$$\int_A x^3 dA = \frac{1.48}{2}[(36.045 - 7.730)^4 - 7.730^4] + \frac{95.99^2 * 1.48}{4}[(36.045 - 7.730)^2 - 7.730^2]$$

$$= 3.0026\text{x}10^6 \text{ mm}^5$$

$$\int_A xy^2 dA = -[\frac{t_i x_c' b_{cw}^3}{12} + t_i (x_c')^3 b_{cw}]$$

$$\int_A xy^2 dA = -(\frac{1.48 * 7.730 * 95.99^3}{12} + 1.48 * 7.730^3 * 95.99)$$

$$= -9.0883\text{x}10^5 \text{ mm}^5$$

Moment of inertia about y-axis $I_y' = b_{cw} t_i (x_c')^2 + 2[\frac{t_i b_{cf}^3}{12} + b_{cf} t_i (\frac{b_{cf}}{2} - x_c')^2]$

$$I_y' = 95.99 * 1.48 * (7.730)^2 + 2 * [\frac{1.48 * 36.045^3}{12} + 36.045 * 1.48 * (\frac{36.045}{2} - 7.730)^2]$$

$$= 3.134\text{x}10^4 \text{ mm}^4$$

$$j = \frac{1}{2I_y'}[\int_A x^3 dA + \int_A xy^2 dA] - x_0'$$

$$= \frac{1}{2 * 31340}(3002600 - 908830) - (-20.212) = 53.616 \text{ mm}$$

Web plate in tension under bending about the minor axis

$C_s = -1$; $C_{TF} = 1$

$$M_e = \frac{C_s As_x[j + C_s\sqrt{j^2 + r_{01}^2(s_t / s_x)}]}{C_{TF}}$$

$$= -1 * 246.719 * 17715.835 * (53.616 - 1 * \sqrt{53.616^2 + 44.235^2 (1352.865/17715.835)})$$

$$= 6.014x10^6 \text{ Nmm}$$

Elastic section modulus of the full unreduced section for the extreme compression fiber

$$S_f = \frac{I_y'}{(b_{cf} - x_c')} = \frac{31340}{36.045 - 7.730} = 1106.834 \text{ mm}^3$$

Moment causing initial yield at the extreme compression fiber of the full section

$M_y = S_f f_y = 6.0876x10^5$ Nmm

if $M_e / M_y = 9.879 > 2.78$

the critical moment $M_c = M_y = 6.0876x10^5$ Nmm

Compute the effective section modulus S_c at a stress $f_c = M_c / S_f = 550$ MPa in the extreme compression fibre:

The web is in tension under bending about the minor y axis.

$b_f / b_w = 34.44 / 92.78 = 0.3712$

$k_f = 0.1451 * b_f / b_w + 1.2555 = 0.1451 * 0.3712 + 1.2555 = 1.3094$

$$D = \frac{Et_i^3}{12(1-u^2)} = \frac{210000 * (1.48)^3}{12(1-0.3^2)} = 6.2342\text{x}10^4$$

$$f_{cr} = \frac{p^2 k_f D}{b_f^2 t_i} = \frac{p^2 * 1.3094 * 6.2342x10^4}{(34.44)^2 (1.48)} = 458.949\text{MPa}$$

$$l = \sqrt{\frac{f_c}{f_{cr}}} = \sqrt{\frac{550}{458.949}} = 1.0947 > 0.859$$

if $l > 0.859$

$$r = 0.925(f_{cr} / f_c)^{1/3.9} = 0.925 * (458.949/550)^{1/3.9} = 0.883$$

$b_{fe} = r b_f = 0.883 * 34.44 = 30.411$ mm

$A_e = (b_w + 2b_{fe} + 2u)t_i = 234.793$ mm^2

$$x_{ce\_a} = t_i[2b_{fe}(r_c + b_{fe}/2) + 2u(r_c - \frac{2}{p} r_c)] / A_e$$

$$x_{ce\_a} = 1.48 * [2 * 30.411 * (1.605 + 30.411/2) + 2 * 2.521 * (1.605 - \frac{2}{p} * 1.605)] / 234.793$$

$$= 6.463 \text{ mm}$$

$$I_{ye\_a} = b_w t_i x_{ce\_a}^2 + 2[\frac{t_i b_{fe}^3}{12} + b_{fe} t_i (r_c + \frac{b_{fe}}{2} - x_{ce\_a})^2] + 2[(\frac{p^2 - 8}{4p}) t_i r_c^3 + u t_i (x_{ce\_a} - r_c + \frac{2}{p} r_c)^2]$$

$I_{ye\_a} = 22571.109 \text{ mm}^4$

$$S_c = \frac{I_{ye\_a}}{(r_c + b_{fe} - x_{ce\_a})} = 883.306 \text{ mm}^3$$

$$M_{ny} = S_c(\frac{M_c}{S_f}) = 4.858x10^5 \text{ Nmm}$$

5. Determine the beam-column strength P_u according to Beam-Column interaction equations Equation C5.2.2-1 and C5.2.2-2

Unfactored design strength $f_c = 1,\ f_b = 1$

$C_{my} = C_m = 1$

$$\frac{P_u}{P_n} + \frac{C_{my}P_u e_{s2}}{M_{ny}(1 - \frac{P_u}{P_{Ey}})} \le 1.0$$

$$P_{Ey} = \frac{p^2 EI_y}{(K_y L_y)^2} = \frac{p^2 * 210000 * 3.121x10^4}{(1 * 814.9)^2} = 9.741x10^4 \text{ N}$$

let $a = \frac{M_{ny}}{P_{Ey}} = \frac{4.858x10^5}{9.741x10^4} = 4.987$

$$b = \frac{-M_{ny}P_n}{P_{Ey}} - M_{ny} - e_{s2}P_n$$

$$= \frac{-4.858x10^5 * 46766.68}{9.741x10^4} - 4.858x10^5 - 1.928x46766.68$$

$$= -8.092x10^5$$

$$c = M_{ny}P_n = 4.858x10^5 * 46766.68$$

$$= 2.272x10^{10}$$

$$P_{u\_1} = \frac{-b + \sqrt{b^2 - 4ac}}{2a} = 126146.3189 \text{ N}$$

$$P_{u\_2} = \frac{-b - \sqrt{b^2 - 4ac}}{2a} = 36115.562 \text{ N}$$

$$\frac{P_u}{P_{no}} + \frac{P_u e_{s1}}{M_{ny}} \le 1.0$$

$$P_{u\_3} = \frac{M_{ny}P_{no}}{M_{ny} + e_{s1}P_{no}} = \frac{4.858x10^5 * 66452.65}{4.858x10^5 + 2.571 * 66452.65} = 49162.73 \text{ N}$$

The minimum beam-column strength $P_u = 36115.562$ N

Therefore,

$P_u / N_{test} = 36115.562 / 40900 = 0.883$

REFERENCE:

Cold-Formed Steel Design Manual, 1996 Edition, American Iron and Steel Institute

Teoman Pekoz(1987). Development of a Unified Approach to the Design of Cold-Formed Steel Members

Cohen, J. M. (1987). Local Buckling Behavior of Plate Elements, Department of Structural Engineering Report, Cornell University, Ithaca, New York.

Mulligan, G. P. and Pekoz, T. (1984). "Local Buckled Thin-Walled Columns", Journal of Structural Engineering, ASCE, vol. 110, No. 11, 2635-2654.

Mulligan, G. P. and Pekoz, T. (1987). "Local Buckling Interaction in Cold-Formed Columns", Journal of Structural Engineering, ASCE, Vol. 113, No. 3, 604-620

El Mahi, A. (1985). "Behavior of Unstiffened Elements in Bending", M. S. Thesis, Dept. Of Mechanics of Materials, University of Strathclyde, Glasgow, UK

Rhodes, J. (1985). "Final Report on Unstiffened Elements", University of Strathclyde, Glasgow, UK

Ben Young (1997). "The Behavior and Design of Cold-formed Channel Columns", Ph. D Dissertation, Dept. Of Civil Engineering, University of Sydney, Australia

Teoman Pekoz (1987). Development of A Unified Approach to the Design of Cold-Formed Steel Members

Asko Talja (1990). "Design of the Buckling Resistance of Compressed HSS Channels", Research Note 1163, Technical Research Centre of Finland

Asko Talja (1992). "Design of Cold-Formed HSS Channels for Bending and Eccentric Compression", Research Note 1403, Technical Research Centre of Finland

Venkatakrishnan Kalyanaraman (1976). " Elastic and Inelastic Local Buckling and Postbuckling Behavior of Unstiffened Compression Elements", Ph.D Dissertation, Dept. Of Civil Engineering, Cornell University, USA

Vahik Enjily (1985). "The Inelastic Post Buckling Behavior of Cold-Formed Sections", Ph.D Dissertation, Dept. of Civil Engineering, Building and Cartography, Oxford Polytechnic, UK

Thiam Sin Loh (1985). "Combined Axial Load and Bending in Cold-formed Steel Members", PhD Dissertation, Dept. of Structural Engineering, School of Civil and Environmental Engineering, Cornell University

P. Jayabalan (1989). " Behavior of Non-Uniformly Compressed Thin Unstiffened Elements", Ph.D Dissertation, Dept. of Civil Engineering, India Institute of Technology, Madras

K. Srinivasa Rao (1998). " Coupled Local and Torsional-Flexural Buckling of Cold-Formed Steel Members", Ph.D Dissertation, Dept. of Civil Engineering, India Institute of Technology, Madras

American Iron and Steel Institute

1140 Connecticut Avenue, NW
Suite 705
Washington, DC 20036

www.steel.org

Research Report RP-01-2